

University of California

Santa Cruz

The Mono Craters-Mono Lake Islands Volcanic Complex,
Eastern California: Evidence for Several Magma Types,
Magma Mixing, and a Heterogeneous Source Region

A Thesis submitted in partial fulfillment
of the requirements for the degree of

MASTER OF SCIENCE

in

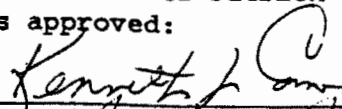
Earth Science

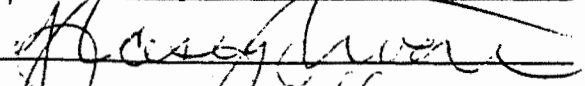
by

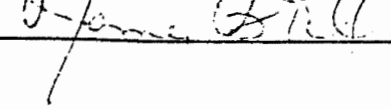
Patrick Clayton Kelleher

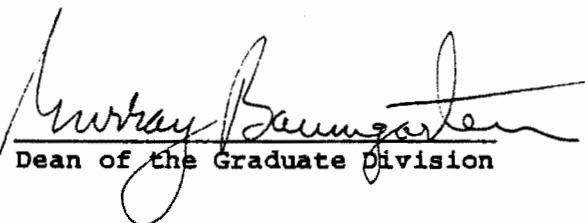
September 1986

The Thesis of Patrick Clayton Kelleher
is approved:









Dean of the Graduate Division

QE
461
K134
1986
C.2

Abstract

The Mono Craters (MC)-Mono Lake Islands (MLI) volcanic complex of eastern California, consists of Late Pleistocene to Recent basalt through high silica rhyolite lavas (HSR). Major and trace element, and Nd and Sr isotopic data establish that the major rock types that comprise the complex are not directly related by fractional crystallization or variable degrees of partial melting of a single source. Petrogenetic modeling suggest the following: 1) The MLI dacite lavas were derived from basaltic magmas, enriched in the incompatible trace elements, similar to the basalts at Black Point. 2) Andesitic inclusions within the HSR lavas, and the MC dacite dome are the products of two component mixing between basalt and highly evolved rhyolite. The mixing endmembers, however, cannot be any of the lavas presently exposed, and involve chemically distinct basalt/rhyolite constituents for each of the two rock types. 3) The HSR of the Mono Craters are petrologically and chemically variable, and fall into three groups: biotite-, orthopyroxene-, and fayalite + crystal poor lavas. The biotite-bearing domes are the oldest and most chemically distinct, and constitute a separate magma batch. The orthopyroxene-bearing domes are the most LREE and Zr enriched HSRs of the chain; the fayalite and crystal poor lavas are chemically homogeneous. The trace element data is consistent with their derivation from the orthopyroxene-bearing domes by crystal fractionation of a feldspar dominated, allanite-bearing assemblage. 4) The fp series of the Inyo domes (Sampson and

Cameron, in review) is chemically similar to the MC HSRs and the MLI rhyolites, but does not appear to be directly related.

Nd and Sr isotopic data document source region heterogeneity. Combined with other Late Cenozoic volcanic rocks of the Sierra Nevada Province, the data constitute two isotopically distinct mantle sources, one enriched at $^{87}\text{Sr}/^{86}\text{Sr}$ of about .7060 and ϵ_{Nd} between +1.5 and -6, and the other, less enriched at about .7045 and $\epsilon_{\text{Nd}} > +4$. Melts derived from the isotopically enriched source requires either garnet or hornblende in the residue. Moreover, overprinting the isotopically distinct mantle source regions, are two trace element signatures. The dominant component is characterized by an arc-like trace element pattern and is present in all the volcanic rocks of the region. The second component has a "within plate basalt" trace element signature, and within the Sierran Province, correlates with the isotopically more primitive mantle source.

Table of Contents

| | |
|------------------------------------------------------------|-----|
| Abstract | |
| Acknowledgements | iv |
| Table of Contents | v |
| List of Figures and Tables | vi |
| Introduction | 1 |
| Geologic Setting | 3 |
| Description of Rock Units | 4 |
| Petrography and Mineral Chemistry | 8 |
| Major Element Chemistry | 36 |
| Trace Element Chemistry | 47 |
| Nd-Sr Isotopes | 63 |
| Discussion | 73 |
| High-Ba Rocks | 73 |
| Low-Ba Rocks | 84 |
| Mono Craters High Silica Rhyolites | 87 |
| Relationship Between Inyo Domes and MC-MLI Rhyolites | 89 |
| Constraints on Source Regions | 96 |
| Summary | 103 |
| References | 105 |
| Appendix A | |

List of Figures and Tables

| | | |
|-------------|----------------------------------------------------------------------------------------------|----------------|
| Figure 1 | Generalized map of Mono Basin area | 2 |
| Figure 2 | Table showing subdivision of rock types | 5 |
| Figure 3a | Map of Mono Craters showing distribution of dome types | 9 |
| Figure 3b | Map of MC with subdivision of porphyritic facies | 11 |
| Figure 4a-h | Photomicrographs of basalt and andesitic inclusions | 26,28 30,32 |
| Figure 5 | quadrilateral diagrams; mafic phases of MC-MLI lavas | 16 |
| Figure 6 | diagram summary: feldspar analyses | 18 |
| Figure 7a | Harker diagrams of major oxides | 41 |
| Figure 7b | Silica variation diagrams of trace elements | 43 |
| Figure 8 | SiO ₂ vs. FeO*/MgO | 46 |
| Figure 9 | Ba vs. SiO ₂ | 48 |
| Figure 10 | REE diagram: Black Point, June Lake, MLI dacite | 51 |
| Figure 11 | REE diagram: MLI rhyolite, andesitic inclusion, MC dacite | 53 |
| Figure 12a | MORB-normalized HYG diagram; Black Point June Lake basalts, and basaltic inclusions | 55 |
| Figure 12b | MORB-normalized HYG diagram; MC-MLI, SNP, and Devil's Garden basalts | 58 |
| Figure 12c | HYG diagram of andesitic inclusion, Coso inclusion, Kenya Rift andesite | 61 |
| Figure 13a | Ba, Nd vs. Sr; MC HSRs | 64 |
| Figure 13b | Zr vs. Sr; MC HSRs | 66 |
| Figure 14 | REE diagram MC HSRs | 68 |
| Figure 15 | ⁸⁷ Sr/ ⁸⁶ Sr vs eNd; MC-MLI | 72 |

| | | |
|------------|--------------------------------------------------------------------------------------------|-----|
| Figure 16a | REE Rayleigh fractionation modeling basalt to MLI dacite | 76 |
| Figure 16b | Summarized trace element modeling basalt to MLI dacite | 77 |
| Figure 17 | REE diagram; MLI dacite and rhyolite | 82 |
| Figure 18 | WR/groundmass glass REE analyses, MC HSR | 88 |
| Figure 19 | REE model; HSR opx-bearing to HSR fayalite-bearing rhyolite | 90 |
| Figure 20a | Summarized trace element modeling; Inyo fp to MC HSR fay.-bearing rhyolite | 92 |
| Figure 20b | REE model; Inyo fp to MC HSR fayalite bearing rhyolite | 94 |
| Figure 21 | FeO*/MgO, Ba/Sr, Zr/Y, Zr/Nb vs SiO ₂ ; Inyo fp and MLI rhyolite lavas | 97 |
| Figure 22 | Nd-Sr isotopic diagram; MC-MLI and SNP basalts, granites, and mantle xenoliths ... | 100 |

Tables

| | | |
|---------|------------------------------------------------------------------|----|
| Table 1 | Summarized petrography and modes of MC-MLI rocks | 14 |
| Table 2 | EDS microanalyses of MC-MLI phenocrysts | 20 |
| Table 3 | Major and trace element XRF analyses | 37 |
| Table 4 | Isotope dilution REE analyses | 50 |
| Table 5 | Nd-Sr isotopic ratios MC-MLI lavas | 71 |
| Table 6 | Distribution coefficients used in petrogenetic modeling | 79 |

Introduction

The Mono Craters-Mono Lake Islands (MC-MLI) volcanic complex is located a few kilometers east of the Sierra Nevada fault scarp in eastern California (fig. 1). The lavas range from basalt through high silica rhyolite (HSR) and erupted onto, and south of, the western floor of the Mono Basin in Latest Pleistocene to Recent time (Russell, 1889; Mayo, 1948; Curry, 1960; Lajoie, 1968; Sieh and Bursik, 1986). The dramatic landforms of the complex have attracted the attention of geologists for nearly a century. To date however, the chemistry, petrogenetic inter-relationships, and evolution of this magmatic system has received little attention. This paper presents 52 major and trace element, 11 isotope dilution rare earth element (REE), and 7 Nd and Sr isotopic analyses of the MC-MLI lavas.

The MC-MLI volcanic rocks represent some of the most recent, Sierran front range volcanic activity. Other major silicic centers along the eastern Sierran front include: the Pleistocene Coso Volcanic Field approximately 160 kms. to the southeast (Bacon, et al., 1980, 1981), the seismically active Long Valley magmatic system (Bailey, 1976), and the 600 yr. B.P. (Miller, 1985) Inyo domes just south of the Mono Craters (fig. 1). The temporal proximity of the Mono, Inyo, and Long Valley lavas has stimulated controversy over the relationship between these volcanic centers. Some believe that the three systems are chemically related (eg Bailey, 1981-1984, Sieh, in press, Tanzer and Macdougall, 1984). Others (Sampson et al, 1983, 1984, Kelleher

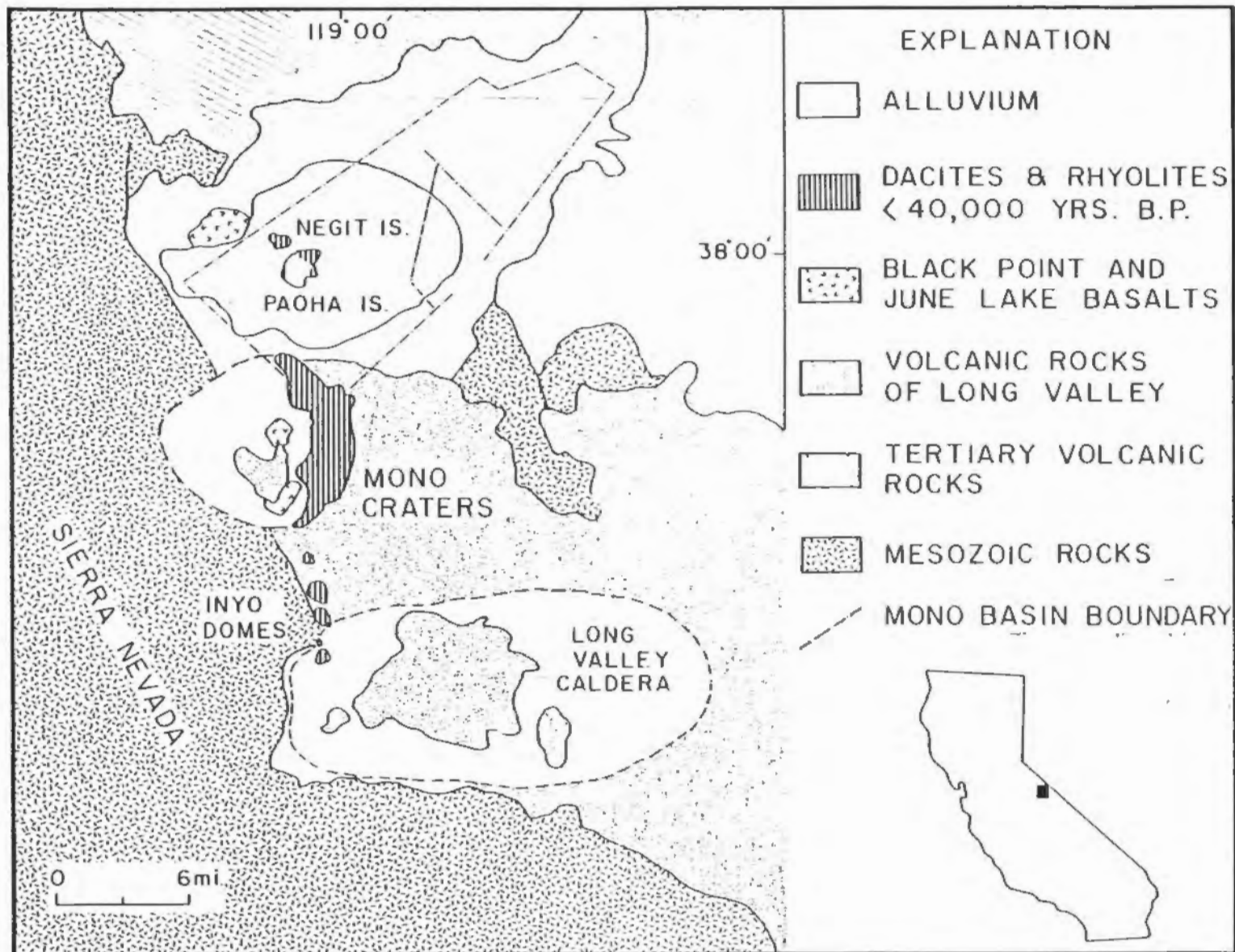


Figure 1:

Generalized geologic map of Late Pleistocene to Recent volcanic rocks in the MC-MLI area (redrafted from Bailey, et al., 1976). The geophysical boundary of the Mono Basin is shown in the dot-dash line. Silicic rocks are shown in the ruled pattern; the basalts of Black Point and June Lake are in the checked pattern. The June Lake lavas are more extensive than shown. A detailed map of the Mono Craters is located in Appendix A.

and Cameron, 1984, 1985) have presented chemical and isotopic arguments that suggests several unrelated magmas. Bailey et al. (fig. 2, 1984) have proposed: 1) a single, zoned magma body which includes all of the Mono Craters lavas and Inyo domes, 2) a single magma chamber for the Mono Lake Islands dacites and rhyolites, and 3) a separate magmatic system for the Long Valley lavas. The purposes of this paper are to investigate the petrogenetic history and inter-relationships of the lavas that comprise the Mono Craters, Mono Lake Islands, and contemporaneous basalts, and to resolve the controversy over the relationship between the silicic rocks of the MC-MLI complex and the Inyo domes. The petrologic, chemical, and isotopic data presented here demonstrates several liquid lines of descent for the silicic rocks of the complex and the unlikelihood that any of these lavas are directly related to the Inyo rhyolites.

Geologic Setting

The MC-MLI erupted within and south of the Mono Basin, a post-Miocene, rectilinear depression (fig 1). The region is underlain by Mesozoic basement with lithologies similar to metamorphic and intrusive rocks found in the Sierra Nevada (Kistler, 1966, Bateman and Eaton, 1967, Oliver, 1977). Volcanic activity in the region, began in Early to Mid-Miocene time and is characterized by intermediate to silicic, calc-alkaline lavas. (Gilbert, et al., 1968). Approximately 4MY ago, the character of volcanism changed, erupting more alkalic, olivine basalts, latites, and bimodal basalt-

rhyolitic lavas. Deformation and faulting has been roughly continuous and associated with volcanism for at least the last 10 M.Y. (ibid).

The most recent faulting and volcanism in the Mono Basin area follows a north-northwest regional trend within a zone, termed the Walker Lane belt by Stewart et al. (1975). This zone is distinctly different from the N-S striking normal faults of the Basin and Range to the east. The belt is characterized by: 1) NNW-NW striking normal faults, 2) conjugate right- and left-lateral, strike slip faults, and 3) greater extension rates Wright, (1976). Leeman (1982) defined a petrologic subprovince of the Basin and Range based on enriched Sr contents and Sr isotopic compositions that is generally similar to the tectonically defined Walker Lane belt. This suggests that the chemical signature of the volcanism here, is tectonically controlled.

Description of Rock Types

The volcanic rocks of the complex are discussed in terms of five groups. These are: 1) 50-54% SiO₂ basalts, 2) 58-62% SiO₂ andesites, 3) 64-69% SiO₂ dacites 4) 70-72% SiO₂ rhyolites and 5) high silica rhyolites (HSR, >75% SiO₂) (fig. 2). A brief description of the different rock types follows.

Basalt occurs as cinders and bombs at Black Point, a 13,000 year old maar volcano (Wood, 1977; Lajoie, 1968) well exposed on the northwest shore of Mono Lake (fig. 1). The June Lake basalts erupted onto, and south of, the western floor of the Mono Basin from several

Pleistocene - Recent Volcanic Rocks
of the Mono Basin

| | <u>BASALT</u> | <u>ANDESITE</u> | <u>DACITE</u> | <u>RHYOLITE</u> | <u>HIGH SILICA RHYOLITE</u> |
|-----------|----------------------------------------------------------------------|-------------------------------------------------------------------------|-----------------------------------------------------------------|--------------------------------------------------------------------|--------------------------------------------|
| higher Ba | 50-54 % SiO ₂ June Lake Black Point lavas | | 64-69% SiO ₂ Mono Lake Islands dacite lavas | 70-72 % SiO ₂ Mono Lake Islands rhyolite lavas | |
| lower Ba | 53-55% SiO ₂ basaltic inclusions in MC Dacite | 58-62% SiO ₂ andesitic inclusions in MC Rhyolite | 67-69% SiO ₂ Mono Craters Dacite Dome | | 76-77% SiO ₂ Mono Craters |

Figure 2:

Subdivision of MC-MLI rock types and their distribution into high- and low-Ba groups as discussed in the text. Note that the Mono Craters high silica rhyolites are excluded from the Ba distinctions.

cinder cones and fissures. The age of the June Lake eruptions has not been dated radiometrically but is bracketed between the Tahoe and Tiogan glacial periods (Putnam, 1938) or between about 12,000 and >50,000 yrs. B.P. The sample analyzed for this study represents the most areally extensive June Lake lava exposed. A third occurrence of basalt is as inclusions within the MC dacite dome (dome #12, fig. 3a). The inclusions are dark gray to reddish colored, finely vesicular and have megacrysts of plagioclase up to 2.5 cm. in length. Several textural features suggest that the inclusions were incorporated as partially molten material. These features are: 1) irregular, rounded shapes, 2) 1-2mm chill margins, 3) vesicular habit, 4) crenulated margins, and 5) re-entrants of host material (fig. 4e-h).

Andesite in the MC-MLI is found only as inclusions in two HSR domes (domes #14, #18, fig.3a). These inclusions are abundant within the HSR host comprising 10-15% by volume. Contacts between host and inclusion are sharp with occasional re-entrants of HSR (fig. 4a).

The single dacite dome of the Mono Craters chain (fig. 3a) represents the initial silicic volcanism of the MC-MLI complex 40,000 yrs. B.P. (Lajoie, 1968). The dome is slightly perlitic, sparsely porphyritic, and contains abundant basaltic inclusions up to 25 cm. in diameter (fig. 4e). Flowbanded rhyolitic xenoliths also occur but are sparse.

A cinder cone and at least two lava flows of dacitic composition comprise Negit Island in Mono Lake. Dacite also occurs with rhyolite

lavas and plug domes on Paoha Island, and many of the smaller islands. Stein (pers. comm., 1983) and Sieh et al. (1983) suggest Paoha is slightly younger than Negit at <300 yrs. B.P.

The Mono Craters form an arcuate chain of 27 gray, glassy, pumiceous, HSR lavas and one dacite dome (fig. 3a). Wood (1977) classified the lavas into porphyritic, sparsely porphyritic, and aphyric types. His classification is adopted here with some modification of the aphyric and sparsely porphyritic facies domes based on more detailed field and petrologic work. The porphyritic domes are further subdivided based on the presence of: biotite, orthopyroxene, or fayalitic olivine phenocrysts (Kelleher and Cameron, 1984). Field studies and hydration rind ages (Wood, 1977) correlate with the subdivisions. HSR volcanism began with the eruption of biotite-bearing lavas approximately 25,000 yrs. B.P.. The three biotite-bearing domes (#'s 11, 19, and 24, fig. 3b), are thickly mantled by younger tephras and are poorly exposed. Orthopyroxene-bearing and fayalite-bearing HSRs were the next porphyritic domes to be deposited. Eruption of the sparsely porphyritic lavas generally followed the emplacement of the porphyritic facies. The aphyric lavas are the youngest deposits of the chain erupting during two magmatic pulses, 1200 and 550 yrs. B.P. (Sieh, 1983, in press).

Petrography/Mineral Chemistry

The petrographic characteristics and mineral chemistry of the different rock types are summarized in tables 1 and 2 and figures 5

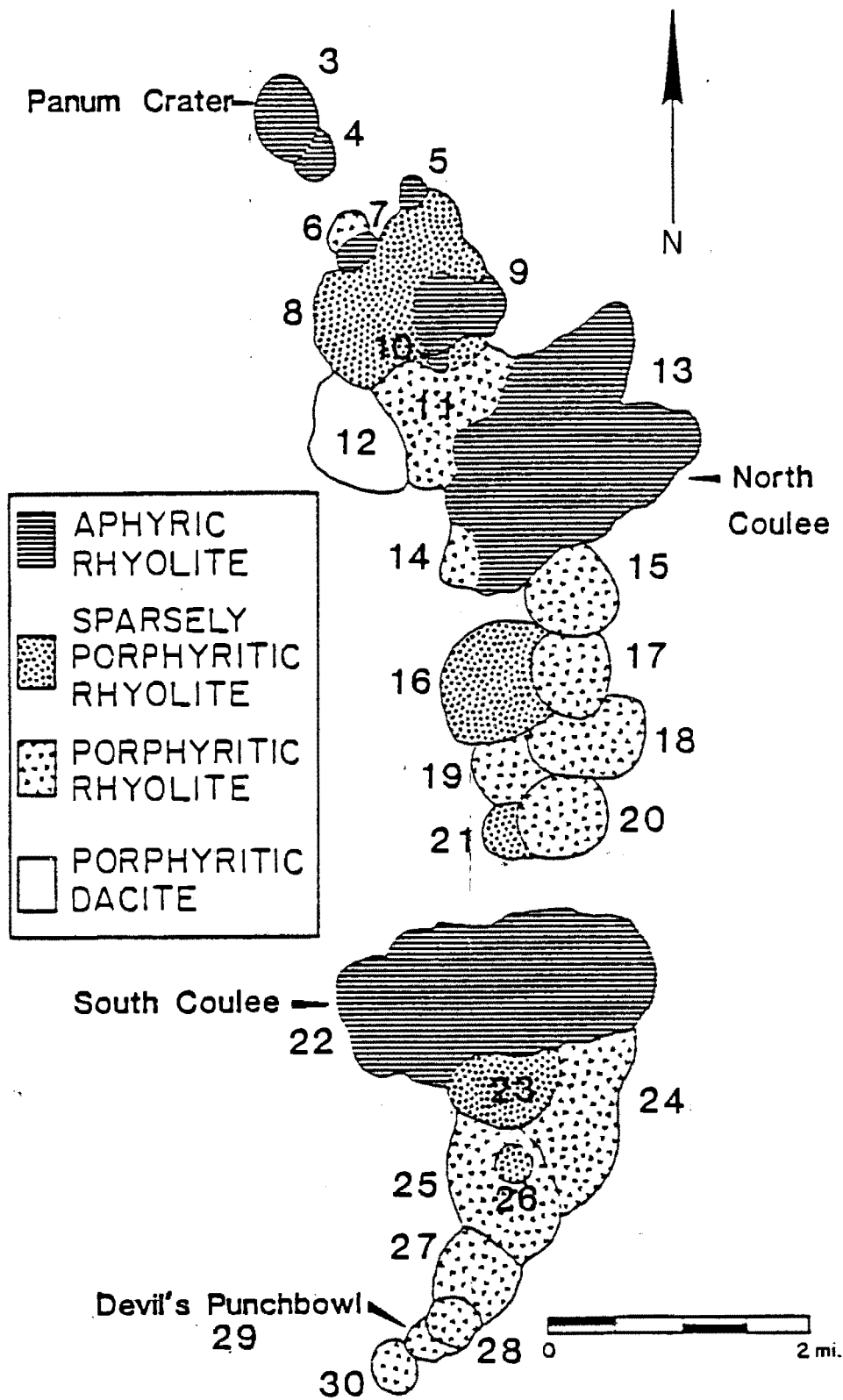


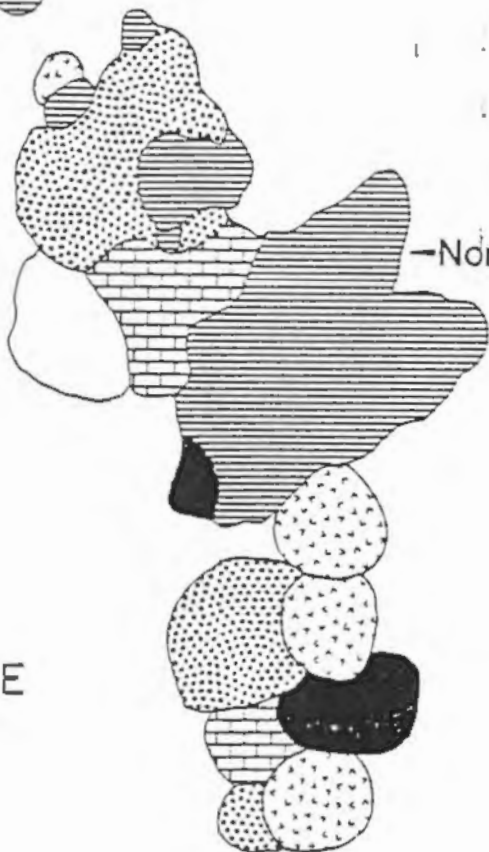
Figure 3a:

Simplified map of the Mono Craters, showing the distribution of aphyric, sparsely porphyritic, and porphyritic domes (modified from Wood, 1977). The single dacite dome of the chain is unpatterned. The dome numbers correlate with the numbering system of Wood (1977) and the geochemical sample numbers in the tables, figures, and text. There is no correlation of age with dome number, but hydration rind dating (Wood, 1977) indicates that the oldest HSRs are porphyritic followed by sparsely porphyritic, and aphyric lavas (see text).

Panum Crater

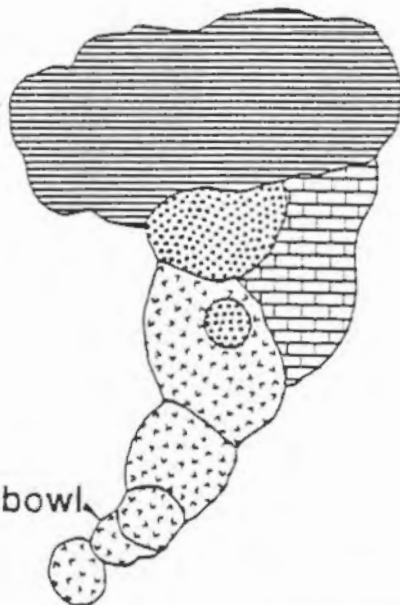


North Coulee



-  OLIVINE RHYOLITE
-  ORTHOPYROXENE RHYOLITE
-  BIOTITE RHYOLITE

South Coulee



Devil's Punchbowl



Figure 3b:

Simplified map of the Mono Craters highlighting the different porphyritic facies domes. The biotite-bearing lavas (brick pattern) are the oldest HSRs and have limited exposures. The orthopyroxene-bearing domes (black) are riddled with vesicular, andesitic inclusions. The 9 fayalite-bearing rhyolites (carrot pattern) are the most extensive porphyritic facies lavas.

and 6. The following descriptions highlight the most important petrologic observations.

Mafic Rocks

The physical evidence for contamination by crustal rocks and/or mixing with compositionally distinct magmas is typical of the mafic to intermediate rocks of the MC-MLI complex. All of the observed samples are porphyritic, averaging 23% by volume, with 1-3mm sized phenocrysts. Plagioclase is the dominant phenocryst phase with subordinate olivine, minor titaniferous clinopyroxene, and sparse Fe-Ti oxides (table 2). The Black Point basalt has the least evidence for contamination. Microanalyses, made with an energy dispersive system (EDS) equipped scanning electron microscope (SEM) (table 2), indicate that plagioclase (An70) and olivine (Fo85) are compositionally homogeneous, and all phenocryst phases, including clinopyroxene, are eu- to subhedral and texturally uniform. Rounded pre-Cenozoic(?) quartzite clasts and quartz xenocrysts up to 7mm in length with fine grained Fe-oxide reaction rims are present in minor amounts (<1% by vol.). In contrast, the June Lake sample has abundant disequilibrium textures. Olivine phenocrysts are resorbed and have variable compositions ranging from Fo88 to Fo65. Plagioclase phenocrysts are commonly resorbed or sieve textured and have extremely variable anorthite contents ranging from An90 to An33 (fig. 6). Quartz xenocrysts with kelyphitic reaction rims of pyroxene, and sanidine and orthoclase(?) xenocrysts are also common.

Table 1: Petrographic modes of Mono-Craters-Mono Lake Islands volcanic rocks (in volume percent)

| Sample rock type | Mafic Rocks | | | | Mono Lake Islands Dacites | | | | | | | |
|---------------------|--------------|-------------|---------------|---------------|---------------------------|------------|------------|-------------|------------|------------|------------|------------|
| | BP83 bas. | JLB bas. | incl. bas. | incl. and. | N1 dac. | N2 dac. | N3 dac. | MLI dac. | N4 dac. | P6 dac. | P2 dac. | P4 dac. |
| % phenocr. | 20 | 38 | 45 | 8 | 8 | 6 | 6 | 10 | 9 | 4 | 5 | 4 |
| Olivine | 11 | 11 | 16 | 21 | - | - | - | - | - | - | - | - |
| Opx | - | - | - | 4 | 4 | 2 | 2 | 1 | - | 3 | 4 | 5 |
| Cpx | 7 | 3 | 9 | 2 | + | + | + | + | - | 2 | + | - |
| Hblde. | - | - | - | - | 4 | 19 | 16 | 31 | 15 | - | - | 12 |
| Biotite | - | - | - | - | 1 | + | + | 3 | 1 | + | + | 12 |
| Magnetite | + | + | 4 | + | 10 | 12 | 18 | 7 | 13 | 30 | 24 | 7 |
| Plag | 82 | 86 | 71 | 72 | 15 | 16 | 5 | 2 | 4 | 24 | 21 | 66 |
| micro | a | a | a | a | 66 | 61 | 60 | 54 | 66 | 43 | 51 | a |
| megacr. | | | 4 | | | | | | | | | |
| apatite | - | - | - | + | + | + | + | + | + | + | + | + |
| Xenocrysts | q | q,p | - | q,s,p | | | | | | | | |
| # sections counted | 1 | 6 | 4 | 4 | 1 | 1 | 2 | 2 | 2 | 2 | 1 | 3 |

| Sample rock type | MLI rhyolites | | | | Mono Craters | | | |
|---------------------|---------------|------------|------------|------------|--------------|------------|-------------|------------|
| | P1 rhy. | P3 rhy. | P5 rhy. | P7 rhy. | bt. HSR | opx HSR | fay. HSR | MC dac. |
| % phenocr. | 3 | 6 | 5 | 2 | 5 | 5 | 8 | 12 |
| plag | 52 | 70 | 69 | 53 | 26 | 42 | 25 | 33 |
| sanidine | - | - | - | - | 25 | 42 | 40 | - |
| quartz | - | - | - | - | 33 | 0.3 | 26 | - |
| hblde | + | - | - | + | 0.8 | 7 | 6 | 30 |
| biotite | 28 | 28 | 27 | 37 | 13 | - | -,b | - |
| magnetite | 16 | 2 | 4 | 10 | 2 | 4 | 3 | 7 |
| opx | - | - | - | - | - | 6 | -,b | 33 |
| cpx | - | - | - | - | - | - | - | 30 |
| olivine | - | - | - | - | - | - | 1 | - |
| apatite | + | + | + | - | | | + | + |
| zircon | + | + | + | - | 0.3 | 0.8 | + | - |
| allanite | - | - | - | - | | | + | - |
| Xenocrysts | - | - | - | - | - | - | | p,o,c |
| # sections counted | 1 | 2 | 2 | 2 | 6 | 6 | 9 | 1 |

+: present

-: not observed

a: a, not distinguished; b: occurs in 2 sections of ol-bearing domes

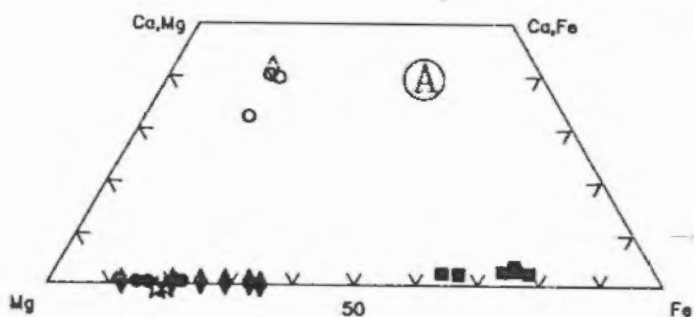
p,s,q: plag, sanidine, quartz

o,c: olivine, clinopyroxene

Table 1:

Summarized petrographic modes (58) of each of the different rock types. Each thin section represents ≥ 1000 point counts. The silicic rocks (MLI dacites, rhyolites, and MC HSRs) are all crystal poor and average $< 1\text{mm}$ in length. Note the higher relative percentage of accessory phases in the orthopyroxene-bearing domes; Hornblende is rare in biotite-bearing dome, M-19, and allanite is absent. Sample numbers: BP and JLB = Black Point and June Lake basalts respectively; bas. incl. = basaltic inclusions in MC dacite; and. incl. = andesitic inclusions in orthopyroxene-bearing domes; N- = Negit Island dacites; P- = Paoha Island dacites and rhyolites; Mono Craters lavas, as indicated.

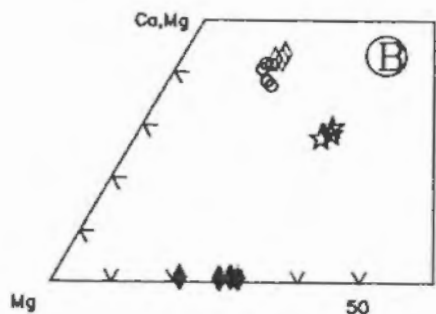
EDS Analyses: Mafic Phenocrysts



(A)

Mafic Rocks

- ☆ olivine: Black Point basalt
- ◆ olivine: June Lake basalt
- ◇ cpx: June Lake basalt
- olivine: andesitic inclusions
- cpx: andesitic inclusions
- opx: andesitic inclusions



(B)

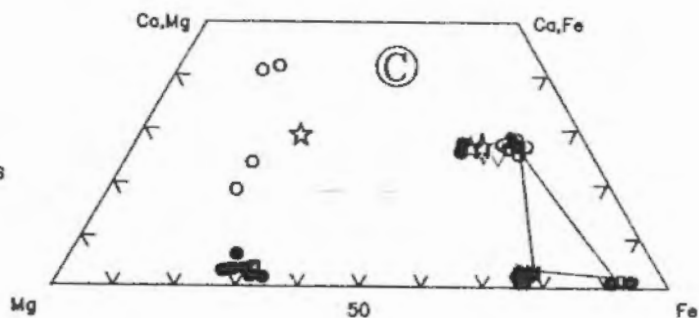
MC dac. & basalt incl.

- ◇ cpx: basaltic inclusions
- ◆ olivine: basaltic inclusions
- cpx: MC dacite
- ☆ hornblende: MC dacite

(C)

MLI

- cpx: MLI dacites
- opx: MLI dacites
- ☆ hornblende: MLI dacites
- opx: MLI rhyolites



(C)

HSR

- hornblende: biotite-bearing domes
- ◇ hornblende: orthopyroxene-bearing domes
- ◆ opx: orthopyroxene-bearing domes
- hornblende: fayalite-bearing domes
- opx: fayalite-bearing domes M6 & M28
- fayalite: fayalite-bearing domes
- ☆ hornblende: M16

Figure 5:

EDS-microanalyses of mafic silicates. Hornblendes are plotted as 100 mol% Ca+Mg+Fe. Note the diverse assemblage and composition of the andesitic inclusions (A) and subcalcic cpx analyses from the MLI dacites (C). In (C) the biotite-bearing dome M-24, has the most Mg-rich hornblende compositions of the HSRs (Mg-rich, black dot). Hornblende is rare in biotite-bearing rhyolite, M-19, and no hornblende analyses were obtained. The orthopyroxene-bearing lavas, and the sparsely porphyritic dome M-16 also have more Mg-rich hornblende compositions than the other porphyritic HSRs. The tie line connects coexisting phases in the two fayalite-bearing domes that have orthopyroxene.

EDS Feldspar Analyses

18

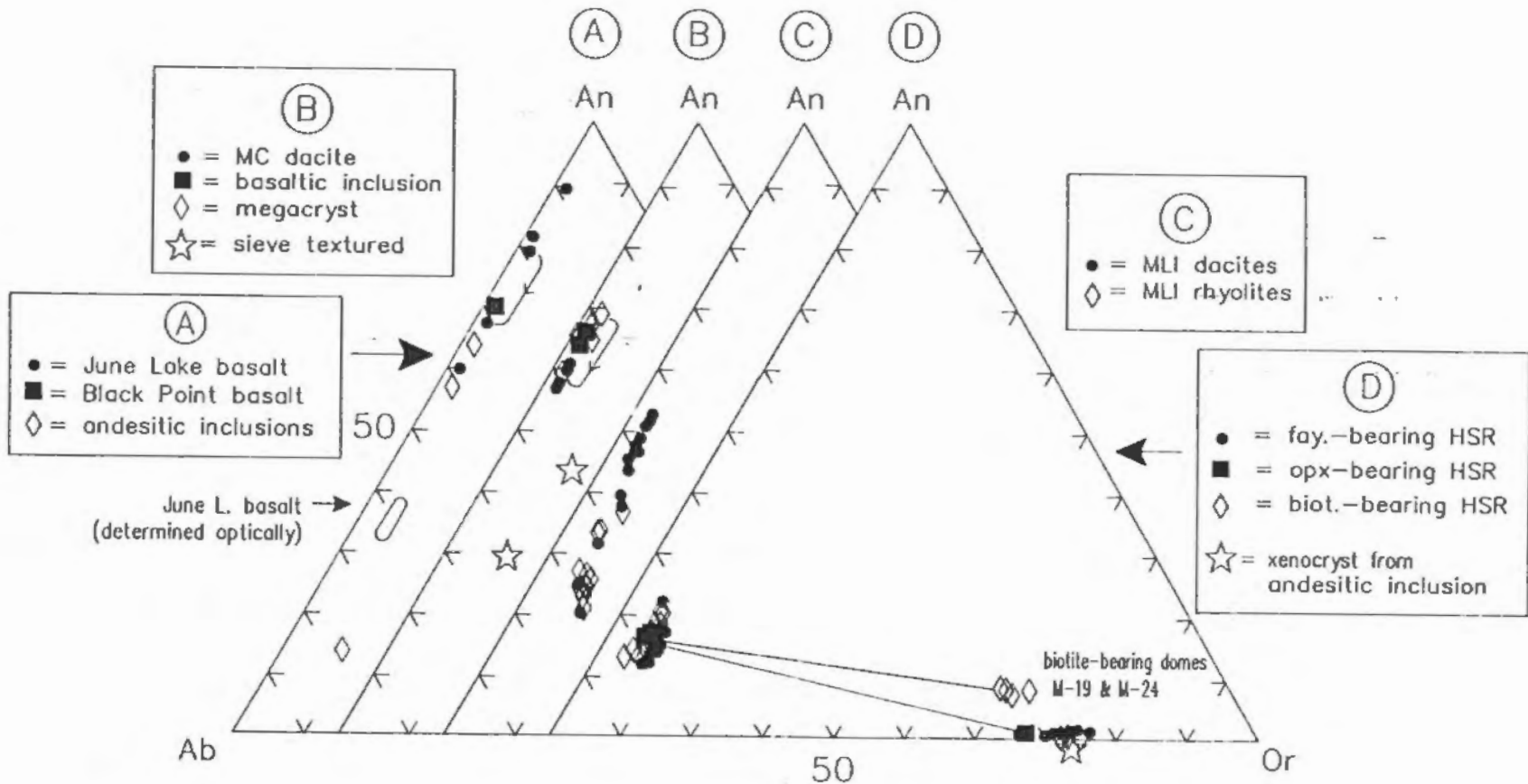


Figure 6:

EDS-microanalyses of MC-MLI feldspars: (A), June Lake, Black Point basalts, and andesitic inclusions. Note the extreme range of compositions in the June Lake sample (An90-35) and the andesite (An70-14). (B), MC dacite and basaltic inclusions. (C), MLI dacites (dots) and MLI rhyolites (diamonds). (D), MC hSRs, tie lines connect coexisting sanidine and plagioclase. Note the more calcic sanidine of the biotite bearing domes M-19- and M-24, and the sanidine xenocryst from the andesitic inclusion (star).

Table 2 Mineral Analyses

mafic phenocrysts

| | Sp83-1 | J1b-1 | J1b-1 | M-12-2b | M-18-1b | M-18-1b | J1b-1 | M-12-2b | M-12-2b | M-12-1a | M-12-1a | M-18-1b | M-18-1b | M-12-1a | M-12-1a | M-12-1a |
|-------|---------|---------|----------|---------|---------|---------|----------|----------|----------|----------|----------|---------|-----------|----------|----------|----------|
| SiO2 | 37.99 | 35.80 | 38.37 | 37.15 | 37.25 | 38.05 | 48.73 | 51.52 | 49.56 | 50.93 | 49.56 | 48.11 | 48.37 | 43.05 | 44.47 | 43.89 |
| Al2O3 | 0.30 | 0.41 | 0.36 | 0.42 | 0.35 | 0.25 | 4.91 | 2.56 | 4.13 | 2.96 | 3.96 | 0.82 | 0.69 | 11.38 | 9.96 | 10.19 |
| TiO2 | 0.00 | 0.00 | 0.00 | 0.00 | 0.00 | 0.00 | 1.59 | 0.68 | 1.25 | 0.84 | 1.37 | 0.05 | 0.05 | 2.37 | 2.39 | 2.38 |
| Cr2O3 | 0.00 | 0.00 | 0.00 | 0.04 | 0.00 | 0.00 | 0.26 | 0.14 | 0.21 | 0.19 | 0.13 | 0.03 | 0.05 | 0.05 | 0.04 | 0.10 |
| FeO | 15.97 | 30.71 | 11.54 | 19.49 | 20.45 | 14.98 | 9.51 | 9.16 | 9.13 | 10.60 | 9.65 | 40.64 | 39.97 | 16.59 | 16.01 | 16.53 |
| MnO | 0.10 | 0.51 | 0.13 | 0.25 | 0.18 | 0.14 | 0.12 | 0.08 | 0.12 | 0.25 | 0.16 | 2.55 | 2.52 | 0.25 | 0.23 | 0.28 |
| MgO | 44.90 | 31.92 | 48.47 | 41.95 | 40.78 | 45.59 | 14.87 | 16.20 | 14.99 | 16.08 | 14.69 | 6.43 | 6.95 | 11.79 | 12.95 | 12.19 |
| CaO | 0.10 | 0.33 | 0.12 | 0.15 | 0.18 | 0.15 | 19.90 | 19.61 | 20.33 | 18.05 | 20.38 | 1.34 | 1.39 | 11.79 | 11.40 | 11.66 |
| Na2O | 0.63 | 0.33 | 1.02 | 0.55 | 0.80 | 0.85 | 0.00 | 0.00 | 0.17 | 0.00 | 0.01 | 0.00 | 0.00 | 2.05 | 1.76 | 1.86 |
| K2O | 0.00 | 0.00 | 0.00 | 0.00 | 0.00 | 0.00 | 0.10 | 0.05 | 0.12 | 0.11 | 0.08 | 0.01 | 0.01 | 0.02 | 0.79 | 0.92 |
| phase | olivine | olivine | ol, core | olivine | olivine | olivine | cpx | cpx | cpx | cpx | cpx | opx | opx, core | hb1a | hb1a | hb1a |
| comp | Fe83 | Fe65 | Fe88 | Fe79 | Fe78 | Fe84 | 41,43,16 | 40,46,14 | 42,43,15 | 37,46,17 | 42,42,16 | En21 | En23 | 29,40,31 | 27,43,30 | 28,41,31 |

plagioclase phenocrysts

| | Sp83-1 | J1b-1 | J1b-1 | J1b-1 | J1b-1 | J1b-1 | M-12-2b | M-12-2b | M-12-2b | M-18-1b | M-18-1b | M-18-1b | M-18-1b | M-12-1a | M-12-1a | M-12-2 |
|-------|--------|-------|-------|-----------|-------------|------------|-------------|------------|------------|----------|---------|---------|---------|----------|----------|----------|
| SiO2 | 51.08 | 47.47 | 48.56 | 52.94 | 51.66 | 49.54 | 52.39 | 51.97 | 53.81 | 46.13 | 44.53 | 52.43 | 53.90 | 62.34 | 61.07 | 53.65 |
| Al2O3 | 30.91 | 33.74 | 32.75 | 29.60 | 30.42 | 32.39 | 30.44 | 30.81 | 28.84 | 19.31 | 21.81 | 30.00 | 26.91 | 23.49 | 23.99 | 29.03 |
| TiO2 | 0.01 | 0.00 | 0.00 | 0.00 | 0.00 | 0.00 | 0.00 | 0.00 | 0.02 | 0.00 | 0.00 | 0.00 | 0.03 | 0.00 | 0.00 | 0.00 |
| Cr2O3 | 0.10 | 0.13 | 0.13 | 0.02 | 0.05 | 0.13 | 0.11 | 0.00 | 0.11 | 0.00 | 0.02 | 0.13 | 0.12 | 0.00 | 0.01 | 0.09 |
| FeO | 0.56 | 0.48 | 0.45 | 0.58 | 0.60 | 0.42 | 0.23 | 0.27 | 0.66 | 0.00 | 0.12 | 0.37 | 0.54 | 0.28 | 1.01 | 0.53 |
| MnO | 0.00 | 0.00 | 0.00 | 0.00 | 0.00 | 0.00 | 0.00 | 0.00 | 0.00 | 0.00 | 0.00 | 0.00 | 0.00 | 0.00 | 0.00 | 0.00 |
| MgO | 0.22 | 0.16 | 0.06 | 0.11 | 0.16 | 0.01 | 0.08 | 0.00 | 0.09 | 0.00 | 0.00 | 0.11 | 0.13 | 0.00 | 0.16 | 0.11 |
| CaO | 13.67 | 16.84 | 15.89 | 12.15 | 13.31 | 15.26 | 12.82 | 0.00 | 11.60 | 0.23 | 2.73 | 12.67 | 11.39 | 5.75 | 7.44 | 11.67 |
| Na2O | 3.19 | 0.95 | 1.94 | 4.12 | 3.50 | 2.05 | 3.67 | 13.35 | 4.45 | 3.14 | 9.19 | 3.91 | 4.52 | 6.71 | 4.54 | 4.54 |
| K2O | 0.28 | 0.22 | 0.22 | 0.49 | 0.29 | 0.25 | 0.29 | 3.26 | 0.42 | 11.19 | 1.61 | 0.38 | 0.48 | 1.43 | 1.58 | 0.38 |
| phase | plag | plag | plag | p, sieved | p, sub, rml | p, sub, cr | pl, neg, cr | pl, mg, oc | pl, mg, cr | sanidine | plag | plag | plag | p, sieve | p, sieve | plag, ho |
| comp | An69 | An90 | An81 | An60 | An67 | An79 | An65 | An68 | An58 | Or69 | An14 | An63 | An57 | An29 | An63 | An57 |

Table2 (cont'd)

MLI dacites

| | Heg-R42 | Heg-R42 | Heg-R42 | Heg-R42 | Heg-R42 | Heg-R42 | Heg-R42 | Fao-Rhy4 | Fao-Rhy4 | Fao-Rhy4 | Fao-Rhy4 | Fao-Dac6 | Fao-Dac6 | Fao-Dac6 | Fao-Dac6 | Fao-Dac6 |
|-------|---------|---------|---------|----------|---------|---------|---------|----------|----------|----------|----------|----------|----------|----------|----------|----------|
| SiO2 | 52.22 | 51.64 | 52.31 | 51.52 | 36.74 | 36.18 | 36.53 | 51.86 | 43.06 | 36.65 | 36.72 | 50.02 | 50.93 | 52.41 | 52.44 | 51.53 |
| Al2O3 | 2.31 | 1.75 | 1.71 | 2.56 | 14.70 | 14.48 | 14.42 | 1.51 | 11.12 | 14.31 | 14.57 | 3.21 | 3.26 | 1.88 | 1.50 | 1.63 |
| TiO2 | 0.34 | 0.20 | 0.22 | 0.68 | 7.21 | 6.56 | 6.23 | 0.15 | 3.84 | 3.99 | 6.41 | 0.80 | 0.68 | 0.40 | 0.08 | 0.23 |
| Cr2O3 | 0.00 | 0.00 | 0.00 | 0.14 | 0.00 | 0.00 | 0.00 | 0.00 | 0.01 | 0.00 | 0.00 | 0.20 | 0.12 | 0.05 | 0.00 | 0.01 |
| FeO | 17.81 | 17.90 | 18.91 | 9.16 | 22.01 | 23.88 | 23.95 | 21.00 | 13.48 | 23.70 | 22.44 | 9.79 | 13.22 | 13.82 | 18.22 | 18.95 |
| MnO | 0.50 | 0.58 | 0.72 | 0.08 | 0.11 | 0.17 | 0.13 | 0.72 | 0.20 | 0.23 | 0.17 | 0.30 | 0.42 | 0.45 | 0.58 | 0.61 |
| MgO | 24.88 | 24.66 | 24.36 | 16.20 | 10.17 | 9.31 | 9.28 | 23.28 | 13.56 | 9.53 | 10.23 | 14.94 | 19.01 | 21.91 | 24.58 | 24.64 |
| CaO | 1.83 | 3.04 | 1.43 | 19.61 | 0.00 | 0.00 | 0.00 | 1.23 | 11.15 | 0.00 | 0.00 | 19.53 | 11.26 | 9.04 | 1.27 | 1.34 |
| Na2O | 0.11 | 0.22 | 0.14 | 0.00 | 0.05 | 0.02 | 0.00 | 0.27 | 2.56 | 0.00 | 0.01 | 0.08 | 0.24 | 0.02 | 0.03 | 0.04 |
| K2O | 0.00 | 0.00 | 0.00 | 0.05 | 9.01 | 9.39 | 9.46 | 0.00 | 1.02 | 9.59 | 9.44 | 0.07 | 0.06 | 0.03 | 0.00 | 0.00 |
| phase | opx | opx | opx | cpx | biotite | biotite | biotite | opx | bblda | biotite | biotite | cpx | cpx | cpx | opx | opx |
| comp | En69 | En67 | En68 | 40,46,14 | Fe55 | Fe59 | Fe59 | En65 | 28,46,26 | Fe58 | Fe55 | 41,43,16 | 23,56,21 | 18,61,21 | En67 | En68 |

| | Heg-R42 | Fao-Rhy4 | Fao-Rhy4 | Fao-Rhy4 | Fao-Rhy4 | Fao-Dac6 | Fao-Dac6 | Fao-Dac6 |
|-------|---------|---------|---------|---------|---------|---------|----------|----------|----------|----------|----------|----------|----------|----------|
| SiO2 | 55.63 | 55.09 | 36.68 | 61.98 | 56.23 | 36.65 | 60.08 | 57.67 | 56.84 | 58.55 | 56.54 | 57.99 | 55.10 | |
| Al2O3 | 27.84 | 27.98 | 27.29 | 23.57 | 27.43 | 27.29 | 24.77 | 26.59 | 27.15 | 25.84 | 27.12 | 26.19 | 27.91 | |
| TiO2 | 0.00 | 0.00 | 0.01 | 0.03 | 0.00 | 0.01 | 0.09 | 0.00 | 0.02 | 0.09 | 0.00 | 0.03 | 0.01 | |
| Cr2O3 | 0.13 | 0.08 | 0.05 | 0.05 | 0.08 | 0.05 | 0.01 | 0.11 | 0.10 | 0.09 | 0.01 | 0.07 | 0.11 | |
| FeO | 0.47 | 0.53 | 0.44 | 0.15 | 0.43 | 0.41 | 0.27 | 0.36 | 0.37 | 0.34 | 0.45 | 0.32 | 0.49 | |
| MnO | 0.00 | 0.00 | 0.00 | 0.00 | 0.00 | 0.00 | 0.00 | 0.00 | 0.00 | 0.00 | 0.00 | 0.00 | 0.00 | |
| MgO | 0.03 | 0.01 | 0.01 | 0.00 | 0.00 | 0.00 | 0.04 | 0.00 | 0.02 | 0.09 | 0.08 | 0.08 | 0.12 | |
| CaO | 10.08 | 10.48 | 9.38 | 4.93 | 9.79 | 9.39 | 4.49 | 8.23 | 8.99 | 7.62 | 9.30 | 8.14 | 10.58 | |
| Na2O | 5.30 | 5.22 | 5.56 | 8.01 | 5.50 | 5.57 | 7.21 | 5.89 | 5.63 | 6.52 | 5.93 | 6.44 | 5.12 | |
| K2O | 0.52 | 0.62 | 0.58 | 1.29 | 0.55 | 0.62 | 1.05 | 0.65 | 0.68 | 0.83 | 0.60 | 0.74 | 0.56 | |
| phase | plag | plag | p.cuh | p.cuh | p.cuh | plag | plag,cuh | plag | plag | plag | plag | plag | plag | |
| comp | An58 | An51 | An47 | An26 | An48 | An46 | An31 | An43 | An46 | An37 | An45 | An29 | An52 | |

MLI rhyolites

| | Fao-Rhy3 | |
|-------|----------|----------|----------|----------|----------|----------|----------|----------|----------|----------|----------|----------|----------|----------|-------|
| SiO2 | 52.25 | 38.14 | 36.60 | 36.43 | 36.38 | 36.67 | 36.67 | 40.30 | 61.60 | 61.23 | 61.88 | 62.23 | 61.37 | 61.44 | 59.72 |
| Al2O3 | 1.39 | 15.00 | 14.34 | 14.03 | 14.14 | 14.84 | 15.05 | 24.64 | 23.90 | 24.16 | 23.89 | 23.59 | 24.05 | 23.97 | 23.33 |
| TiO2 | 0.19 | 6.34 | 6.40 | 6.03 | 6.08 | 6.79 | 6.68 | 0.05 | 0.00 | 0.00 | 0.00 | 0.01 | 0.00 | 0.00 | 0.02 |
| Cr2O3 | 0.08 | 0.00 | 0.00 | 0.00 | 0.00 | 0.00 | 0.00 | 0.06 | 0.00 | 0.09 | 0.02 | 0.00 | 0.02 | 0.08 | 0.03 |
| FeO | 20.16 | 14.68 | 23.97 | 25.74 | 25.69 | 21.50 | 20.89 | 0.41 | 0.12 | 0.20 | 0.23 | 0.16 | 0.15 | 0.26 | 0.14 |
| MnO | 0.74 | 0.00 | 0.19 | 0.17 | 0.22 | 0.05 | 0.05 | 0.00 | 0.00 | 0.00 | 0.00 | 0.00 | 0.00 | 0.00 | 0.00 |
| MgO | 23.86 | 16.04 | 9.24 | 8.03 | 7.92 | 10.84 | 11.29 | 0.00 | 0.00 | 0.00 | 0.00 | 0.00 | 0.00 | 0.00 | 0.00 |
| CaO | 1.21 | 0.00 | 0.00 | 0.00 | 0.00 | 0.00 | 0.00 | 6.75 | 3.09 | 5.74 | 4.98 | 4.82 | 5.43 | 5.40 | 6.77 |
| Na2O | 0.00 | 0.27 | 0.00 | 0.00 | 0.00 | 0.20 | 0.20 | 6.40 | 8.00 | 7.76 | 7.83 | 7.79 | 7.72 | 7.68 | 7.04 |
| K2O | 0.00 | 9.51 | 9.28 | 9.54 | 9.56 | 9.31 | 9.17 | 1.33 | 1.29 | 1.32 | 1.37 | 1.40 | 1.26 | 1.23 | 0.95 |
| phase | opx | biotite | biotite | biotite | biotite | biotite | biotite | plag | plag |
| comp | En66 | Fe736 | Fe59 | Fe64 | Fe65 | Fe53 | Fe51 | An33 | An24 | An25 | An24 | An23 | An26 | An26 | An33 |

table2
(cont'd)

| | M-27-1 | M-30-1 | M-17-1 | M-28-1 |
|-------|----------|----------|----------|----------|
| SiO2 | 42.96 | 42.93 | 41.59 | 41.93 |
| Al2O3 | 7.93 | 8.38 | 8.75 | 9.12 |
| TiO2 | 1.57 | 1.87 | 1.92 | 1.91 |
| Cr2O3 | 0.04 | 0.13 | 0.01 | 0.00 |
| FeO | 31.06 | 29.21 | 29.17 | 28.44 |
| MnO | 0.90 | 0.87 | 0.80 | 0.78 |
| MgO | 3.10 | 3.97 | 4.52 | 3.75 |
| CaO | 9.87 | 10.23 | 9.75 | 9.83 |
| Na2O | 1.64 | 1.34 | 1.46 | 2.27 |
| K2O | 0.92 | 1.06 | 1.04 | 0.98 |
| phase | hb1de | hb1de | hb1de | hb1de |
| comp | 26,11,63 | 27,14,59 | 15,16,59 | 26,14,60 |

| | M-14-1 | M-14-1 | M-18-1 | M-18-1 |
|-------|----------|----------|----------|----------|
| SiO2 | 42.18 | 41.92 | 42.16 | 42.96 |
| Al2O3 | 8.56 | 8.92 | 8.90 | 8.80 |
| TiO2 | 1.99 | 1.97 | 1.93 | 1.69 |
| Cr2O3 | 0.04 | 0.00 | 0.04 | 0.01 |
| FeO | 28.47 | 28.34 | 27.99 | 27.72 |
| MnO | 0.78 | 0.71 | 0.72 | 0.77 |
| MgO | 5.10 | 3.13 | 5.03 | 5.10 |
| CaO | 9.86 | 10.00 | 10.06 | 9.77 |
| Na2O | 2.04 | 1.90 | 2.16 | 2.25 |
| K2O | 0.98 | 1.08 | 1.01 | 0.93 |
| phase | hb1de | hb1de | hb1de | hb1de |
| comp | 18,57,25 | 18,56,26 | 18,56,26 | 19,56,25 |

| | M-11-1 | M-24-1 |
|-------|----------|----------|
| SiO2 | 43.21 | 43.02 |
| Al2O3 | 8.36 | 9.12 |
| TiO2 | 1.14 | 1.40 |
| Cr2O3 | 0.13 | 0.02 |
| FeO | 30.45 | 28.13 |
| MnO | 0.96 | 0.82 |
| MgO | 3.45 | 5.84 |
| CaO | 9.99 | 10.19 |
| Na2O | 1.37 | 2.71 |
| K2O | 0.93 | 1.04 |
| phase | hb1de | hb,core |
| comp | 13,59,28 | 21,53,28 |

| | M-16-1 | M-20-2 | M-25-2 | M-27-2 |
|-------|--------|--------|--------|--------|
| SiO2 | 61.60 | 64.60 | 64.61 | 64.67 |
| Al2O3 | 22.57 | 21.96 | 21.87 | 21.83 |
| FeO | 0.08 | 0.07 | 0.01 | 0.13 |
| CaO | 3.57 | 3.10 | 2.80 | 2.75 |
| Na2O | 8.83 | 8.91 | 9.22 | 9.13 |
| K2O | 1.24 | 1.35 | 1.49 | 1.46 |
| phase | plag | plag | plag | plag |
| comp | Ab75 | Ab77 | Ab77 | Ab79 |

| | M-14-1 | M-14-1 | M-18-1 | M-18-1 |
|-------|--------|--------|--------|--------|
| SiO2 | 64.11 | 63.82 | 63.52 | 63.19 |
| Al2O3 | 22.12 | 22.16 | 22.78 | 22.97 |
| FeO | 0.00 | 0.02 | 0.06 | 0.05 |
| CaO | 3.23 | 3.19 | 3.28 | 3.65 |
| Na2O | 9.05 | 9.22 | 9.14 | 9.02 |
| K2O | 1.33 | 1.35 | 1.22 | 1.12 |
| phase | plag | plag | plag | plag |
| comp | Ab77 | Ab78 | Ab78 | Ab77 |

| | M-11-1 | M-24-1 | M-19-1 |
|-------|--------|--------|--------|
| SiO2 | 64.51 | 62.68 | 60.82 |
| Al2O3 | 21.99 | 23.47 | 24.63 |
| FeO | .13 | 0.03 | 0.04 |
| CaO | 2.26 | 4.13 | 3.05 |
| Na2O | 8.84 | 8.63 | 10.49 |
| K2O | 1.12 | 1.02 | 0.97 |
| phase | plag | plag | plag |
| comp | Ab78 | Ab74 | Ab81 |

| | M-30-1 | M-17-1 | M-28-1 | M-29-1 |
|-------|--------|--------|--------|--------|
| SiO2 | 66.30 | 66.23 | 65.80 | 66.05 |
| Al2O3 | 19.16 | 18.79 | 19.62 | 19.62 |
| FeO | 0.03 | 0.00 | 0.00 | 0.00 |
| CaO | 0.15 | 0.11 | 0.15 | 0.24 |
| Na2O | 2.85 | 3.27 | 3.28 | 2.90 |
| K2O | 11.50 | 11.47 | 11.14 | 11.17 |
| phase | sanid | sanid | sanid | sanid |
| comp | Or72 | Or69 | Or68 | Or71 |

| | M-14-1 | M-14-1 | M-18-1 | M-18-1 |
|-------|--------|--------|--------|--------|
| SiO2 | 66.06 | 66.17 | 65.91 | 64.66 |
| Al2O3 | 19.37 | 19.37 | 19.50 | 19.39 |
| FeO | 0.00 | 0.00 | 0.00 | 0.00 |
| CaO | 0.24 | 0.21 | 0.26 | 0.14 |
| Na2O | 3.37 | 3.27 | 3.35 | 3.45 |
| K2O | 10.95 | 10.99 | 10.97 | 10.62 |
| phase | sanid | sanid | sanid | sanid |
| comp | Or67 | Or68 | Or68 | Or66 |

| | M-11-1 | M-24-1 | M-19-1 |
|-------|--------|--------|--------|
| SiO2 | 66.10 | 64.96 | 65.01 |
| Al2O3 | 18.74 | 21.14 | 20.97 |
| FeO | .03 | 0.00 | 0.00 |
| CaO | 0.11 | 1.30 | 1.35 |
| Na2O | 2.94 | 3.20 | 2.98 |
| K2O | 12.10 | 9.40 | 9.68 |
| phase | sanid | sanid | sanid |
| comp | Or73 | Or61 | Or63 |

| | M-20-2 | M-27-2 | M-17-1 | M-28-1 |
|-------|---------|---------|---------|---------|
| SiO2 | 30.59 | 30.85 | 30.28 | 30.12 |
| Al2O3 | 0.41 | 0.34 | 0.00 | 0.00 |
| Cr2O3 | 0.04 | 0.00 | 0.07 | 0.08 |
| FeO | 62.82 | 62.23 | 61.15 | 63.50 |
| MnO | 1.54 | 4.00 | 3.42 | 3.37 |
| MgO | 2.47 | 2.49 | 3.00 | 2.85 |
| CaO | 0.08 | 0.08 | 0.08 | 0.08 |
| phase | olivine | olivine | olivine | olivine |
| comp | Fs94 | Fs93 | Fs92 | Fs93 |

| | M-14-1 | M-14-1 | M-18-1 | M-18-1 |
|-------|--------|--------|--------|--------|
| SiO2 | 46.90 | 46.78 | 47.74 | 47.25 |
| Al2O3 | 0.93 | 0.95 | 1.20 | 1.07 |
| TiO2 | 0.07 | 0.03 | 0.00 | 0.01 |
| Cr2O3 | 0.08 | 0.00 | 0.04 | 0.00 |
| FeO | 40.81 | 41.38 | 40.55 | 40.82 |
| MnO | 2.59 | 2.65 | 2.44 | 2.66 |
| MgO | 6.96 | 6.84 | 6.40 | 6.63 |
| CaO | 1.37 | 1.34 | 1.23 | 1.26 |
| Na2O | 0.25 | 0.03 | 0.37 | 0.28 |
| K2O | 0.04 | 0.00 | 0.01 | 0.00 |
| phase | opx | opx | opx | opx |
| comp | Fs77 | Fs77 | Fs78 | Fs78 |

| | M-11-1 | M-24-1 | M-19-1 |
|-------|--------|--------|--------|
| SiO2 | 34.97 | 35.67 | 36.19 |
| Al2O3 | 13.47 | 14.03 | 14.34 |
| TiO2 | 4.29 | 4.89 | 5.31 |
| Cr2O3 | 0.00 | 0.08 | 0.00 |
| FeO | 32.94 | 29.72 | 27.83 |
| MnO | 0.42 | 0.38 | 0.19 |
| MgO | 4.28 | 5.87 | 7.17 |
| CaO | 0.00 | 0.10 | 0.06 |
| Na2O | 0.39 | 0.13 | 0.06 |
| K2O | 9.26 | 9.19 | 9.44 |
| phase | biot. | biot. | biot. |
| comp | Fs781 | Fs774 | Fs768 |

Table 2:

Summarized microanalyses of phenocryst phases in MC-MLI volcanic rocks. Analyses were done at UCSC using an EDS (PGT Systems4) equipped scanning electron microscope. Analytical uncertainty is 5% relative for all elements except Na which is 10%. Compositions are reported in mol% for all phases. Iron is assumed as 100% Fe²⁺. Pyroxene is reported as mol% Wo, En, Fs in that order; hornblende as 100 mol% Ca, Mg, Fe. Fe-rich orthopyroxene, fayalite, and biotite as Fe/Fe+MgO x 100; olivine and Mg-rich orthopyroxene as Mg/Mg + Fe (total) x 100; and feldspars as mol% An, Ab or Or. Definition of phases: ol = olivine; cpx = clinopyroxene; opx = orthopyroxene; hblde = hornblende; plag, pl, or p = plagioclase; cr = core; oc = outer core; rm = rim; meg = megacryst; hs = host; in or inc = inclusion; euh = euhedral; sieve = sieve textured.

The basaltic inclusions have euhedral clinopyroxene phenocrysts with homogeneous compositions (Wo40-43, En40-44, Fs14-18, fig. 5, table 2). Olivine phenocrysts are also compositionally uniform (Fo85-Fo75, fig. 5). Two populations of plagioclase occur in the basaltic inclusions, normally zoned megacrysts (An68-An58) up to 2.5 cm. in length, and 1-2mm euhedral laths (An63-An59, fig. 6, table 2). Although the inclusions do not show signs of contamination, there is clear evidence that they have intimately mixed and reacted with the host dacite. The inclusions have coarse reaction margins up to 3mm, crenulated contacts, and re-entrants of host magma; quench textured dendritic magnetite and acicular groundmass hornblende are ubiquitous (fig. 4e-h). These textures indicate that the inclusions were incorporated into the dacite as fragments of molten material. Furthermore, isolated clinopyroxene and olivine crystals with coarse reaction rims of hornblende, and disaggregating basaltic clots are common constituents within the dacite host (fig. 4h).

Similar textures between hosts and their inclusions have been described at the Coso volcanic field (Bacon and Metz, 1984) and other localities (Bacon, 1986).

The andesitic inclusions in the two HSR domes have unambiguous mixing textures. All of the primary phenocryst phases are resorbed or sieve textured. Olivine is uniform in composition (Fo80) and commonly has fine grained Fe-oxide reaction rims. Plagioclase phenocrysts are texturally and compositionally diverse ranging from An63 to An14 (fig.

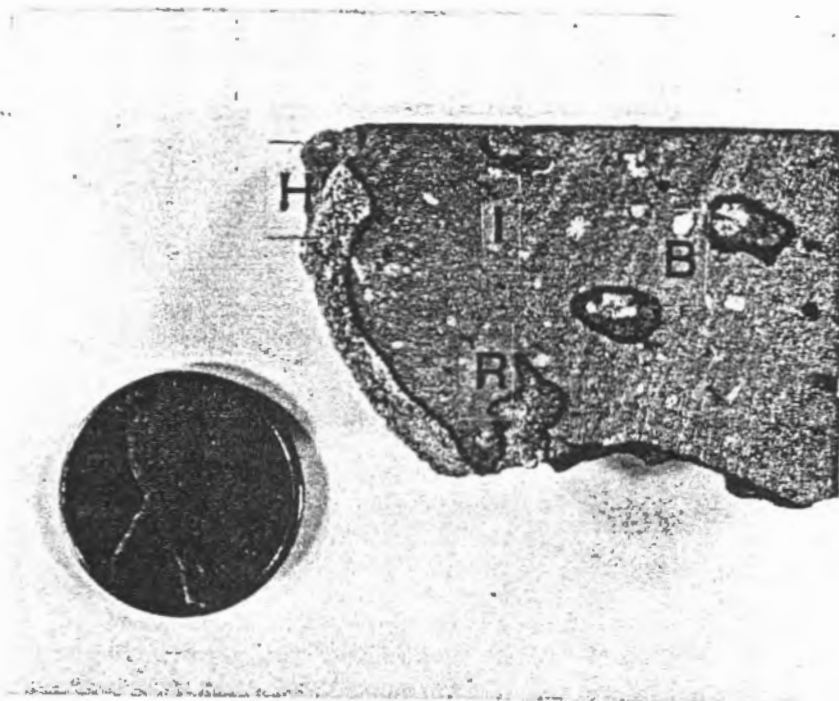
6). Orthopyroxene crystals in the inclusions are sub- to anhedral, up to 3mm in length, and have reaction rims of granular Fe-oxides, hornblende, and pyroxene(?) (fig. 4c). They are Fe-rich (Fs77-65), and clearly out of equilibrium with the Mg-rich olivines (fig. 5). Quartz and sanidine xenocrysts up to 3mm in length are also common (fig. 4d). The groundmass of the andesitic inclusions have abundant needles of hornblende and apatite. Sharp, crenulated contacts with HSR host, occasional reentrants of host lava, and disaggregating microscopic clots in the HSR host, are also common textures. The andesitic inclusions also contain ≤ 7 mm sized, rounded, inclusions of more mafic(?) rock. In hand specimen, these smaller inclusions are reddish brown colored, fine grained, and vesicular (fig. 4a). In thin section, they are plagioclase and olivine phyric; the groundmass is predominantly composed of dendritic magnetite and minor, acicular hornblende. These observations indicate that the andesitic inclusions themselves are mixed, and were incorporated into the HSR while still partially molten.

Silicic Rocks

Modal abundances and mineral analyses of the silicic rocks are summarized in table 2 and figures 5 and 6. All of the lavas are glassy, sparsely porphyritic, and, except for the MC dacite, lack the mixing relationships found in the mafic portion of the suite.

The MC dacite is plagioclase, hornblende, and clinopyroxene(?) phyric with crystals averaging 1mm. Plagioclase (An56-60), is

a



— .6 mm

b

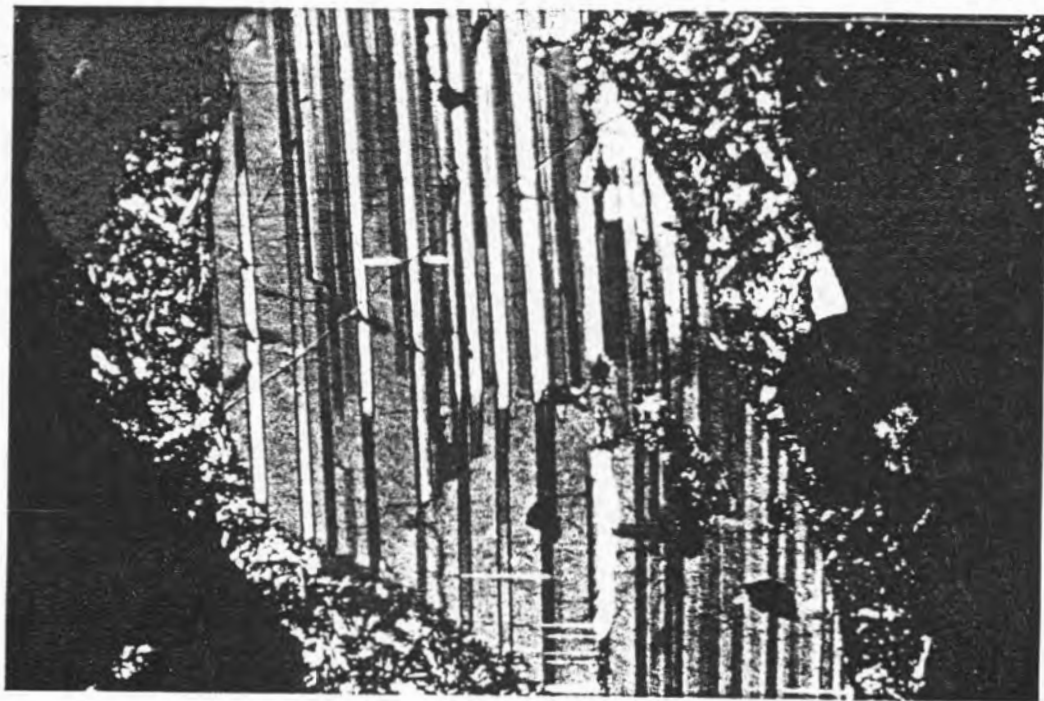


Figure 4 a,b:

(a): Rock chip of a typical andesitic inclusion (I) in the orthopyroxene-bearing HSR domes (H). Note the sharp host/inclusion contact, and re-entrant of host lava (R). Two rounded, mafic inclusions (B) are outlined. See text for discussion.

(b): Typical anhedral, resorbed labradorite phenocryst (P) in andesitic inclusions. Crossed nichols, magnification x80.

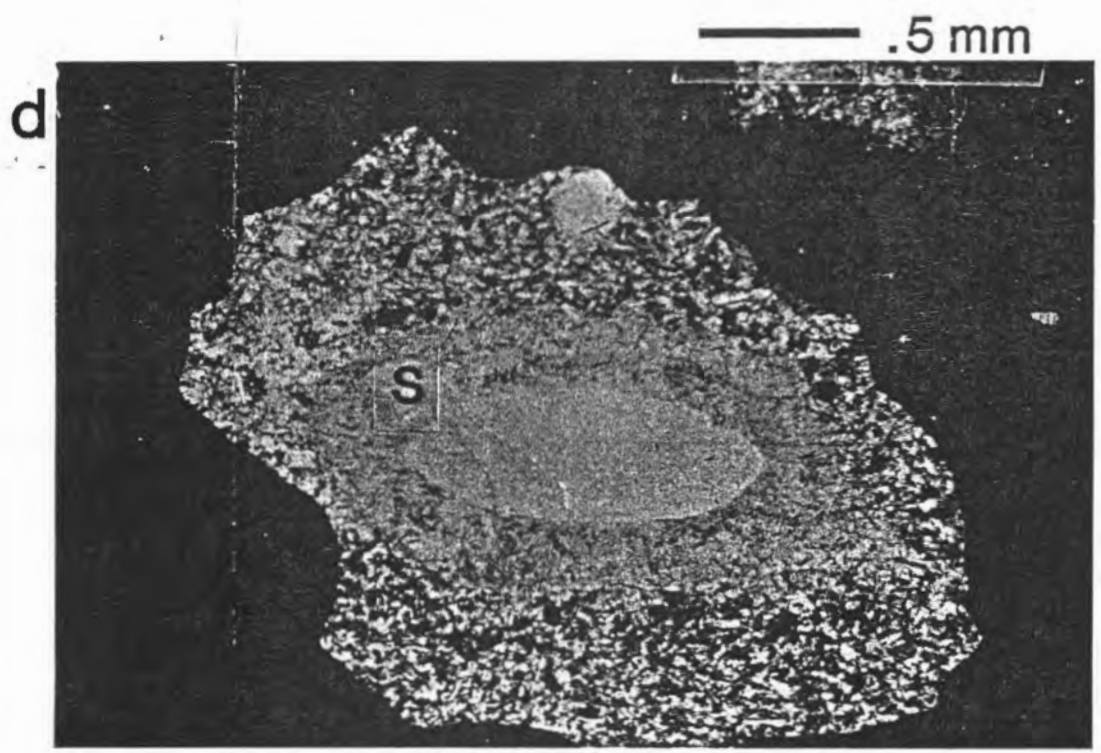
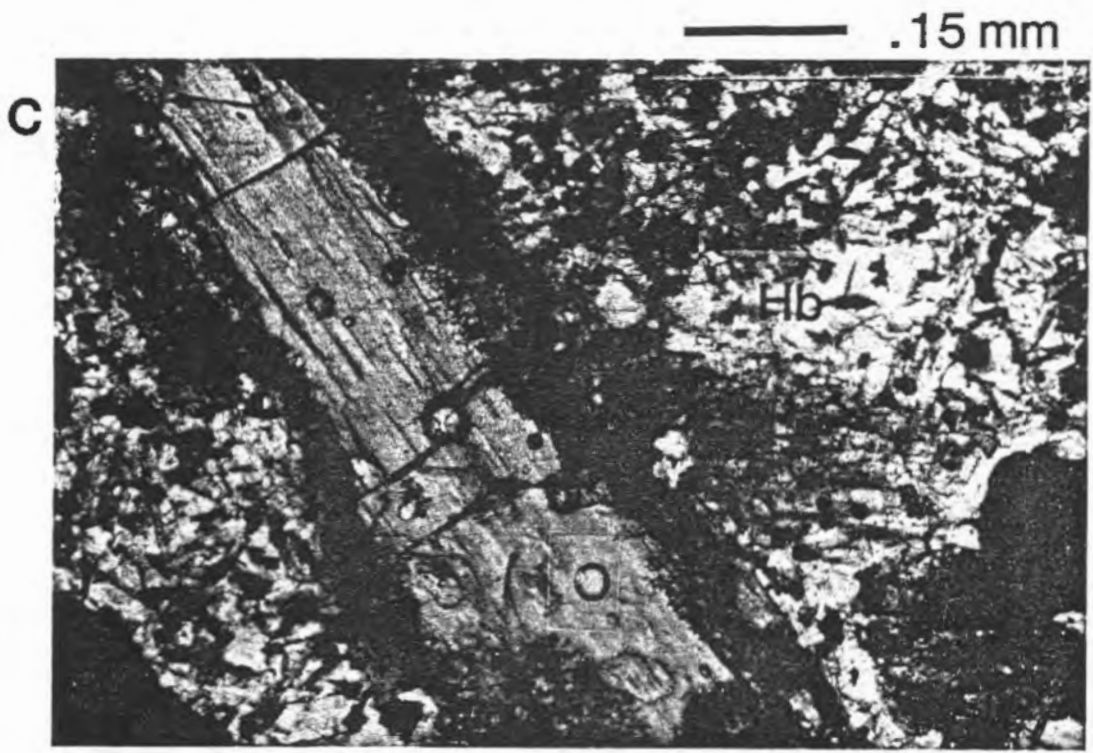
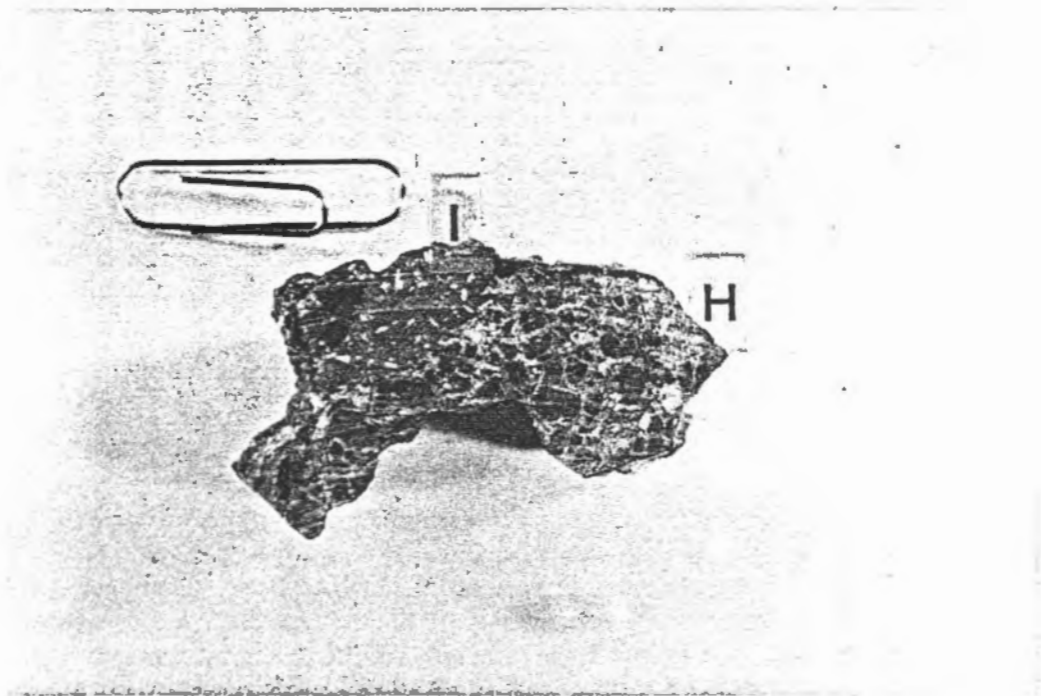


Figure 4 c,d:

(c): Resorbed orthopyroxene (Fs 73) phenocryst (O) in andesitic inclusion. Note the coarse reaction rim and dendritic magnetite. The groundmass of the inclusions are invariably rich in acicular hornblende (e.g. above and to the right of (Hb)) and dendritic magnetite. Plane polarized light, magnification: x80.

(d): Sanidine xenocryst (S) in groundmass of inclusion. Note the coarse reaction corona. Plane polarized light, magnification: x80.

e



— .5 mm

f

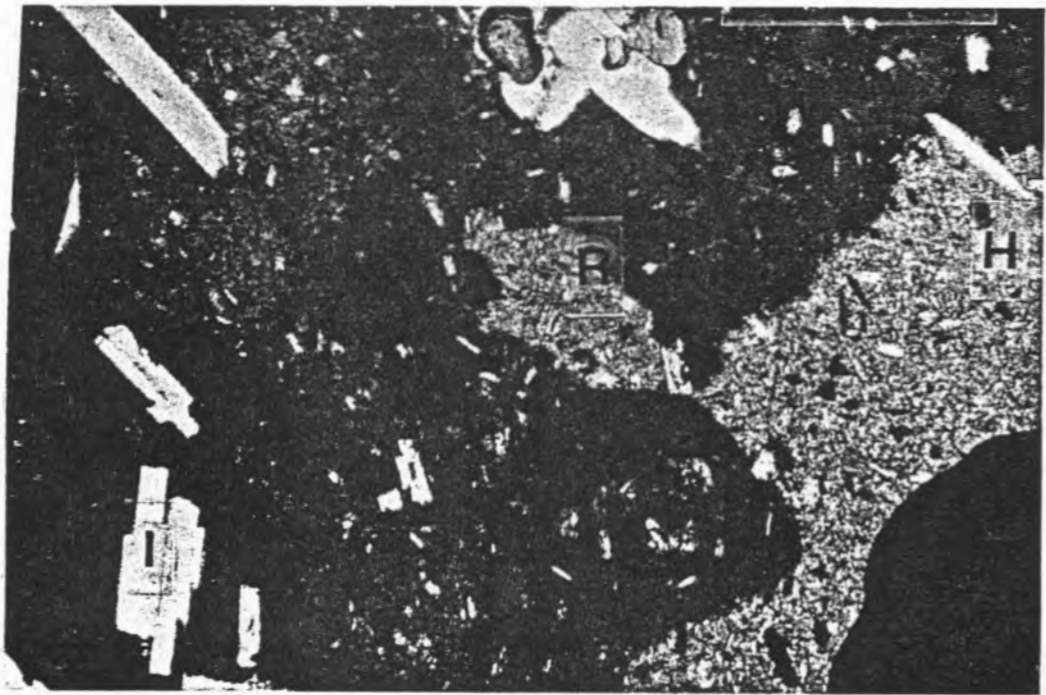


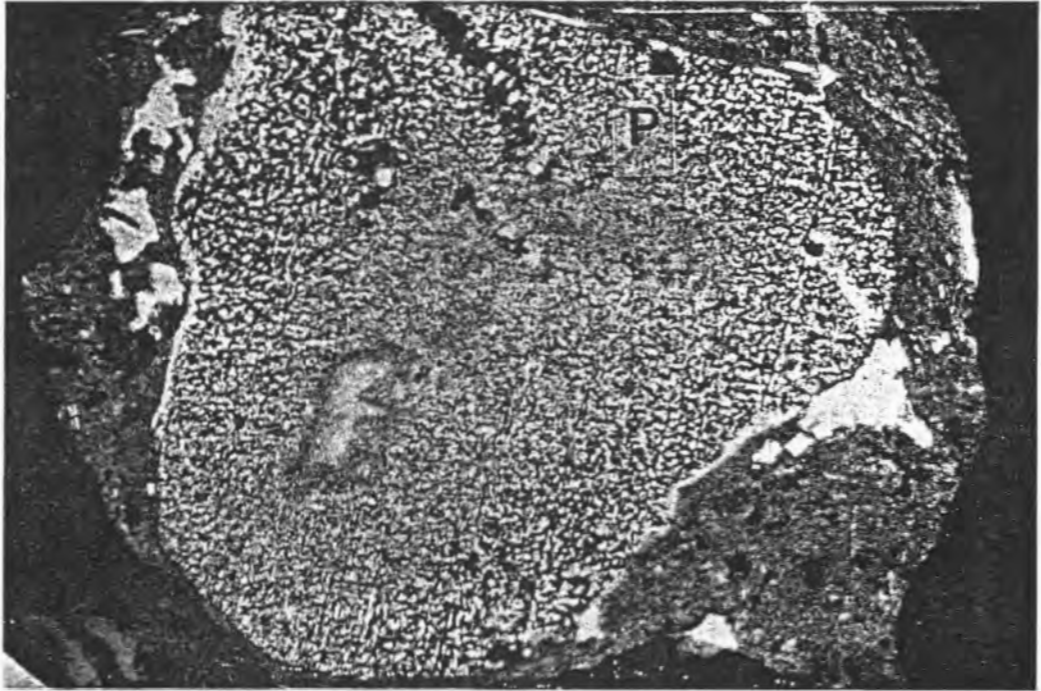
Figure 4 e,f:

(e): Cross section of MC dacite hand specimen (H) and rounded, basaltic inclusion (I). Note the perlitic cracks in the dacite and crenulated contacts with the inclusion.

(f): Photomicrograph (plane polarized light) showing typical inclusion (I, left side of photo)/ host (H, right side of photo) contact. Coarse reaction margin and re-entrant of dacite host (R) are in center. Magnification, x17.

g

— .5 mm



h

— .5 mm

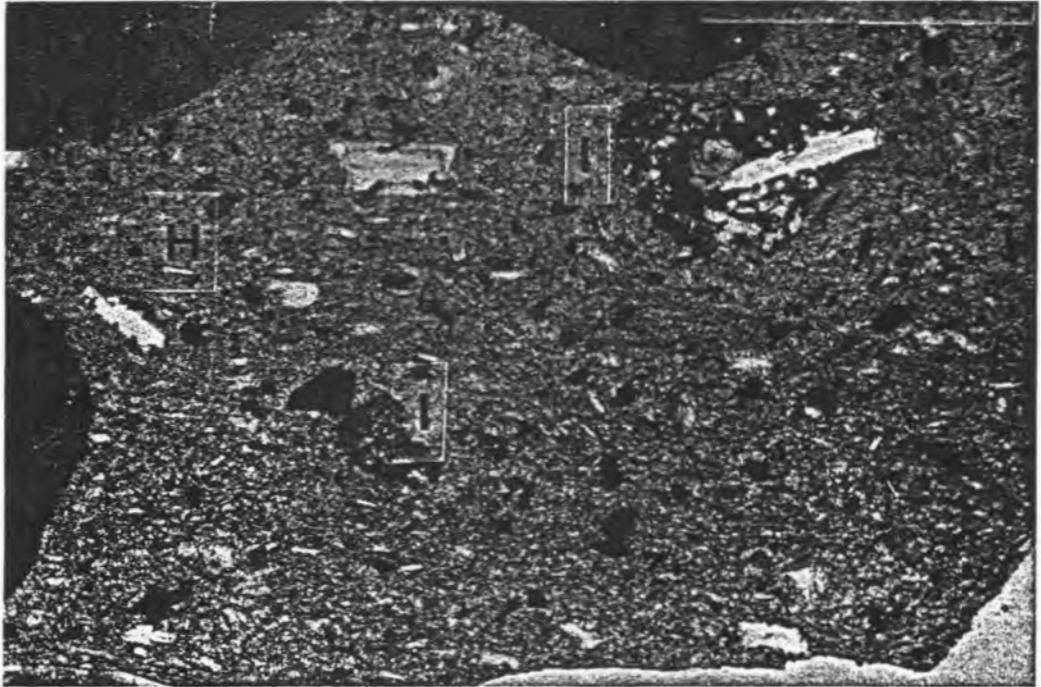


Figure 4 g,h:

(g): Sieve textured andesine xenocryst (P) in the MC dacite. Planepolarized light, magnification, x80.

(h): Microscopic basaltic inclusions (I, left center and upper right) in MC dacite host (H). The larger inclusion is disaggregating (plane polarized light, magnification, x80).

typically eu- to subhedral, although sparse, distinctly more sodic rich (An43-An29), sieve textured feldspars also occur (fig. 4g). The hornblende phenocrysts are euhedral, homogeneous, and slightly Ti and alkali rich (table 2, fig. 5). Clinopyroxene in the dacite is euhedral and occasionally clusters with euhedral plagioclase (An60-An50) and magnetite. The clinopyroxene is chemically similar to clinopyroxene xenocrysts from the disaggregating basaltic inclusions but lacks hornblende reaction rims.

The Mono Lake Islands dacites and rhyolites are sparsely porphyritic to nearly aphyric; crystals are less than 10% by volume and average .5mm (table 1). All phenocryst assemblages are dominated by plagioclase with variable textures and compositions. The plagioclase crystals in the dacites have more calcic compositions (An52-37), and are more commonly fritted and charged with brown glass inclusions than those in the rhyolite (An33-20, fig. 6). Euhedral, occasionally skeletal, orthopyroxene and clinopyroxene phenocrysts are present in all of the dacites and rare in the rhyolites. Orthopyroxene predominates over clinopyroxene and is chemically uniform (En67-65). EDS data indicates that clinopyroxene is also homogeneous (table 2), although two spongy textured, subcalcic clinopyroxene grains were analyzed. Hornblende appears as the dominant mafic phase in most of the MLI dacites except for the flow on Paoha island where it is conspicuously absent. Hornblende is a minor phenocryst phase in the MLI rhyolites. Biotite phenocrysts are present but sparse in the MLI dacites and

predominates as the mafic phase in the rhyolites. Biotite compositions are somewhat variable in the rhyolites; in general, they have intermediate to Fe rich contents (Annite 51- 65) and are Ti rich (5-7 wt.%, table 2). Apatite is a minor but ubiquitous accessory phase in both the dacites and rhyolites; zircon was found petrographically, only in the rhyolites.

The porphyritic facies HSR lavas of the Mono Craters contain 3-8% phenocrysts of predominantly ($\geq 85\%$), albitic plagioclase (An12- 20), sanidine, (Or57-74) and quartz. Hornblende is always present in minor amounts, and magnetite, apatite, and zircon are ubiquitous accessory phases; ilmenite is rare (table 1, Carmichael, 1967). Petrographic analysis of heavy mineral separates indicate that the LREE enriched mineral allanite is also present in all porphyritic domes except M-19, which is biotite-bearing. In the orthopyroxene-bearing domes, allanite crystals reach 1mm in length. Fayalitic olivine (Fa93), and orthopyroxene (En77-74), have homogeneous, Mn rich compositions (table 2, fig. 5). Annite contents in the biotite phenocrysts increase systematically with decreasing Sr concentration, a useful measure of differentiation, concentrations in the three biotite-bearing domes from: annite 68 in M-19, through annite 74 in M-24, to annite 81 in M-11. In addition, the biotite bearing domes show subtle distinctions in their petrographic modes and mineral chemistries. 1) Sanidine from M-19 and M-24 has higher molar calcium (An10, fig. 6) than M-11 or any of the other porphyritic facies lavas,

2) In the least differentiated dome, M-19, hornblende is rare. 3) In the second least differentiated dome, M-24, hornblendes are more Mg-rich than the other porphyritic facies domes (fig. 5, table 2).

The sparsely porphyritic facies domes contain <3%, and usually <1%, phenocrysts. Heavy mineral concentrates from these five domes produced assemblages identical to the fayalite-bearing porphyritic facies domes. The most crystal rich (3%), sparsely porphyritic dome, M-16, has hornblende compositions that are distinct from the fayalite-bearing lavas and is also chemically unique (see below).

The seven aphyric lavas have occasional, 1mm sized, subhedral feldspar crystals in 25 m² of outcrop area. Vapor phase(?), felsic spherulites with iddingsitized fayalite(?) and hematite(?) also occur, and are concentrated within dense obsidian bands of the aphyric domes.

Major elements

Major element analyses of the MC-MLI volcanic rocks are presented in table 3 and summarized on silica variation diagrams in figure 7a. The basaltic lavas of the complex are slightly alkalic and have high Al₂O₃ (17.5-18.5 %), TiO₂ (1-2.1%), and alkali contents (avg. Na₂O + K₂O 5.5%); moderate FeO*/MgO ratios (1.4-2.1); and low CaO/Al₂O₃ ratios (.44-.48). Major element compositions are similar to alkali olivine basalts from other volcanic centers within the Sierra Nevada Province (e.g. Van Kooten, 1983, Bacon and Metz, 1984), and average late Cenozoic alkali olivine basalts of the Basin

Table 3. Major and Trace Element Analyses
 HC-MLI Volcanic Complex

| Sample | BP83-1 | JLB-1 | M12-1B | M12-2B | M14-1B | M18-1B | M12-1A | M12-2A | Neg-RD1 | Neg-RD2 | Neg-RD3 | Neg-RD4 | MLI-1 | Pao1 | Pao2 | Pao3 | Pao4 | Pao5 | Pao6 | Pao7 | |
|--------------------------------|-------------|-----------|--------|--------|--------|--------|-------------|-------------|---------|---------|---------|---------|---------|---------|---------|---------|---------|---------|---------|---------|---------|
| Rock Type | Black Point | Juna Lake | incl. | incl. | incl. | incl. | HC dac dome | HC dac dome | MLI dac | MLI rhy | MLI dac | MLI rhy | MLI rhy | MLI rhy | MLI rhy | MLI dac | MLI rhy |
| SiO ₂ (wt.%) | 50.44 | 53.56 | 54.59 | 52.60 | 57.85 | 61.73 | 66.67 | 68.26 | 64.44 | 64.96 | 65.36 | 69.35 | 67.60 | 70.31 | 65.14 | 71.73 | 67.96 | 72.00 | 64.07 | 69.79 | |
| TiO ₂ | 1.49 | 1.48 | .94 | 2.08 | 1.49 | 1.20 | .84 | .78 | .88 | .81 | .79 | .32 | .55 | .29 | .87 | .20 | .55 | .19 | .95 | .24 | |
| Al ₂ O ₃ | 18.41 | 18.19 | 17.46 | 17.48 | 15.87 | 15.31 | 14.86 | 14.35 | 16.56 | 16.71 | 16.54 | 15.32 | 16.00 | 15.59 | 16.39 | 15.01 | 14.08 | 14.88 | 16.54 | 15.13 | |
| Fe ₂ O ₃ | 9.41 | 8.43 | 9.23 | 10.15 | 8.02 | 6.63 | 4.59 | 4.19 | 4.98 | 4.55 | 4.52 | 2.72 | 3.57 | 2.72 | 4.67 | 2.27 | 3.34 | 2.21 | 4.95 | 2.51 | |
| HgO | 5.86 | 3.90 | 4.47 | 4.25 | 4.04 | 3.01 | 1.99 | 1.65 | 1.44 | 1.37 | 1.24 | .49 | .77 | .20 | 1.07 | .15 | .65 | .15 | 1.36 | .26 | |
| CaO | 8.80 | 8.27 | 7.76 | 7.64 | 5.84 | 4.82 | 3.52 | 2.99 | 3.49 | 3.31 | 3.28 | 1.88 | 2.38 | 1.45 | 3.02 | 1.02 | 1.94 | 1.00 | 3.76 | 1.45 | |
| Na ₂ O | 3.90 | 3.87 | 3.38 | 3.79 | 3.84 | 3.99 | 3.68 | 3.78 | 4.27 | 4.42 | 4.35 | 4.87 | 4.74 | 4.36 | 4.48 | 4.24 | 4.64 | 4.18 | 4.64 | 5.39 | |
| K ₂ O | 1.26 | 1.72 | 1.66 | 1.58 | 2.55 | 2.96 | 3.54 | 3.76 | 3.52 | 3.47 | 3.54 | 4.81 | 4.07 | 4.89 | 3.91 | 5.21 | 4.53 | 5.22 | 3.73 | 5.04 | |
| P ₂ O ₅ | .31 | .42 | .39 | .31 | .37 | .27 | .15 | .15 | .32 | .30 | .27 | .09 | .17 | .08 | .33 | .08 | .15 | .04 | .34 | .07 | |
| Rb (ppm) | 14.6 | 31.0 | 44.9 | 34.7 | 71.1 | 87.0 | 124.3 | 131.8 | 76.6 | 77.8 | 77.2 | 111.4 | 89.6 | 111.2 | 95.9 | 123.5 | 111.5 | 128.1 | 91.4 | 113.9 | |
| Sr | 774.4 | 945.0 | 592.2 | 642.7 | 374.0 | 308.4 | 276.9 | 234.7 | 489.4 | 497.6 | 485.2 | 213.6 | 365.1 | 197.5 | 453.0 | 110.3 | 307.1 | 104.2 | 488.2 | 150.1 | |
| Zr | 158.6 | 167.1 | 158.9 | 170.5 | 211.8 | 198.4 | 126.3 | 125.3 | 278.6 | 273.6 | 265.8 | 353.8 | 294.8 | 367.3 | 323.5 | 325.1 | 410.7 | 336.2 | 306.5 | 382.2 | |
| Hf | 11.6 | 12.5 | 17.8 | 18.5 | 22.1 | 21.4 | 22.0 | 22.2 | 15.4 | 15.6 | 14.3 | 16.9 | 14.9 | 17.6 | 20.9 | 19.3 | 21.6 | 19.4 | 20.2 | 17.2 | |
| Y | 19.1 | 19.9 | 25.4 | 25.6 | 32.1 | 30.1 | 27.1 | 26.3 | 22.5 | 21.1 | 20.1 | 20.9 | 19.3 | 20.6 | 27.4 | 23.7 | 26.5 | 24.3 | 27.5 | 21.2 | |
| Ba | 635.8 | 843.4 | 357.9 | 444.0 | 302.7 | 298.1 | 296.6 | 307.7 | 1376.1 | 1417.8 | 1416.6 | 1148.3 | 1369.0 | 1157.5 | 1355.8 | 1119.9 | 1591.5 | 1039.4 | 1356.8 | 1055.4 | |
| La | 23.9 | 32.1 | 19.5 | 21.2 | 27.2 | 31.4 | 19.8 | 16.9 | 31.8 | 31.6 | 28.8 | 54.9 | 39.4 | 53.3 | 39.8 | 59.8 | 46.3 | 59.0 | 41.3 | 56.5 | |
| Ce | 44.76 | 55.4 | 44.8 | 46.8 | 58.8 | 61.9 | 46.7 | 42.8 | 70.5 | 66.2 | 66.7 | 97.5 | 77.1 | 96.8 | 88.0 | 103.7 | 91.5 | 106.0 | 85.0 | 105.9 | |
| Nd | 22.73 | 28.3 | 22.2 | 26.9 | 28.8 | 28.7 | 18.2 | 17.6 | 30.4 | 28.4 | 28.5 | 34.2 | 29.1 | 33.2 | 39.4 | 36.6 | 39.0 | 37.1 | 49.6 | 34.8 | |
| Sc | 21.0 | 20.6 | 19.3 | 18.0 | 14.5 | 12.2 | 8.5 | 7.6 | 8.0 | 7.5 | 7.6 | 4.9 | 5.3 | 3.9 | 8.0 | 3.9 | 6.7 | 3.9 | 8.4 | 3.9 | |
| V | 188.5 | 202.3 | 197.2 | 195.5 | 135.8 | 110.6 | 81.6 | 68.8 | 55.3 | 46.9 | 44.9 | 7.8 | 22.7 | 5.7 | 32.2 | 2.8 | 11.0 | 2.1 | 39.2 | 3.2 | |
| Ni | 55.9 | 15.8 | 27.0 | 21.1 | 35.2 | 29.8 | 15.2 | 11.6 | 3.3 | 24.6 | 3.9 | 6.0 | 4.1 | 5.3 | 3.1 | 6.0 | 3.7 | 5.3 | 3.5 | 5.9 | |
| Cr | 20.9 | 29.2 | 18.9 | 9.8 | 39.0 | 26.2 | 14.1 | 9.7 | 2.1 | 2.6 | 4.2 | 3.7 | 1.7 | 5.1 | 3.1 | 5.3 | 1.3 | 5.0 | 2.0 | 3.6 | |

Table 3 cont'd.

| Sample | M3-1 | M4-2 | M5-1 | M6-1 | M7-2 | M8-3 | M9-2 | M10-1 | M13-2 | M15-2 | M16-1 | M17-2 | M20-1 | M21-1 | M22-1 | M23-1 | M25-1 | M26-1 | M27-1 | M28-1 |
|--------------------------------|-------|-------|-------|-------|-------|-------|-------|-------|-------|-------|-------|-------|-------|-------|-------|-------|-------|-------|-------|-------|
| Rock Type | A | A | A | Ol | Sp | Sp | A | A | A | ol | sp | ol | ol | sp | A | Sp | ol | Sp | ol | ol |
| SiO ₂ | 76.44 | 76.30 | 76.34 | 76.36 | 76.88 | 76.64 | 76.89 | 76.82 | 76.49 | 76.43 | 76.50 | 76.45 | 76.21 | 76.45 | 76.21 | 76.42 | 76.43 | 76.26 | 76.06 | 76.32 |
| TiO ₂ | .08 | .07 | .08 | .07 | .07 | .06 | .06 | .07 | .07 | .07 | .08 | .07 | .07 | .07 | .07 | .07 | .07 | .07 | .07 | .07 |
| Al ₂ O ₃ | 12.87 | 12.80 | 12.93 | 12.97 | 12.70 | 12.64 | 12.62 | 12.63 | 12.90 | 12.84 | 12.96 | 12.92 | 12.96 | 12.92 | 12.87 | 12.94 | 12.92 | 12.87 | 12.95 | 12.90 |
| Fe ₂ O ₃ | 1.31 | 1.26 | 1.31 | 1.34 | 1.25 | 1.24 | 1.24 | 1.23 | 1.32 | 1.29 | 1.27 | 1.31 | 1.31 | 1.31 | 1.30 | 1.31 | 1.30 | 1.29 | 1.34 | 1.35 |
| MgO | .07 | .05 | .06 | .04 | .04 | .04 | .02 | .02 | .04 | .02 | .05 | .02 | .10 | .07 | .13 | .06 | .06 | .05 | .05 | .04 |
| CaO | .60 | .61 | .62 | .63 | .66 | .81 | .58 | .59 | .62 | .61 | .67 | .61 | .61 | .61 | .85 | .62 | .61 | .77 | .78 | .61 |
| Na ₂ O | 3.79 | 3.81 | 3.79 | 3.59 | 3.59 | 3.67 | 3.71 | 3.77 | 3.59 | 3.78 | 3.59 | 3.73 | 3.79 | 3.61 | 3.61 | 3.62 | 3.70 | 3.73 | 3.83 | 3.81 |
| K ₂ O | 4.75 | 4.71 | 4.77 | 4.86 | 4.74 | 4.78 | 4.75 | 4.77 | 4.81 | 4.83 | 4.77 | 4.68 | 4.79 | 4.81 | 4.79 | 4.82 | 4.77 | 4.82 | 4.80 | 4.78 |
| P ₂ O ₅ | .04 | .05 | .04 | .05 | .02 | .02 | .01 | .02 | .06 | .05 | .06 | .04 | .06 | .07 | .08 | .05 | .05 | .05 | .04 | .03 |
| Rb (ppm) | 185.2 | 183.8 | 186.6 | 187.4 | 183.8 | 184.8 | 185.8 | 184.4 | 184.0 | 190.8 | 193.5 | 184.1 | 184.8 | 189.3 | 188.0 | 188.5 | 186.3 | 187.7 | 182.7 | 181.8 |
| Sr | 6.5 | 5.5 | 6.4 | 5.7 | 5.7 | 6.7 | 6.7 | 6.4 | 6.2 | 5.6 | 11.3 | 5.3 | 6.4 | 6.5 | 6.0 | 6.6 | 6.2 | 6.3 | 6.7 | 5.4 |
| Zr | 119.0 | 117.5 | 119.9 | 122.7 | 115.8 | 117.4 | 118.2 | 117.8 | 121.3 | 124.5 | 105.9 | 117.3 | 119.7 | 121.5 | 119.1 | 118.4 | 122.7 | 119.6 | 121.5 | 120.3 |
| Nb | 25.6 | 25.1 | 24.4 | 25.2 | 24.8 | 24.7 | 24.6 | 24.4 | 25.0 | 25.3 | 24.3 | 24.4 | 24.8 | 24.9 | 24.8 | 25.2 | 25.2 | 25.2 | 24.8 | 25.0 |
| Y | 31.0 | 31.5 | 32.1 | 31.9 | 30.3 | 30.4 | 30.6 | 30.5 | 30.4 | 33.2 | 32.1 | 30.6 | 31.1 | 32.2 | 31.6 | 30.3 | 31.0 | 32.1 | 30.1 | 30.4 |
| Ba | 49.3 | 48.3 | 49.9 | 48.8 | 48.6 | 49.4 | 50.4 | 53.2 | 50.7 | 37.2 | 61.1 | 39.7 | 47.5 | 45.5 | 48.6 | 46.4 | 43.6 | 46.5 | 47.1 | 43.2 |
| La | 19.2 | 21.5 | 22.5 | 19.5 | 19.0 | 20.9 | 23.5 | 21.9 | 22.1 | 17.9 | 18.2 | 16.3 | 17.0 | 21.1 | 19.8 | 19.0 | 19.5 | 21.2 | 18.8 | 17.1 |
| Ce | 54.8 | 52.6 | 54.0 | 49.4 | 51.2 | 52.8 | 54.8 | 52.5 | 55.5 | 48.1 | 48.1 | 48.2 | 48.6 | 52.5 | 52.5 | 52.5 | 50.3 | 54.5 | 49.2 | 49.4 |
| Hf | 21.2 | 19.7 | 20.1 | 19.1 | 19.8 | 20.2 | 20.6 | 19.8 | 20.7 | 18.2 | 19.6 | 18.7 | 18.9 | 20.8 | 20.0 | 19.6 | 19.3 | 21.2 | 19.1 | 18.6 |
| V | 1.4 | .7 | 1.0 | 1.1 | 1.1 | .3 | 1.0 | .6 | 1.4 | 1.9 | 1.1 | .8 | 1.6 | 1.0 | 1.0 | .7 | .4 | 1.1 | 1.5 | .3 |

Table 3 (cont'd)

| Sample | M29-2 | M30-1 | M1-k | M22-k | M11-1 | M11-2 | M11-3 | M19-1 | M24-1 | M24-3 | M14-1A | M18-1A |
|--------------------------------|-------|-------|-------|-------|-------|-------|-------|-------|-------|-------|--------|--------|
| Rock Type | ol | ol | A | ol | bt. | bt. | bt. | bt. | bt. | bt. | opx | opx |
| SiO ₂ | 76.52 | 76.29 | 76.40 | 76.49 | 76.87 | 76.76 | 77.04 | 76.36 | 76.52 | 76.63 | 75.86 | 75.40 |
| TiO ₂ | .07 | .07 | .07 | .07 | .06 | .06 | .06 | .09 | .07 | .07 | .08 | .08 |
| Al ₂ O ₃ | 12.86 | 12.97 | 13.06 | 13.03 | 12.61 | 12.73 | 12.70 | 13.15 | 12.93 | 12.67 | 13.12 | 13.21 |
| Fe ₂ O ₃ | 1.31 | 1.30 | 1.25 | 1.23 | 1.19 | 1.22 | 1.21 | 1.15 | 1.21 | 1.15 | 1.46 | 1.44 |
| MgO | .01 | .06 | .04 | .05 | .05 | .01 | .01 | .01 | .04 | .02 | .04 | .12 |
| CaO | .61 | .64 | .62 | .60 | .63 | .64 | .61 | .74 | .72 | .86 | .65 | .91 |
| Na ₂ O | 3.80 | 3.69 | 3.73 | 3.73 | 3.77 | 3.81 | 3.61 | 3.55 | 3.52 | 3.78 | 3.61 | 3.73 |
| K ₂ O | 4.69 | 4.84 | 4.73 | 4.69 | 4.67 | 4.65 | 4.65 | 4.85 | 4.86 | 4.70 | 4.98 | 4.96 |
| P ₂ O ₅ | .03 | .04 | .01 | .01 | .03 | .02 | .01 | .05 | .05 | .01 | .06 | .06 |
| Bb (ppm) | 185.0 | 179.6 | 185.9 | 181.9 | 191.7 | 192.8 | 195.1 | 177.0 | 178.5 | 180.0 | 170.8 | 170.2 |
| Sr | 5.1 | 6.6 | 5.5 | 5.1 | 10.4 | 8.1 | 9.0 | 46.4 | 29.8 | 30.6 | 9.4 | 9.2 |
| Zr | 126.9 | 117.9 | 123.4 | 125.0 | 109.1 | 115.0 | 115.0 | 108.2 | 103.2 | 109.4 | 138.0 | 137.0 |
| Mb | 25.0 | 24.0 | 24.3 | 24.1 | 24.3 | 23.4 | 23.9 | 18.6 | 21.0 | 20.3 | 23.6 | 23.3 |
| Y | 29.8 | 31.0 | 30.0 | 29.7 | 31.5 | 31.6 | 31.7 | 25.4 | 27.7 | 27.9 | 30.1 | 29.2 |
| Ba | 45.1 | 47.6 | n.d. | n.d. | 49.5 | 46.8 | 50.7 | 281.5 | 143.9 | 141.3 | 66.9 | 66.9 |
| La | 18.0 | 20.7 | n.d. | n.d. | 13.1 | 14.6 | 14.4 | 23.3 | 18.3 | 18.3 | 31.6 | 30.0 |
| Ce | 46.4 | 52.2 | n.d. | n.d. | 40.9 | 43.9 | 43.2 | 53.1 | 46.6 | 47.0 | 67.7 | 68.7 |
| Md | 17.4 | 19.6 | n.d. | n.d. | 15.1 | 15.8 | 15.5 | 17.7 | 16.1 | 16.9 | 25.9 | 25.2 |
| V | 1.0 | 1.1 | n.d. | n.d. | 1.2 | 1.8 | 1.1 | 1.3 | 1.3 | 1.7 | 1.2 | 1.8 |

Table 3:

Major and trace element analyses of MC-MLI lavas. All elements were analyzed by XRF using the method of Stork et al. (in review). Major oxides are reported as weight % and normalized to 100% anhydrous; total iron is reported as Fe_2O_3 . MnO was not analyzed. Analytical uncertainties are $\geq 10\%$ for La, 5% for Ce, and $< 5\%$ for all other elements. Sample numbers for the Mono Craters lavas are keyed to the dome numbers on figure 3a (e.g. M3-1 = (M)ono Craters, dome # 3, sample 1). M-12-1 and -2B are basaltic inclusions from the MC dacite dome (dome #12, fig. 3a); M-14-1B and M-18-1B are andesitic inclusions from the two orthopyroxene-bearing domes (fig. 3a). Neg- = samples from Negit Island; Pao- = samples from Paoha Island. Sample MLI-1 is from an islet immediately north of Negit Island (paper volcano isle).

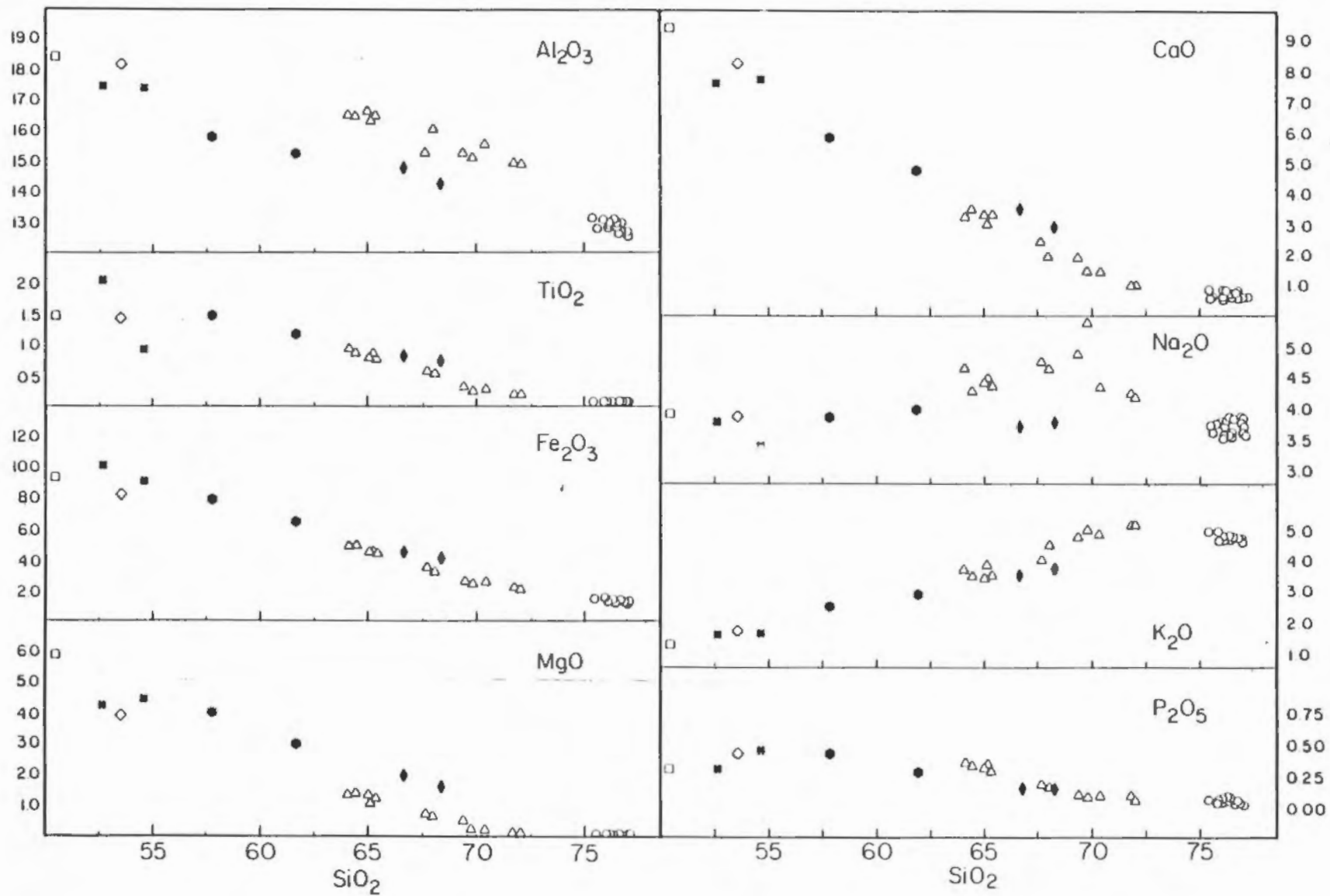


Figure 7a:

Major element silica variation diagrams. Symbols: Black Point (50.4% SiO_2) and June Lake (53.6% SiO_2) basalts, open diamonds; basaltic inclusions, filled crosses, andesitic inclusions, filled hexagons; MLI dacites and rhyolites, open triangles; MC dacite, filled diamonds; MC HSRs, open circles.

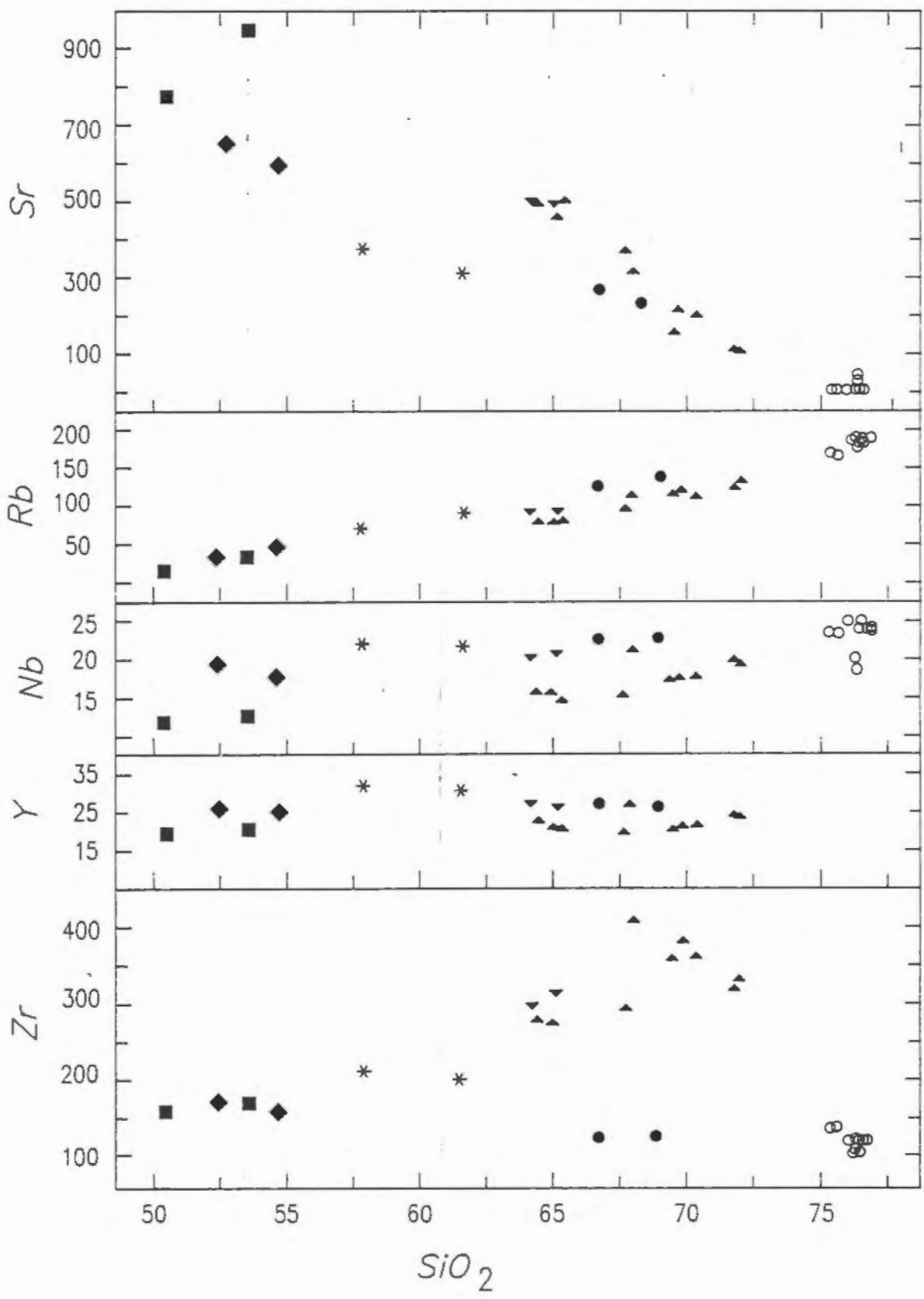


Figure 7b:

Silica variation diagrams of selected trace elements.
Symbols: squares, Black Point (50.4% SiO₂) and June Lake (53.6% SiO₂) basalts; diamonds, basaltic inclusions; stars, andesitic inclusions; triangles, MLI dacites and rhyolites; inverted triangles, dacite flow from Paoha Island; filled circles, MC dacite; open circles, MC HSRs.

and Range (Leeman and Rogers, 1970). Compared to typical low-K, high-Al, olivine tholeiite (HAOT) of the Devil's Garden Lava field in northeastern California (Bullen, in prep, McKee, et al., 1983), and much of the northwestern United States (e.g. Hart, 1985), the MC-MLI basalts are more silica saturated, have higher TiO_2 , alkalis, and P_2O_5 contents, and lower MgO/FeO^* and CaO/Al_2O_3 ratios.

The andesitic inclusions are high-K, calc-alkaline lavas (fig. 8) similar to typical high-K, calc-alkaline, orogenic andesites (Gill, 1981,) and calc-alkaline basalt and associated andesite of the Lassen volcanic field (Clynne, unpublished data). The andesitic inclusions however, have higher TiO_2 contents and FeO^*/MgO ratios than typical calc-alkaline andesite (Gill, 1981, Table 5.2), and higher alkalis, TiO_2 , and FeO^*/MgO than the Lassen andesites (Clynne, unpub. data).

The dacite dome of the Mono Craters and the dacitic lavas of the Mono Lake Islands have very different major element chemistries. Although both are high-K, the MC dacite has lower FeO^*/MgO ratios and plots within the CA field, while the MLI lavas define a slight iron enrichment trend (fig. 8). Additionally, the MC dacite has higher MgO and CaO , and lower Al_2O_3 and Na_2O than the MLI lavas (fig. 7a).

The MLI rhyolites are high-K lavas, and plot at the silicic end of the MLI dacites for all of the major elements except Na_2O . However, the MLI rhyolites have much higher FeO^*/MgO ratios than the dacites

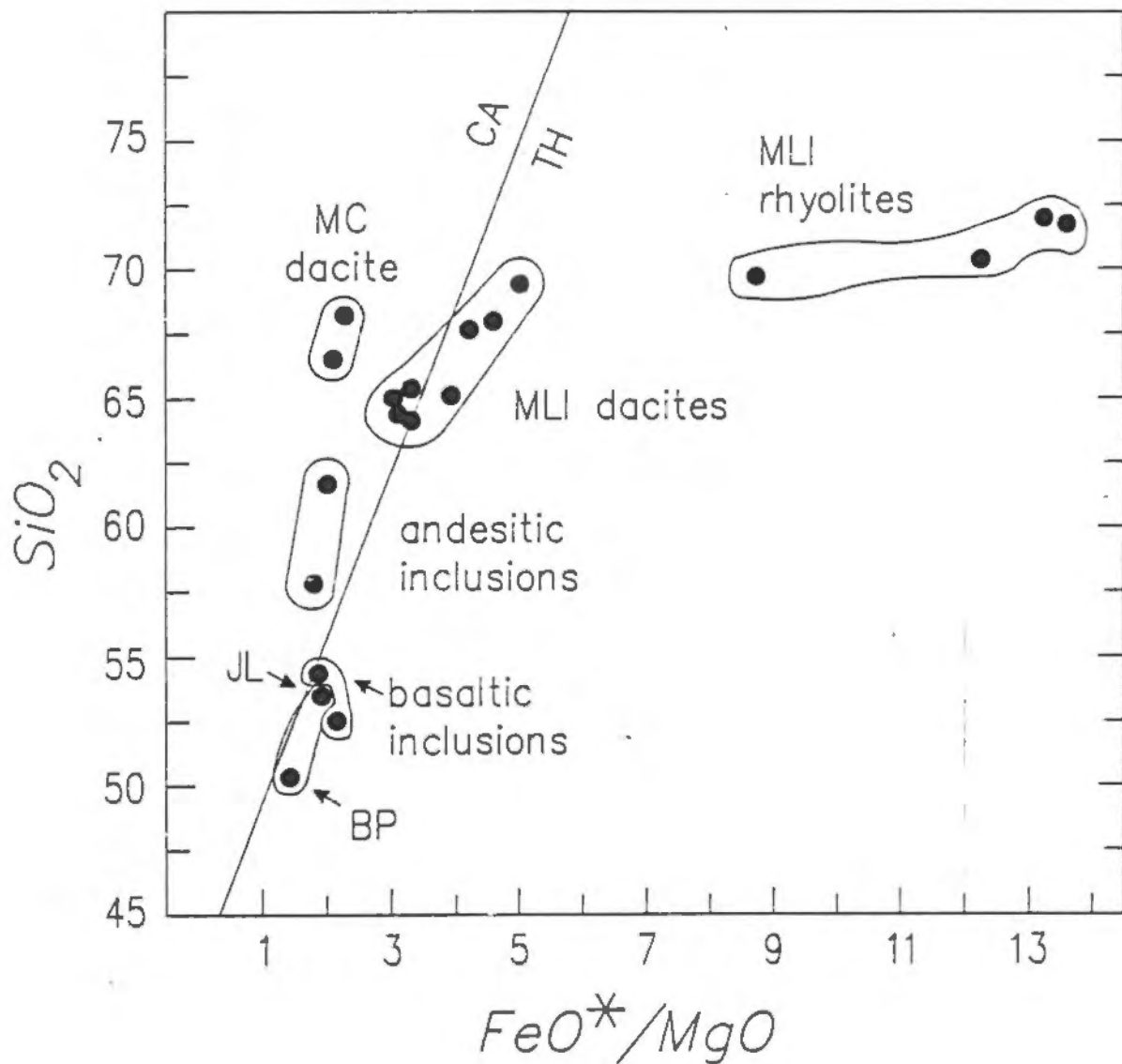


Figure 8:

FeO^*/MgO vs. SiO_2 of MC-MLI volcanic rocks. See figure for identification of rock types. The MLI dacites are more Fe-enriched than the MC dacite, and the MLI rhyolites have higher FeO^*/MgO than the MLI dacites. The HSRs are not plotted because of the extreme Mg depletion.

at similar SiO_2 contents (fig. 8).

The high silica rhyolites of the Mono Craters have nearly homogeneous major element chemistries (Table 3 and fig. 7a). 38 analyses of the 27 HSR flows and domes fall within a range of 1.5 wt.% SiO_2 . All are corundum normative and slightly peraluminous with aluminous indexes (molar $\text{Ca} + \text{Na} + \text{K}/\text{Al}$) between

Trace Elements

The different rock types of the complex are divided into a high-Ba group, including the June Lake and Black Point basalts, and the MLI dacites and rhyolites, and a low-Ba group, including the basaltic inclusions within the MC dacite dome, the andesitic inclusions, and the MC dacite (figs. 2,9). (The MC HSRs are excluded from discussion here, because of the compatibility of Ba.) The extreme contrast in Ba contents between the two subdivisions is illustrated by comparison of the high- and low-Ba dacite lavas in figure 9. The high-Ba, MLI dacites are > 5 times more enriched in Ba than the low-Ba, MC dacite (1600 and 300 ppm Ba respectively). Relative to the low-Ba group, the high-Ba lavas are also characterized by: 1) highly fractionated REE patterns with $(\text{Ce}/\text{Yb})_n$ values between 6 and 12 (table 4), 2) higher Sr, and 3) lower Nb and $(\text{Ba}/\text{Nb})_n$ (9.6-11.8 in the high-Ba basalts compared to 3.5-4.2 in the basaltic inclusions, figure 12a).

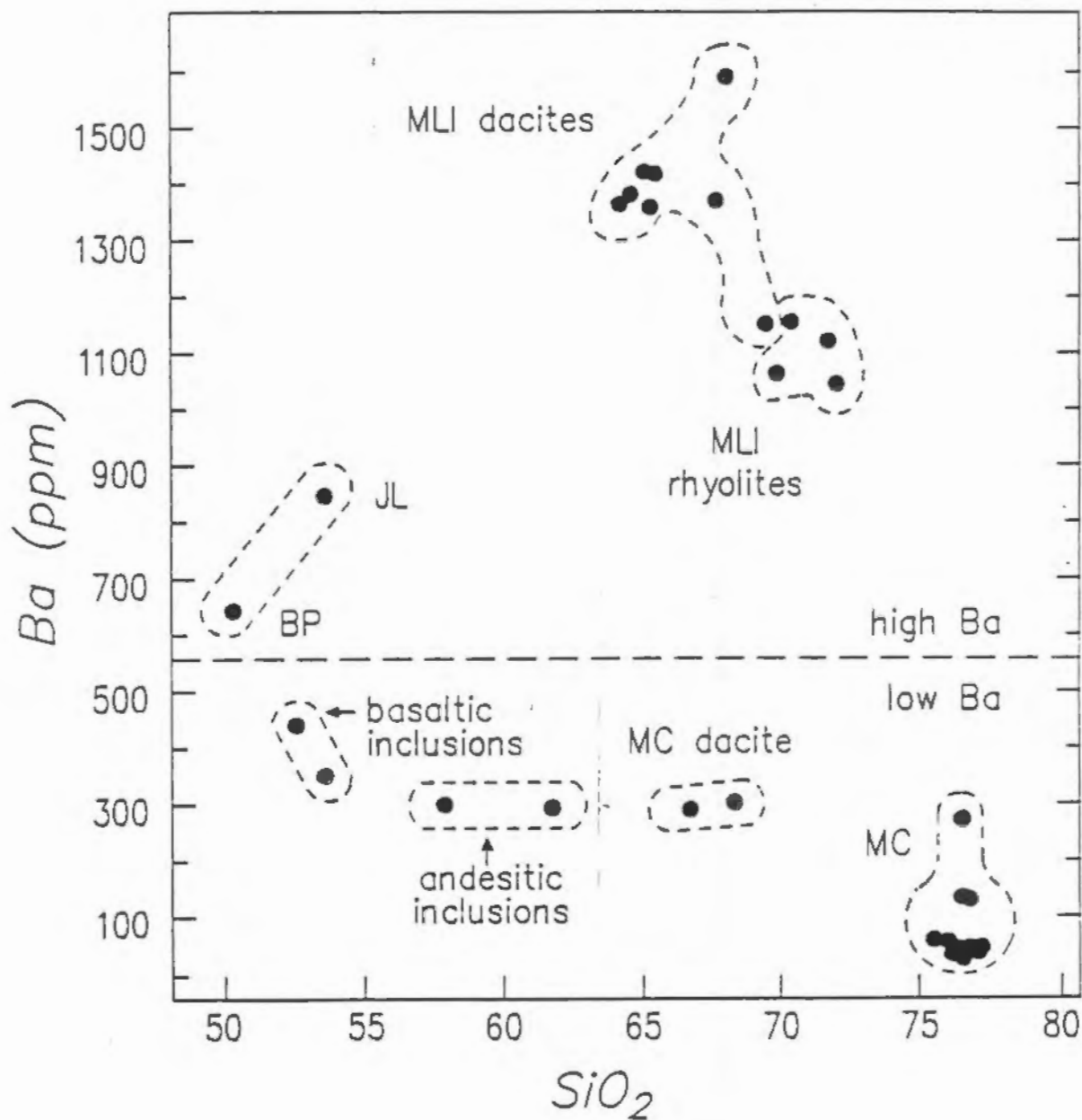


Figure 9:

Ba vs. SiO₂ diagram subdividing the different rock types into high- and low-Ba groups. The dividing line is arbitrary but reflects a significant change in Ba (and other elemental concentrations, see text) at similar SiO₂ contents. The MC HSRs are not grouped on this basis because of sanidine fractionation.

Figure 10 is a REE plot of the two high-Ba basaltic lavas, Black Point and June Lake, and a representative sample of the MLI dacites. All three are similarly LREE enriched with highly fractionated patterns and positive to slightly negative Eu anomalies ($\text{Eu}/\text{Eu}^* = 1.03$ to 0.94). The three patterns are similar in that they are flat to slightly concave downward in the LREE to MREEs (Ce to Sm) and concave upward in the MREE to HREEs (Gd to Yb). In contrast, the low-Ba lavas have, at similar SiO_2 contents, lower LREE concentrations and less fractionated REE patterns with $(\text{Ce}/\text{Yb})_n$ between 3 and 4. For example, figure 11 contrasts the REE patterns of the andesitic inclusions and MC dacite (low-Ba), with the MLI rhyolite (high-Ba). The three patterns have modest to large negative Eu anomalies ($\text{Eu}/\text{Eu}^* .73-.53$), however, the two low-Ba lavas have much lower LREE concentrations and less fractionated patterns.

Both the high- and low-Ba basalts have a distinct, arc-like trace element signature (fig. 12a), similar to alkali olivine basalts from within the Sierra Nevada Province, and basaltic lavas from the Devil's Garden Lava field of northeastern California and southcentral Oregon. Figure 12b is a MORB normalized diagram of incompatible trace elements of: 1) the MC-MLI basalts, 2) uncontaminated basalts of the Coso volcanic field (Bacon and Metz, 1984; Bacon et al., 1984), 3) alkali olivine basalts of the San Joaquin volcanic field (Van Kooten, 1981), 4) a single .08 M.Y. old basalt from

| Sample | Mafic lavas | | | Silicic lavas | | |
|------------------|-------------|-------|---------------|---------------|----------|----------|
| | BP | JLB | and. incl. | MC dac. | MLI dac. | MLI rhy. |
| SiO ₂ | 50.44 | 53.56 | 57.85 | 67.67 | 64.96 | 71.73 |
| Ce | 41.56 | 54.49 | 60.56 | 43.21 | 81.01 | 102.00 |
| Nd | 21.83 | 26.47 | 28.75 | 19.39 | 34.11 | 34.91 |
| Sm | 4.53 | 4.98 | 6.03 | 4.25 | 6.14 | 5.40 |
| Eu | 1.48 | 1.51 | 1.44 | .81 | 1.65 | .76 |
| Gd | 4.08 | 3.82 | 5.16 | 3.78 | 4.73 | 3.77 |
| Dy | 3.75 | 3.54 | 5.31 | 4.12 | 4.20 | 3.63 |
| Er | 1.98 | 1.86 | 2.96 | 2.31 | 2.29 | 2.15 |
| Yb | 1.76 | 1.63 | 2.79 | 2.33 | 2.13 | 2.26 |
| Ce/Yb | 23.7 | 33.49 | 10.32 | 18.51 | 38.05 | 45.23 |

High Silica Rhyolites

| Sample | M19 | M24 | M14 | M28 | M3 | M11 | M28 |
|---------------|-------|-------|-------|----------|----------|-------|-------|
| petrol. group | biot. | biot. | opx | fayalite | aphyrlic | glass | glass |
| Ce | 46.95 | 50.01 | 69.55 | 53.03 | 50.64 | 30.25 | 38.5 |
| Nd | 18.08 | 19.30 | 26.60 | 22.95 | 21.65 | 14.57 | 17.6 |
| Sm | 3.62 | 4.05 | 5.02 | 4.79 | 4.58 | 3.97 | 4.25 |
| Eu | .31 | .26 | .20 | .15 | .15 | .24 | .10 |
| Gd | 3.00 | 3.41 | 3.94 | 4.04 | 3.90 | 3.90 | 3.92 |
| Dy | 3.37 | 3.85 | 4.19 | 4.49 | 4.36 | 4.65 | 4.35 |
| Er | 2.00 | 2.36 | 2.56 | 2.72 | 2.59 | 2.88 | 2.76 |
| Yb | 2.23 | 2.52 | 2.67 | 2.87 | 2.78 | 3.00 | 2.93 |
| Ce/Yb | 21.06 | 19.87 | 26.03 | 18.51 | 18.22 | 10.08 | 13.10 |

Table 4:

Isotope dilution rare earth element analyses of MC-MLI volcanic rocks. Analyses were done in G. Hanson's lab at the State University of New York at Stony Brook. Analytical uncertainty is 1% relative. Sample numbers are as in Table 3.

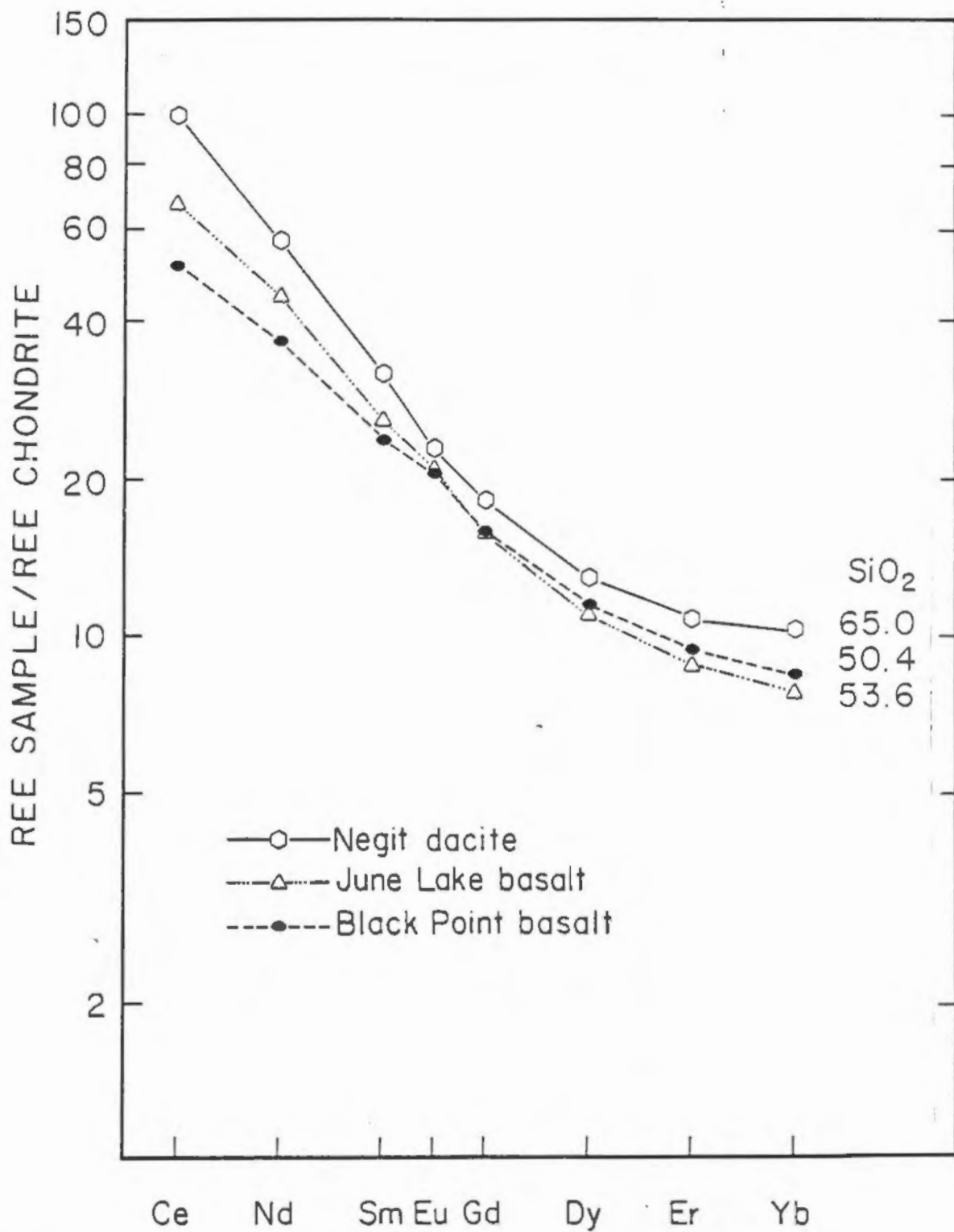


Figure 10:

Chondrite normalized REE diagram of three high-Ba lavas: a MLI dacite (hexagon), and the June Lake (triangle) and Black Point (filled ellipse) basalts. Note the similar shapes in the REE patterns. Normalization factors are 1.2x Leedy chondrites, Hanson, (1980).

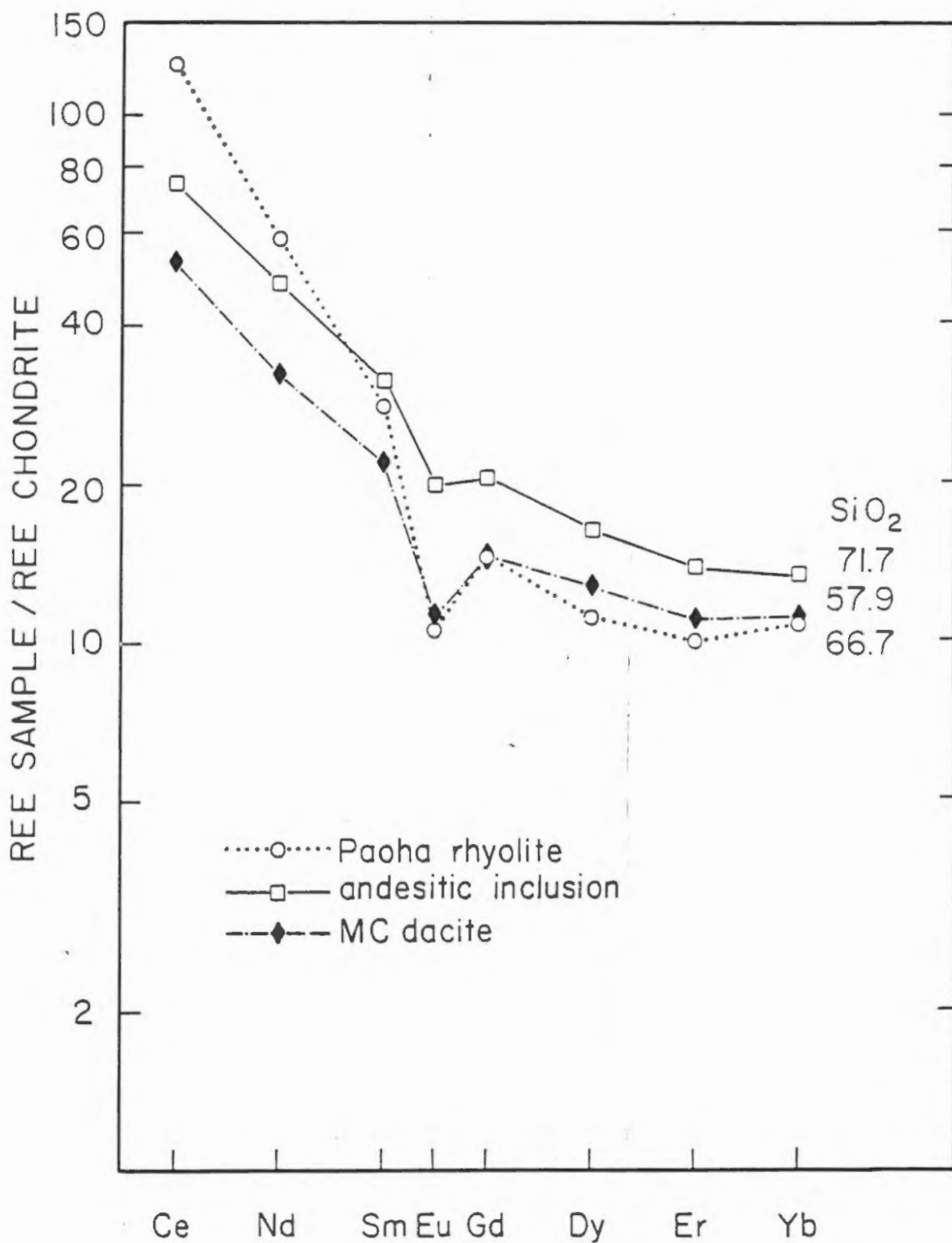


Figure 11:

Chondrite normalized REE diagram contrasting the high-Ba MLI rhyolite (open circle) with the MC dacite (filled diamond) and andesitic inclusion (open square). Both the andesite and the dacite (low-Ba) have much flatter patterns than the rhyolite. The andesite has parallel but higher REE than the dacite, and most of the MC-MLI lava (compare with figures 10 and 14).

Sample/MORB

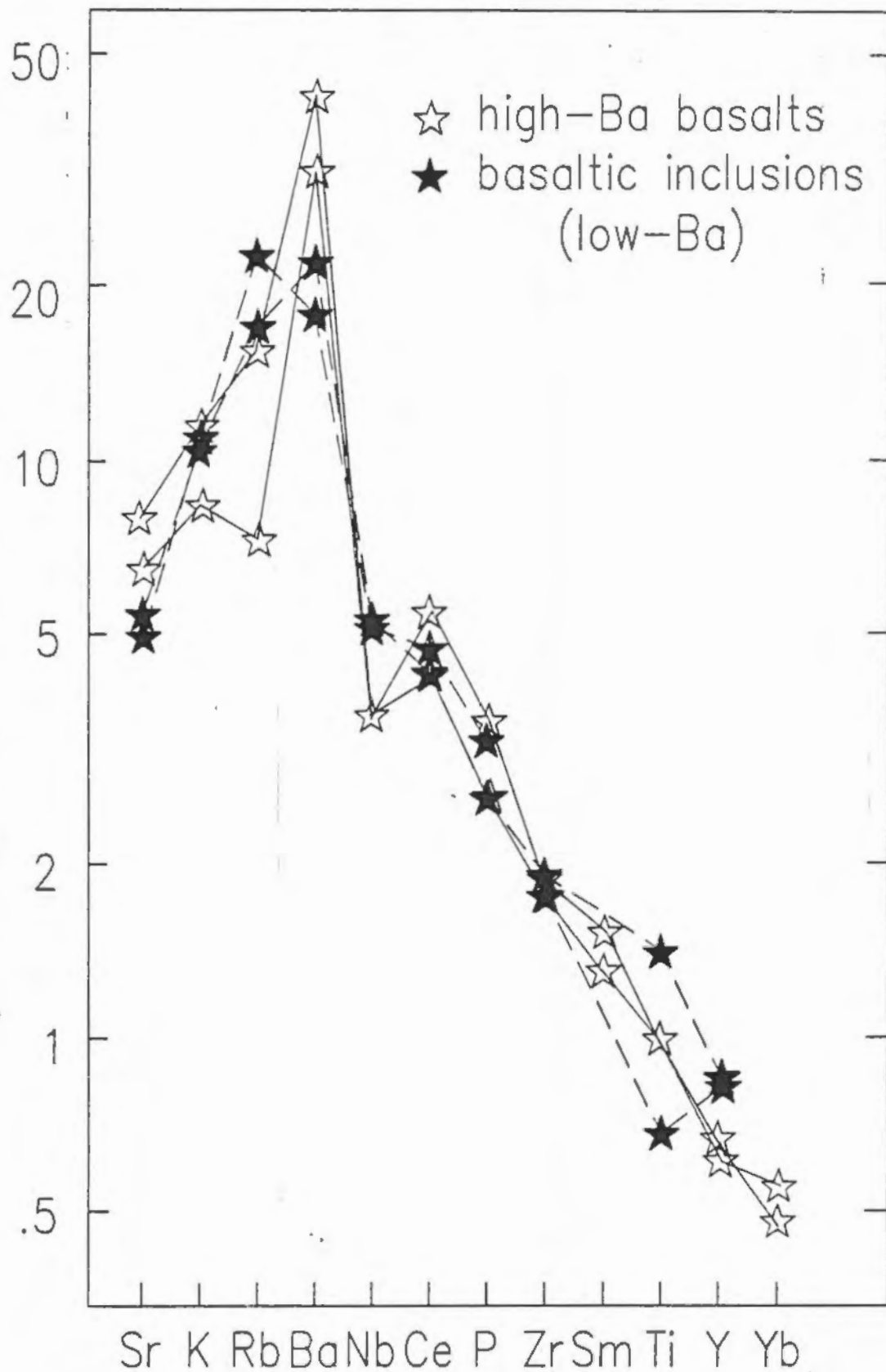


Figure 12a:

MORB normalized hygromagataphile diagram of Black Point and June Lake basalt lavas (open stars, high-Ba), and two analyses of basaltic inclusions from within the MC dacite dome (filled stars, low-Ba). The overall trace element patterns are similar, but the basaltic inclusions lack the Nb depletion relative to the high-Ba lavas, and have lower Ba contents and Ce/Nb, and higher Y (see discussion).

the Long Valley caldera (Sampson, unpublished data), and 5) medium-K, calc-alkaline basalts of the Devil's Garden Lava Field (Bullen, in press). As the figure illustrates, all of the basalts have an arc-like trace element signature characterized by enrichments in LREE, P, alkalis and alkaline earths (especially Ba), and, except for the basalts from the Coso field, a strong Nb depletion. Not shown are typical, low-K HAOT basalts that characterize much of the northwestern U.S.; except for the lowest-K ($< .15\% \text{ K}_2\text{O}$) HAOT lavas, these basalts also have similar incompatible trace element enrichments (Bullen, in press). Several characteristics and distinctions are also apparent on the diagram. First, there is a general trend of increasing alkaline and alkaline earth contents with increasing Ce/Yb (fig. 12b). Second, the medium-K, calcalkaline lavas of the Devil's Garden comprise the lower limit of the trace element enrichments and depletions. Third, this group of basalts are distinct from the Sierra Nevada Province lavas in high field strength (HFS) elements and REE patterns. Specifically, the Devils Garden lavas have flat HFS to HREE patterns, and lower HFS/HFS (e.g. Ti/Y, Nb/Ti), HFS/HREE (e.g. Ti/Yb) and Ce/Yb ratios (5 compared to 8-26, respectively) than the Sierran Province basalts, except for the Coso basalts (fig. 12b). Finally, the uncontaminated basalts of the Coso volcanic field, and the low-Ba basaltic inclusions of the MC-MLI complex have trace element patterns distinct from the other Sierran Province basalts, for which there is available data. These lavas have lower Ba/Nb, Ba/Ta,

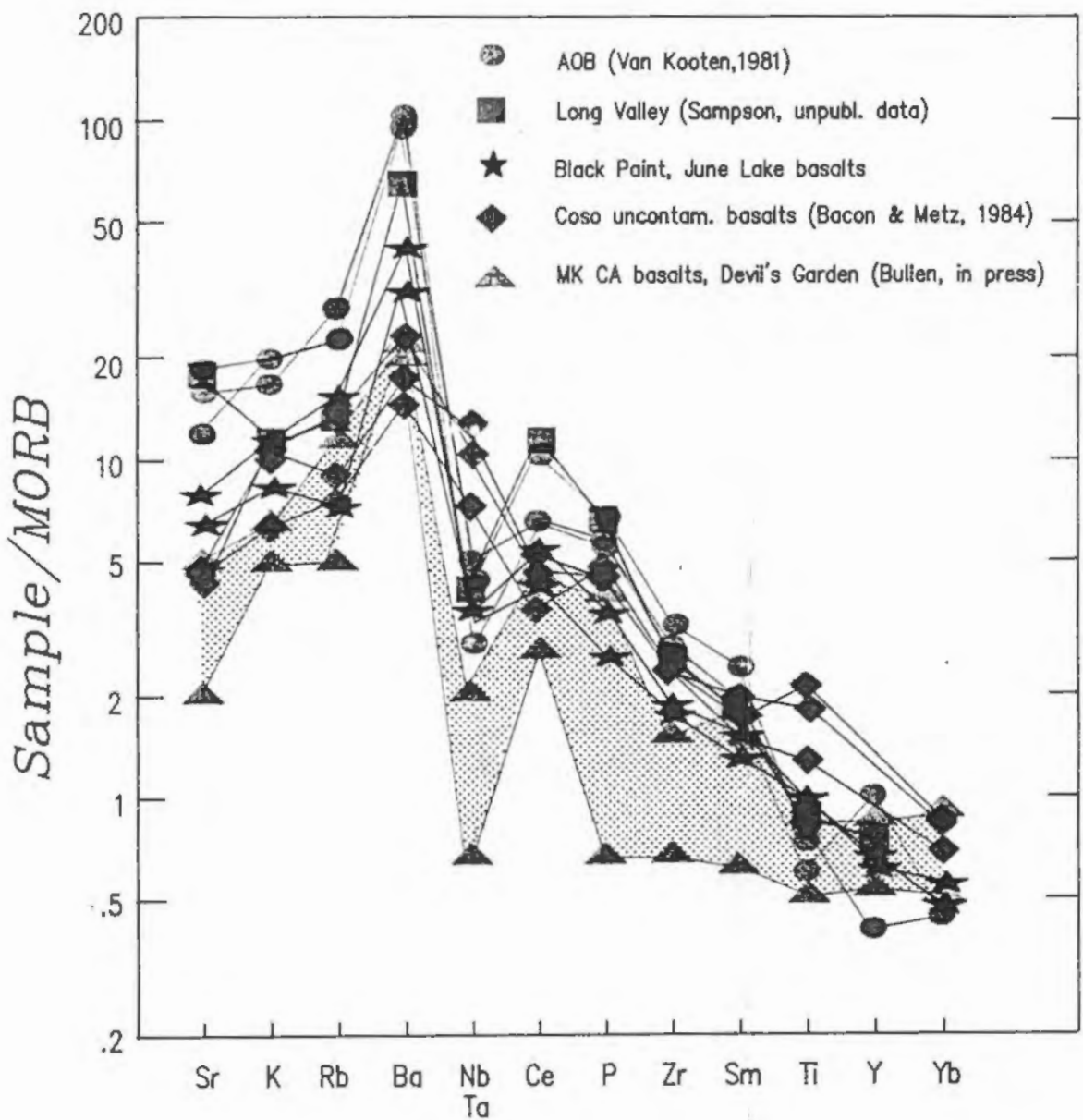


Figure 12b:

MORB normalized hygromagmatophile diagram of several Late Cenozoic basalts of the Sierra Nevada Province. The green stippled pattern represents the range of medium-K CA basalts from the Devil's Garden lava field (Bullen, in press). All of the lavas plotted have a characteristic arc-like trace element pattern. See text for discussion. Normalization factors are from Pearce, (1983).

Ba/K, and Ce/Yb (5-6); and higher Ti, and Nb and Ta than the Sierran Province basalts (figs. 12a,b).

The andesitic inclusions have higher REE concentrations than the high-Ba basalts and MC dacite, higher MREE and HREE concentrations than the MLI rhyolites, and higher HREE than the MC HSRs. Relative to high-K, calcalkaline, acid andesites from continental margin arcs (Gill, 1981), the MC andesitic inclusions have much higher Sr/Rb, and Ti and Nb contents, and lower Ce/Yb and Ba/La ratios (fig. 12c). The MC inclusions are strikingly similar in trace element contents, to the porphyritic andesites that occur as inclusions within the Coso HSR lavas (fig. 12c). This chemical similarity is interesting in light of the parallel mode of occurrence, textures, and petrogenetic origin proposed for both rock types (see discussion).

Mono Craters High Silica Rhyolites

There is a close correlation between phenocryst mineralogy and trace element concentration, and the HSRs are discussed in terms of three groups: 1) biotite, 2) orthopyroxene, and 3) fayalite + sparsely porphyritic + aphyric (collectively referred to as crystal poor) rhyolites (table 3). The fayalite and crystal poor lavas comprise approximately 75% of the Mono Craters' erupted volume and are chemically indistinguishable, except for one sparsely porphyritic dome, M-16. This dome has higher Ba (61ppm), Rb (195 ppm), and Sr (11 ppm); and lower Ce (48 ppm), Nd (17 ppm) and Zr (106 ppm)

Sample/high-K CA
arc andesite (59% SiO₂)

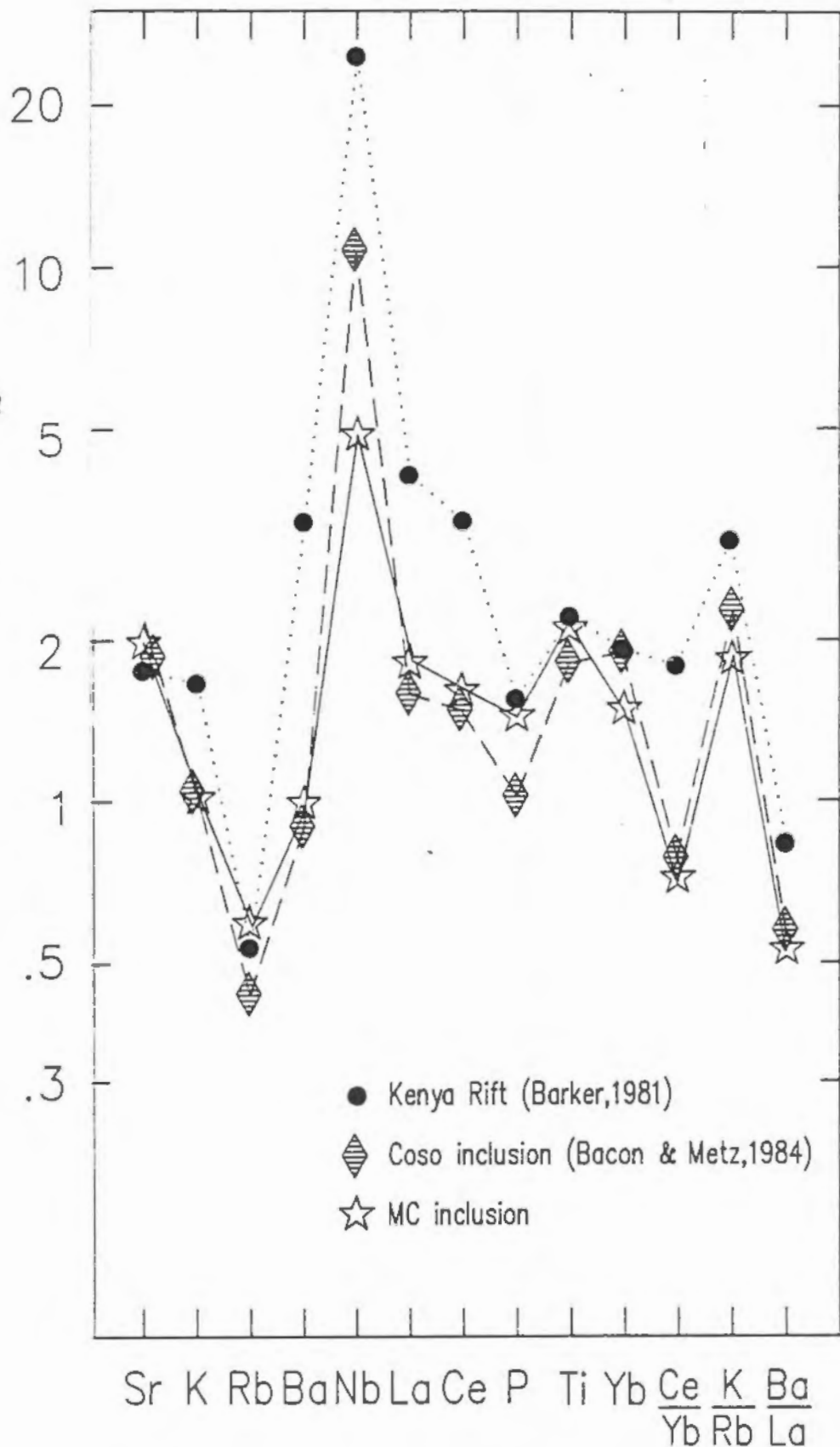


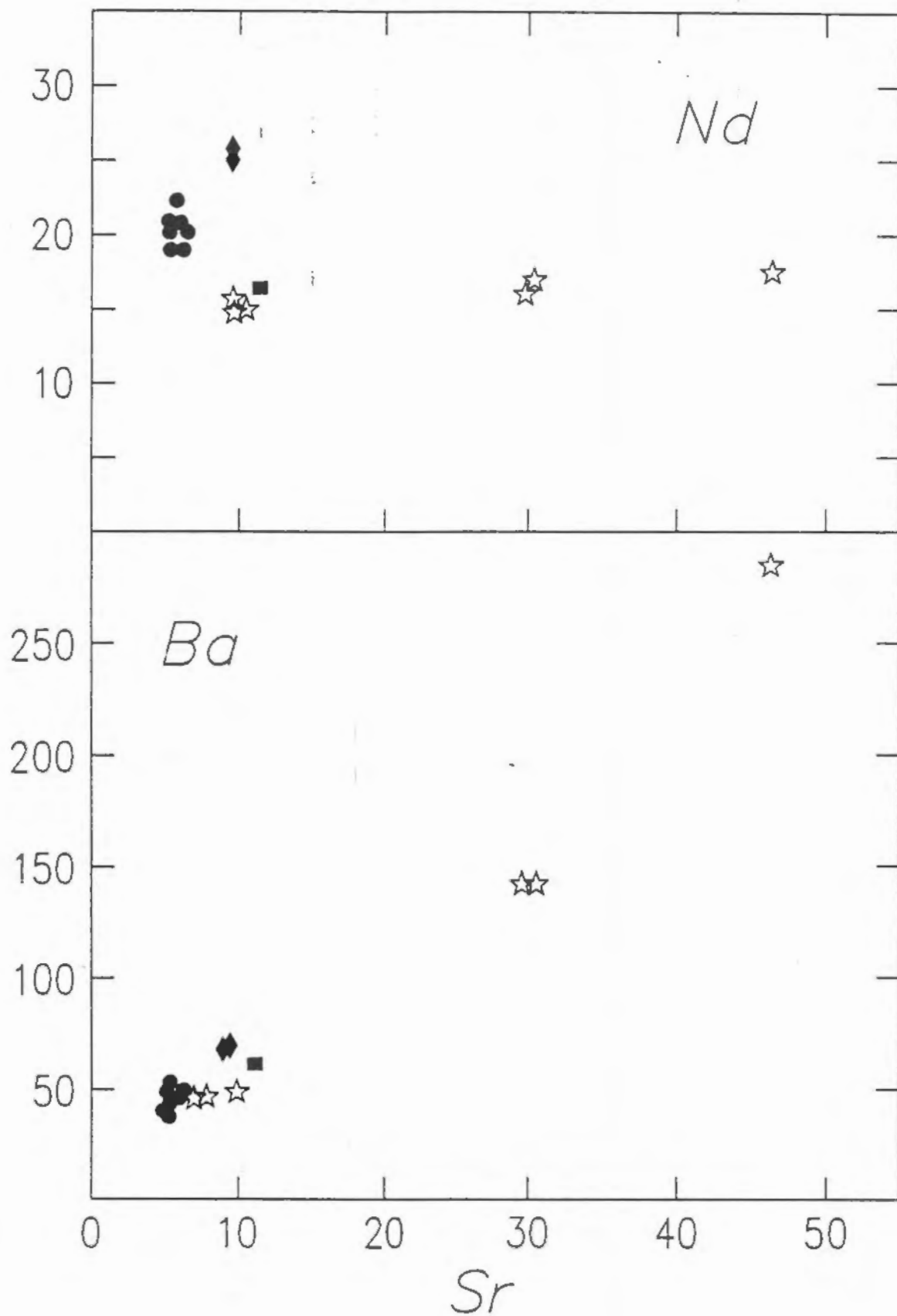
Figure 12c:

HYG plot of the MC andesitic inclusion (57.9%SiO₂), andesitic inclusion from the Coso HSRs (57.8%SiO₂), and Kenya rift (58.5% SiO₂)(Barker, 1977). Samples were normalized to typical high-K acid andesite (Gill,1981). Note the similarity in patterns between the inclusions from Coso and the Mono Craters.

concentrations than any of the other 21 fayalite-bearing and crystal poor lavas (figs. 13a, b). The orthopyroxene-bearing HSRs, though separated by over two kms., have identical trace element contents. These lavas have the highest LREE and Zr (138 ppm), and lowest Rb (170 ppm) concentrations of any of the HSRs. The biotite bearing domes are the most heterogeneous. For example, Sr and Ba concentrations vary from 46-10 ppm and 290-50 ppm respectively (fig. 13a). A regular trend occurs between the individual biotite-bearing domes from M-19 with the highest Sr and Ba and the lowest Rb, Nb, Y, and REE concentrations, through M-24, and finally M-11, which approaches the trace element concentrations of the fayalite and crystal poor rhyolites (figs. 13a, b). Four chondrite normalized REE patterns of the biotite-bearing and fayalite and crystal poor lavas (fig. 14) define a regular pattern of increasing REE concentrations, from the least differentiated biotite bearing dome, M-19, through M-24, to the olivine and crystal poor HSRs. The REE pattern of the orthopyroxene-bearing dome in figure 14 has much higher LREE contents and Ce/Yb compared to the other HSRs.

Nd-Sr Isotopes

Seven Nd and Sr isotopic ratios for the different rock types within the MC-MLI complex are plotted in figure 15 and reported in table 5. For reference, the field of Nd and Sr isotopic values of Cenozoic basalts in the Sierra Nevada Province (Domenick, et al., 1983 and Menzies, et al., 1983) and isotopic ratios of the Bishop Tuff



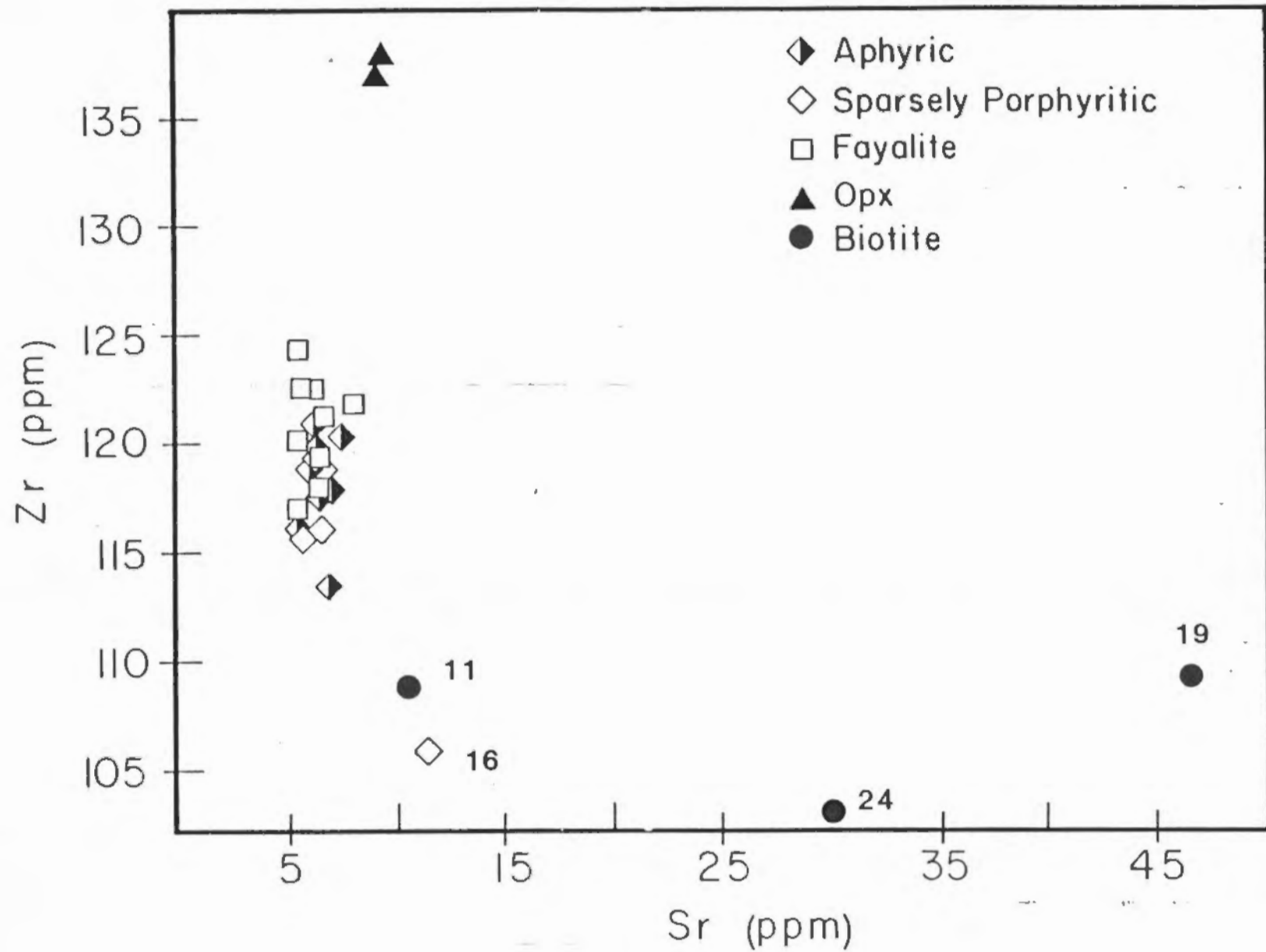


Figure 13b:

Zr vs. Sr plot illustrating the chemical distinctions of the different petrologic facies HSRs. See figure for key. The fayalite + crystal poor lavas are chemically homogeneous except for one sparsely porphyritic lava, M-16 (labeled). The orthopyroxene-bearing HSRs are Zr enriched relative to the other HSRs. The biotite bearing domes are chemically, the most diverse. The dome numbers on the figure correlate with figure 3a.

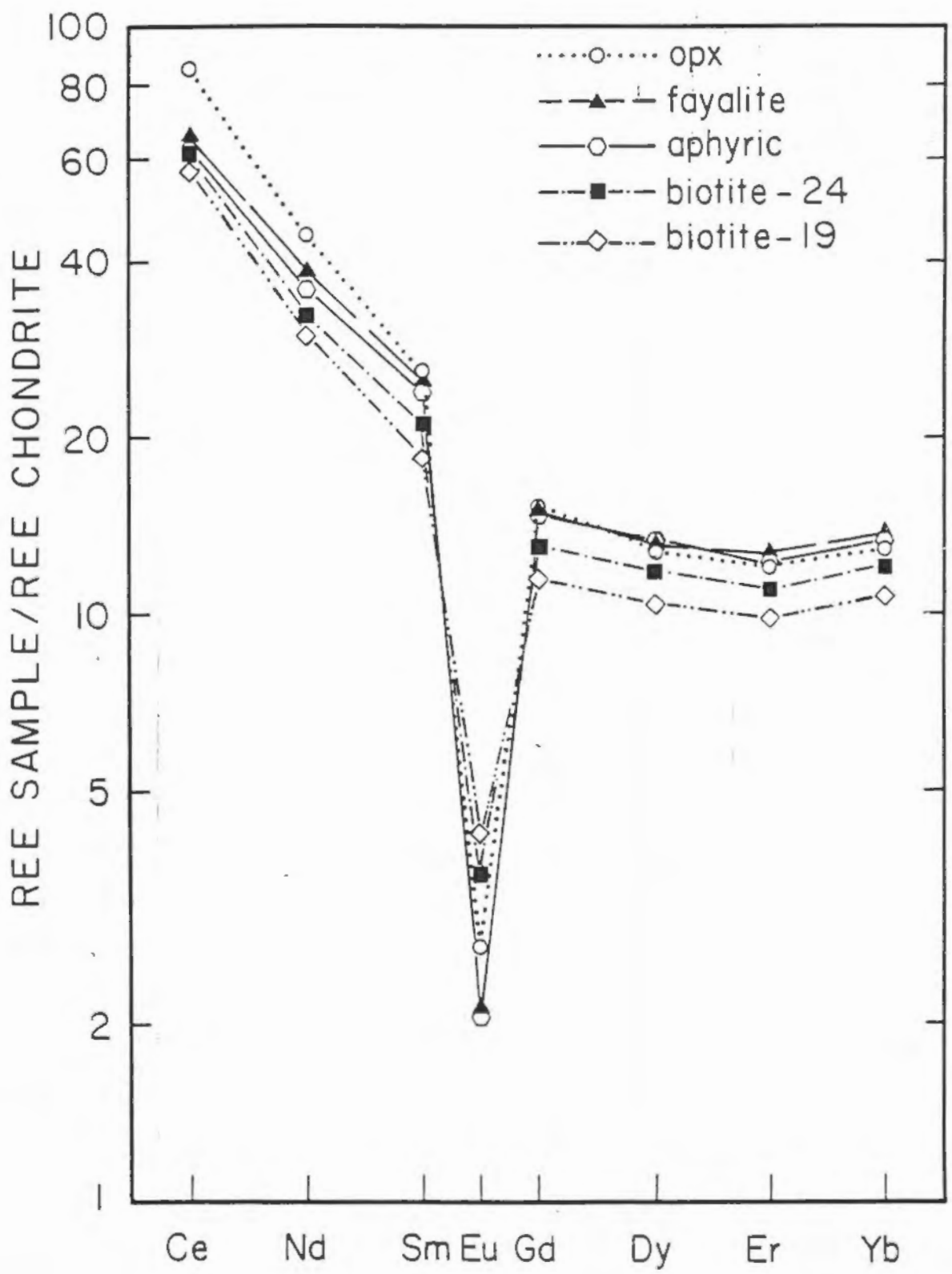


Figure 14:

Chondrite normalized REE diagram of five HSR lavas. See figure for key. Note the systematic increase in all REE except Eu from the biotite-bearing dome, M-19, through M-24, to the fayalite and crystal poor rhyolites. The orthopyroxene-bearing dome is the most LREE enriched, and is similar in HREE content to the HSR lavas.

(Halliday, et al., 1984), and Inyo domes (Sampson and Cameron, in press) are also shown. The most mafic rock types of the complex, the basalts of Black Point and June Lake, are variable in isotopic composition; Black Point has an ϵ_{Nd} value of +1.6 and $^{87}Sr/^{86}Sr$ of .7055, while the June Lake basalt is lower at -1.5 and higher at .7062. These values are similar to, but more $^{87}Sr/^{86}Sr$ enriched at a given ϵ_{Nd} , than isotopic ratios reported by Menzies, et al., (1983), and Domenick et al., (1983) for Late Cenozoic volcanic rocks of the Sierra Nevada Province (fig. 15). They also have much higher $^{87}Sr/^{86}Sr$ and lower $^{143}Nd/^{144}Nd$ ratios than low-K HAOT, and medium-K calcalkaline basalts of the Devils Garden lava field which, have uniform, MORB-like values (Bullen, in press). The andesitic inclusion has higher ϵ_{Nd} (+2.9) than late Cenozoic volcanic rocks analyzed thus far from the Sierran Province.

The two analyzed MLI samples, the Negit dacite and Paohan rhyolite, have identical $^{87}Sr/^{86}Sr$, but significantly different $^{143}Nd/^{144}Nd$ ratios (fig. 15). The MLI dacite sample is isotopically indistinguishable from the June Lake basalt.

The HSR samples (three for Nd and two for Sr isotopes) have similar isotopic ratios and are like the Paohan rhyolite sample. $^{87}Sr/^{86}Sr$ overlaps with the Bishop Tuff and Inyo domes and averages about 1 ϵ unit higher than the Bishop Tuff.

| Sample | $87\text{Sr}/86\text{Sr}$ | $143\text{Nd}/144\text{Nd}$ | ϵ_{Nd} |
|-----------------|---------------------------|-----------------------------|------------------------|
| BP | .70545 | .51272 | +1.6 |
| JLB | .70624 | .51256 | -1.5 |
| andes. incl. | .70526 | .51278 | +2.9 |
| MLI dac. | .70631 | .51253 | -2.0 |
| MLI rhy. | .70633 | .51265 | +0.2 |
| HSR-ol | .70634 | .51268 | +0.8 |
| HSR-opx | n.d. | .51268 | +0.9 |
| HSR-biot. | .70680 | .51263 | -0.1 |

note: analytical uncertainty is .00007 for $87\text{Sr}/86\text{Sr}$
and .00003 for $143/144\text{Nd}$

Table 5:

Nd-Sr isotopic analyses of MC-MLI volcanic rocks.
Analyses were done in G. Hanson's lab at the State University of
New York at Stony Brook. See Table 3 for explanation of sample
numbers.

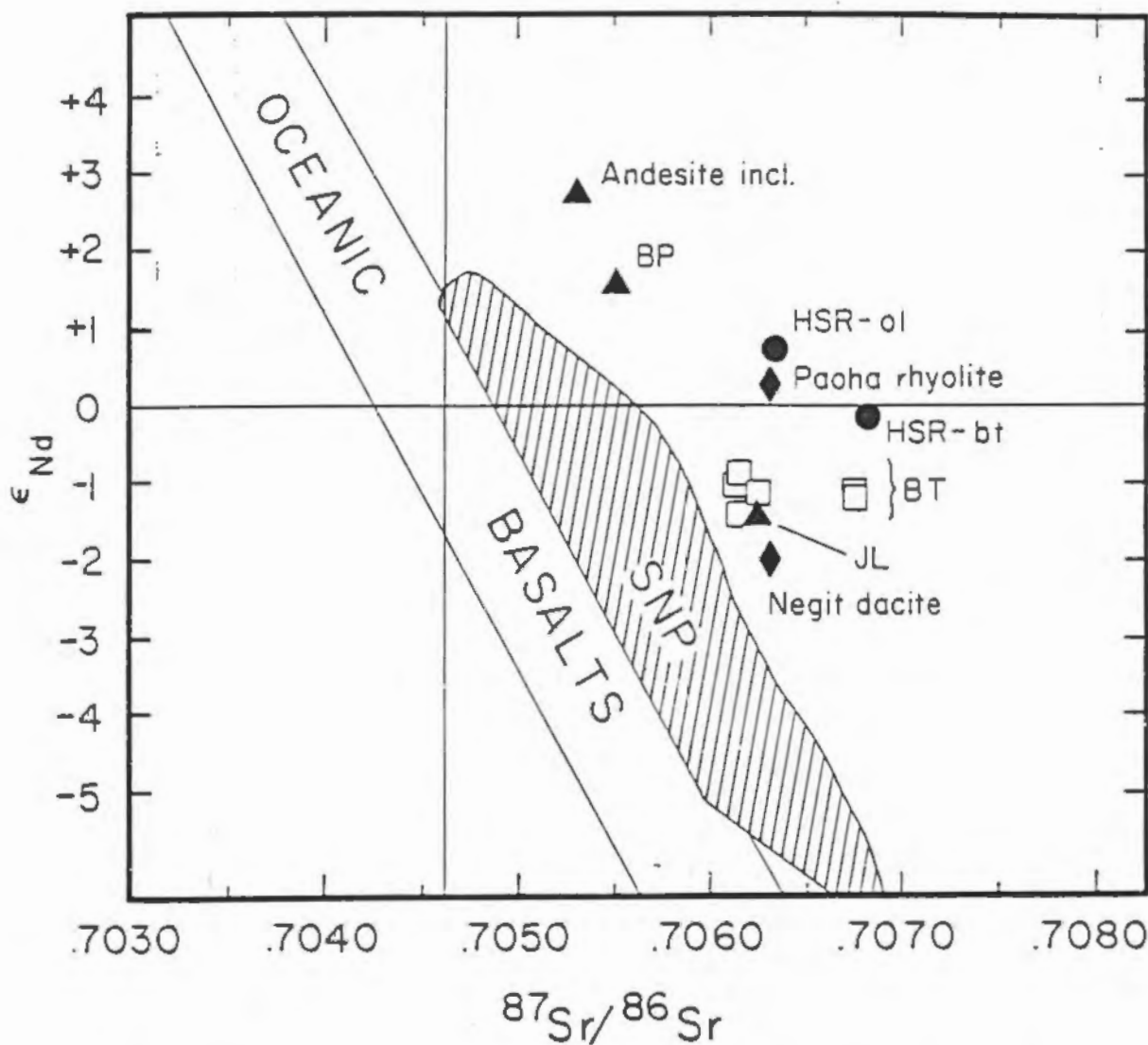


Figure 15:

Nd, Sr isotopic diagram of MC-MLI lavas (see figure for identification of symbols). For reference, present day bulk earth, and the field of oceanic basalts are shown. The ruled pattern represents the range of isotopic values for Late Cenozoic basalts of the Sierra Nevada Province (Menzies, et al., 1983 and Domenick et al., 1983). Nd and Sr values for Bishop Tuff sanidines are also plotted. The MC-MLI mafic rocks are parallel to the Sierran Province basalts. The silicic rocks have similar ratios as the Bishop Tuff, but have higher ϵ_{Nd} , near bulk earth.

Discussion: Relationship Between Rock Types

High-Ba vs. Low-Ba groups

Ba behaves as an incompatible element for all rock types except the MLI rhyolites which have biotite, and thus, it is a useful element for testing possible liquid lines of descent. Figure 9, therefore clearly indicates that none of the lavas from the high-Ba group can be related to the rocks of the low-Ba group by crystal fractionation. Moreover, the major and other trace element abundances, of the high- and low-Ba basalts, precludes their derivation from a single liquid line of descent (figs. 7a, b). For example, the June Lake basalt (high-Ba) has, at the same SiO_2 content and $\text{CaO}/\text{Al}_2\text{O}_3$ ratio, higher Sr and LREE, and lower Nb and Y, than the basaltic inclusions (low-Ba). Similarly, the Ba, Sr, Nb, and LREE data indicates that the high- and low-Ba dacites cannot be comagmatic (figs. 9-11, table 3). The low-Ba andesitic inclusions have such a distinct petrology, REE pattern, and Nd and Sr isotopic signatures, (figs. 11, 15) compared to the high-Ba basalts, that they obviously could not be related by crystal fractionation or small degrees of partial melting of a common source. Likewise, the high-Ba MLI rhyolites do not fall along fractionation or likely mixing lines with the low-Ba dacite.

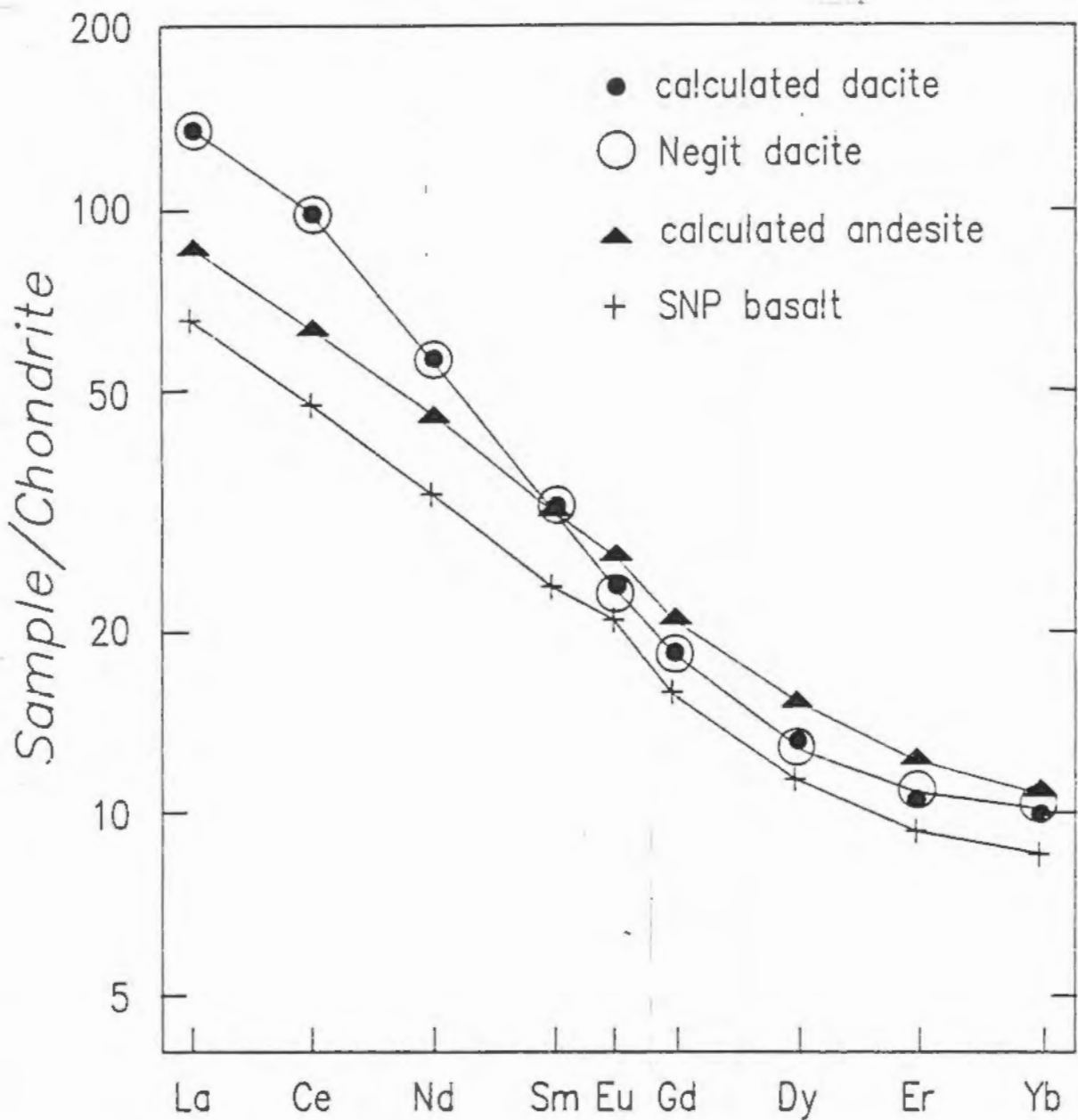
High-Ba group

The two basaltic lavas of the high-Ba group have the same arc-like trace element signature as discussed above, however, the two

lavas were not derived from cognate magmas. The contrasting petrology (table 1), antithetic Ni and Cr behavior (table 3), different Ce/Sm and Gd/Yb ratios, and the distinct Nd and Sr isotopic contents, preclude the two basalts from evolving from a single liquid line of descent. Both basalts show evidence for contamination with either crustal lithologies or highly evolved liquids and the extent of this involvement must be assessed before the trace element signature of the source region can be constrained. Considering the extremely enriched $^{87}\text{Sr}/^{86}\text{Sr}$ (.7330) and highly negative ϵ_{Nd} (-19) character of upper crustal metasedimentary rocks (Kistler and Peterman, 1973; Domenick, et al., 1983), it is unlikely that either the Black Point or June Lake basalts have experienced significant contamination from these rock types. Mesozoic, granitic intrusives are the most common crustal rocks in this area and are likely contaminants. One granitic pluton immediately north of Mono Lake, is substantially lower in Sr, Y, Eu, and HREE concentrations than the Black Point and June Lake lavas (Sofia, MS thesis, 1984); therefore, significant contamination by this pluton, would deplete the basalts in these elements. Geochemical studies document a wide range in chemical compositions of Sierran intrusive rocks (e.g. Kistler and Peterman, 1973), and consequently it is difficult to accurately limit the degree of contamination by unexposed intrusive rocks in this area. However, the systematic trace element pattern for all of the late Cenozoic basalts in the the Sierran Province and elsewhere (above), is not likely to be due to contamination of chemically diverse crustal lithologies. Moreover, the basalts

of the Devil's Garden lava field to the north, and the San Joaquin field to the south of the MC-MLI field (Van Kooten, 1981) have no chemical indication of interaction with crustal material (McKee, et al., 1983; Bullen, pers. comm.), and yet have parallel incompatible trace element enrichments.

The similarity between the REE patterns of the high-Ba basalts and the MLI dacite sample analyzed for REE (fig. 10) is striking and suggests that the dacites could have been derived from chemically similar basalts by crystal fractionation. The high-Ba dacites are isotopically distinct from Black Point and therefore, cannot be directly related. Although the June Lake basalt is isotopically identical to the Negit dacite, it is not a desirable parent liquid for modeling because of the petrographic evidence for a crustal component discussed above. The trace element compositions of the dacites are consistent with plagioclase and hornblende dominated fractional crystallization of a high-Ba basalt with very similar trace element concentrations to Black Point, or other Late Cenozoic volcanic rocks typical of the Sierra Nevada Province. A two stage fractionation model is illustrated in figures 16a and 16b. Although not a unique solution, the model is appropriately constrained by: 1) the the observed phases in the Black Point basalt and Negit dacite, 2) published partition coefficients ($K'ds$; table 6), and 3) proportions and degree of fractionation (f') required to satisfy the major oxides.



Figures 16a:

REE diagram of Rayleigh fractionation model between a typical incompatible trace element enriched Sierran Province basalt, similar to Black Point, and the Negit dacite. The model requires a two stage process, from 1) basalt to mafic andesite, and 2) andesite to dacite. In the first stage, a systematic increase in all the REE occur. In the second, as hornblende and plagioclase dominate the assemblage, Ce/Yb increases and Eu decreases. Phases used are those observed in Black Point and the Negit dacite; proportions were constrained by major element modeling. Partition coefficients are listed in Table 6.

Results of Modeling basalt to MLI Dacite

| | | |
|-------------|----------------------------------------|------------------------------------------------------------------|
| f | .70 | .35 |
| assemblage: | 63 plag 17 oliv 10 cpx 10 mt. | 56 plag 20.5 hbld 8.5 opx 8.0 cpx 3.5 biot 3.5 mt |

| Sample | BASALT | BASALTIC ANDESITE | DACITE |
|--------|--------|-------------------|---------|
| SiO2 | 50.44 | 54.32 | 65.07 |
| TiO2 | 1.49 | 1.20 | .09 |
| Al2O3 | 18.41 | 17.88 | 14.86 |
| Fe2O3 | 9.41 | 8.41 | 4.62 |
| MnO | .07 | .07 | .01 |
| MgO | 5.86 | 3.68 | 1.75 |
| CaO | 8.80 | 7.97 | 4.18 |
| Na2O | 3.90 | 4.78 | 4.84 |
| K2O | 1.26 | 1.84 | 3.59 |
| P2O5 | .31 | .48 | .38 |
| ba | 638.4 | 864.5 | 1416.64 |
| rb | 21.5 | 30.2 | 77.48 |
| sr | 774.4 | 729.9 | 498.79 |
| zr | 105.0 | 143.0 | 274.28 |
| nb | 6.2 | 8.49 | 15.36 |
| y | 15.25 | 21.1 | 21.80 |
| sc | 21.0 | 19.84 | 8.11 |
| v | 189.0 | 110.3 | 46.88 |
| ni | 56.0 | 35.03 | 5.91 |
| cr | 21.0 | 19.88 | 2.58 |
| la | 20.47 | 27.13 | 42.61 |
| ce | 38.65 | 51.23 | 80.46 |
| nd | 20.21 | 27.08 | 34.12 |
| sm | 4.53 | 6.05 | 6.19 |
| eu | 1.48 | 1.91 | 1.72 |
| gd | 4.08 | 5.38 | 4.73 |
| dy | 3.75 | 4.95 | 4.26 |
| er | 1.98 | 2.59 | 2.23 |
| yb | 1.76 | 2.27 | 2.06 |

Figure 16b:

Summarized major and trace element model between typical Sierran basalt and MLI dacite lavas. Major elements were modeled by mass balance/least squares equations; the Rayleigh fractionation equation was used in the trace element modeling. The modeled basalt was adapted from the Black Point concentrations and differ in abundance for Rb, Zr, Nb, and La but have parallel patterns (compare with Table 3).

Table 6: Partition Coefficients

| phase: | basalt | | | | dacite | | | | | |
|--------|--------|-------|-------|-------|--------|-------|------|------|------|------|
| | plag | oliv | cpx | mt | plag | mt | biot | hbld | cpx | opx |
| ba | .23 | .01 | .03 | .01 | .36 | .01 | 6.96 | .39 | .04 | .01 |
| rb | .07 | .01 | .03 | .01 | .02 | .01 | 2.26 | .05 | .01 | .01 |
| sr | 1.83 | .014 | .12 | .01 | 2.29 | .01 | .12 | .33 | .09 | .01 |
| zr | .01 | .01 | .34 | .90 | .03 | .20 | 1.20 | 1.40 | .25 | .08 |
| nb | .01 | .01 | .10 | 1.00 | .03 | 1.00 | 1.80 | 1.30 | .30 | .35 |
| y | .03 | .01 | .50 | .20 | .06 | .50 | 1.20 | 3.50 | 1.50 | .45 |
| la | .28 | .009 | .15 | .20 | .26 | .20 | .32 | 1.77 | .45 | .10 |
| ce | .28 | .009 | .15 | .20 | .24 | .20 | .32 | 1.77 | .55 | .10 |
| nd | .20 | .010 | .31 | .25 | .20 | .20 | .29 | 2.80 | .77 | .17 |
| sm | .17 | .011 | .50 | .30 | .20 | .25 | .26 | 3.75 | .80 | .19 |
| eu | .34 | .010 | .51 | .25 | .99 | .25 | .24 | 2.20 | .80 | .13 |
| gd | .21 | .012 | .61 | .30 | .21 | .25 | .28 | 4.15 | 1.36 | .32 |
| dy | .19 | .014 | .68 | .30 | .19 | .25 | .29 | 4.20 | 1.47 | .46 |
| er | .24 | .017 | .65 | .30 | .24 | .25 | .35 | 4.00 | 1.40 | .66 |
| yb | .30 | .023 | .62 | .30 | .30 | .25 | .35 | 3.55 | 1.29 | .85 |
| sc | .01 | .08 | .90 | 24.00 | .01 | 1.00 | .50 | 7.00 | 3.00 | 1.40 |
| v | .01 | .30 | 9.00 | 2.00 | .01 | 24.00 | 1.00 | 4.00 | .90 | .50 |
| cr | .01 | .20 | 10.00 | 1.00 | .01 | 1.00 | 1.00 | 8.00 | 9.00 | 6.00 |
| ni | .01 | 10.00 | 2.00 | 4.00 | .01 | 4.00 | 1.00 | 7.00 | 5.00 | 8.00 |

High Silica Rhyolite *

| | plag | sani | qtz | fay | hbld | magn | apat | zirc | alla |
|----|-------|------|-----|------|-------|------|-------|--------|------|
| ba | .610 | 6.00 | .00 | .01 | .044 | .01 | .01 | .01 | .01 |
| rb | .041 | .94 | .00 | .01 | .014 | .01 | .01 | .01 | .01 |
| sr | 5.0 | 4.00 | .00 | .01 | .022 | .01 | .01 | .01 | .01 |
| zr | .100 | .10 | .00 | .01 | 4.00 | .80 | .10 | 3487.0 | 1.00 |
| nb | .060 | .06 | .00 | .01 | 4.00 | 4.00 | 4.10 | 30.00 | 4.4 |
| y | .100 | .10 | .00 | .01 | 6.00 | 2.00 | 30.00 | 270.0 | 37.0 |
| la | .20 | .10 | .00 | 1.08 | 1.30 | 11.0 | 50.50 | 7.2 | 2827 |
| ce | .270 | .04 | .00 | .93 | 1.50 | 9.70 | 52.50 | 10.0 | 2494 |
| nd | .210 | .05 | .00 | .77 | 4.30 | 6.90 | 81.10 | 4.6 | 1340 |
| sm | .130 | .03 | .00 | .50 | 7.77 | 3.80 | 89.80 | 11.0 | 977 |
| eu | 2.850 | 3.00 | .00 | .09 | 5.10 | .90 | 50.20 | 20.0 | 100 |
| gd | .097 | .03 | .00 | .31 | 10.00 | 2.00 | 78.00 | 37.0 | 311 |
| dy | .064 | .05 | .00 | .90 | 13.00 | 1.75 | 69.20 | 108.0 | 150 |
| er | .055 | .02 | .00 | .90 | 12.00 | 1.50 | 51.20 | 300.0 | 83 |
| yb | .049 | .05 | .00 | 1.26 | 8.40 | 1.25 | 37.00 | 564.0 | 37 |

* these K'ds are insufficient in the Inyo modeling, see text and figure 20.

Table 6:

Partition coefficients used in trace element modeling,
Sources: Arth, 1976, Mahood and Hildreth, 1983, Pearce and Norry,
1979, Gill, 1981, Leeman and Phelps, 1981, Nash and Creecraft,
1985). Zr in Zr K'd is artificial because of non-Henry's law
behavior; calculated as the concentration of Zr in zircon (EDS
analysis) over the concentration in the whole rock.

Although the major and trace element chemistry is consistent with derivation of the Negit dacites from trace element enriched, basalts by fractional crystallization, the individual MLI dacite eruptive centers have either evolved separately, or not remained a closed system. Specifically, the Paohan dacite lavas and Negit dacites have different petrologies and significantly different LREE, HFS, and V contents that cannot be explained by fractionation of the observed assemblages (fig. 7b, table3).

Linear trends on silica variation diagrams (figs. 7a, b) are present between the MLI dacites and rhyolites that suggest a fractional crystallization origin. Several arguments however, indicate that the MLI dacites cannot be directly parental to the MLI rhyolites:

- 1) The Nd isotopic compositions of the dacites and rhyolites are significantly different; the Negit dacite has ϵ_{Nd} of -2.0 while the Paohan rhyolite is +0.1. (fig. 15).
- 2) It is unlikely that fractionation of either the dacite or rhyolite mineral assemblages could produce the MREE depletion in the rhyolites relative to the dacites (fig. 17).
- 3) Ba concentrations are much lower in the rhyolites (1,000-1200 ppm, compared to 1,400-1,600 ppm in the dacites), and neither the dacites or the rhyolites contain sanidine. Biotite fractionation could explain the lower Ba concentrations, however, the amount required to satisfy the lower Ba in the rhyolites (about 20 wt. %) would deplete the Rb contents by 28% relative to the observed rhyolite Rb concentrations.
- 4) Sr is more depleted in the MLI rhyolites, by a factor of 2,

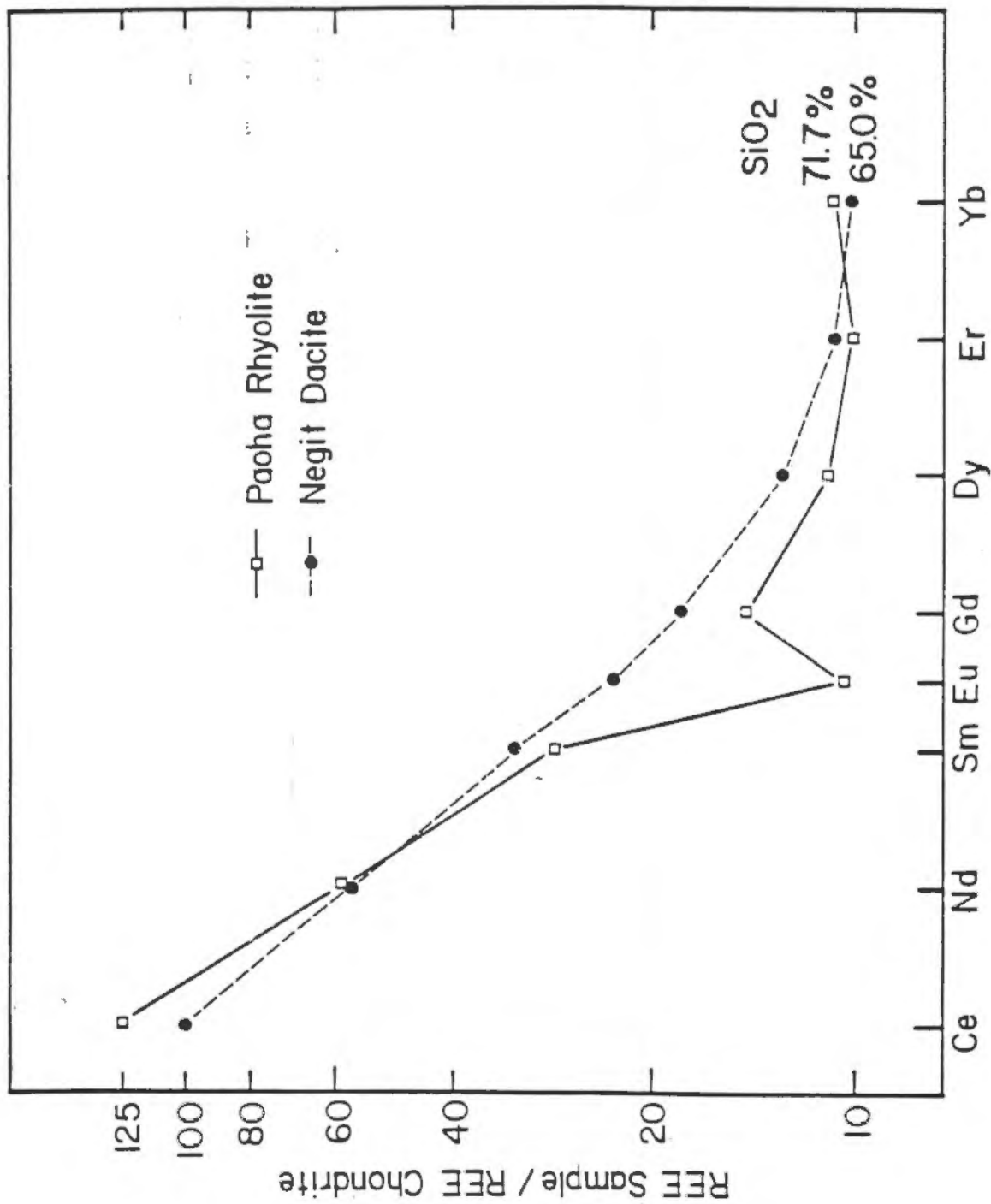


Figure 17:

Chondrite normalized REE diagram of the Negit dacite and Paohan rhyolite. Both are similarly LREE enriched, but have incompatible patterns; the Paohan rhyolite is more depleted in the MREE (Sm to Dy) than can be explained by fractionation of any combination of the observed assemblages. See discussion.

than can be explained by fractionation of either the dacite or rhyolite assemblages.

Low-Ba Rocks

The Ba data of figure 9 indicate that none of the low-Ba rocks can be interrelated by crystal fractionation or variable degrees of partial melting of a single source. The low-Ba basaltic inclusions have similar or higher Ba than either the MC dacite or the andesitic inclusions, and similar LREE to the MC dacite. (table 3). The Ba and other trace element data do not preclude mixing between basaltic and silicic endmembers for either the MC dacite or andesitic inclusions, and the petrographic data (above) is consistent with this hypothesis. However, the andesitic inclusions have higher REE concentrations than the MC dacite (fig. 11) indicating that any mixing hypothesis must involve separate and chemically distinct mafic and silicic endmembers. For the andesitic inclusions, several constraints can be placed on the endmember components based on the petrographic and chemical data: 1) the sanidine, albitic plagioclase, ferrosilite rich opx, and mafic(?) clots, suggest involvement of highly evolved rhyolite and basaltic magmas. 2) The mafic component must have an ϵ_{Nd} value $> +2.9$, higher than any value yet reported for Late Cenozoic basalts of the SNP. 3) Assuming that the silicic component is more LREE enriched than the mafic component, and in order to account for the LREE content of the andesite, the silicic endmember must be $>75x$ chondrite. 4) The low Ce/Yb values (6.7) and high REE concentrations precludes any of the

silicic or mafic rocks presently exposed as potential endmembers; this includes the basalts, the MLI lavas, the HSRs of the Mono Craters, and the Inyo rhyolites.

The likelihood that the andesitic inclusions are the products of mixing between basalt and highly evolved rhyolite is very similar to the proposed origin of the intermediate inclusions of the Coso volcanic field (Bacon and Metz, 1984). In fact, the major and trace element chemistry of both the Mono Craters and Coso inclusions is strikingly parallel (fig. 12c). This is not fortuitous considering the proposed basaltic endmembers have a similar arc-like signature (fig. 12b), and both occur in HSR hosts. Furthermore, the Coso inclusions are more Ta enriched than the andesitic inclusions of the MC-MLI (fig. 12c). This same relationship distinguishes the Black Point and June Lake basalts from the uncontaminated basalts of Coso (fig. 12b, assuming $Nb/Ta = 16$). Bacon and Metz (1984) favor a model for the origin of the intermediate inclusions at Coso in which, either least differentiated HSR, or less evolved, unexposed rhyolite of a single, compositionally zoned magma chamber mixes with underlying basalt. Their model may be applicable to the andesitic inclusions of the MC system, and one likely silicic endmember modeled, has a Ce/Yb ratio (but overall higher REE contents) similar to the MC HSRs. However, the hypothesis cannot be rigorously tested since the REE patterns of the andesites preclude any of the Mono Craters HSRs as silicic endmembers. Furthermore, the trace element chemistry of the MC HSRs, discussed

below, argues against a sustained, compositionally zoned system, and there is no geophysical evidence for a shallow (>10-20km.) magma chamber beneath the Mono Basin (Hermance et al., 1983).

The sieve textured, sodic plagioclase xenocrysts in the MC dacite suggests contamination or mixing. The latter is consistent with the chemical data, and the major element chemistry of the dacite can be modeled by mixing of about 60% rhyolite and 40% basalt. The low Ce/Yb ratio (4.7), and low REE concentrations of the dacite, however, eliminates all of the analyzed basalts or andesites as potential mafic components (fig. 11). Likewise, the HSRs of the Mono Craters, and Inyo and MLI rhyolites can also be eliminated as silicic components; either they are not as LREE enriched as the dacite, or the Eu depletion or LREE enrichment is too large to model with any reasonable basalt by two component mixing. Thus, the origin of the MC dacite is consistent with mixing but is poorly constrained. Other possibilities for the low-Ba dacite involve direct partial melting of lower crustal rocks or fractional crystallization of an andesite with similar but lower REE concentrations as the low-Ba andesite. Amphibolite, pyroxenite, garnet granulite, and gabbroic rocks occur as xenoliths in alkalic basalts or have been proposed as lower or mid-crustal constituents (Domenick, et al., 1983, Oliver, 1977, Bateman and Eaton, 1967). If partial melting of lower crust is proposed, the high HREE concentrations and low Ce/Yb ratio of the dacite requires that HREE enriched residual phases are absent or completely melted, which is unlikely. Thus, all of the

known lower crustal rocks in this area can be excluded except the pyroxenite.

Mono Graters High Silica Rhyolites

The relationship between the biotite and fayalite + crystal poor lavas offers difficulties in being related by a single differentiation process. The biotite bearing domes are the most chemically diverse group of the chain, while the fayalite and crystal poor lavas are nearly homogeneous. The trace element concentrations of both groups are qualitatively consistent with the latter group as differentiates of the former by crystal fractionation of a plagioclase dominated assemblage. The systematic increase in the LREE from the least differentiated biotite bearing dome, M-19, to the fayalite and crystal-poor rhyolites, however is inconsistent with all of the porphyritic domes (except M-19) having allanite as a trace phase. In addition, whole rock/groundmass glass relations of biotite and fayalite bearing domes indicate substantial depletion of the LREE with fractionation (fig. 18). Moreover, in both glasses analyzed, Ce is depleted relative to all HSR whole rock samples. This suggests that either the observed assemblage (e.g. allanite) is not representative of the original fractionating assemblage, or the biotite bearing domes evolved separately from the fayalite and crystal-poor lavas.

In contrast, the trace element variation between the orthopyroxene-bearing and fayalite and crystal poor lavas is consistent with crystal fractionation of an allanite-bearing, plagioclase

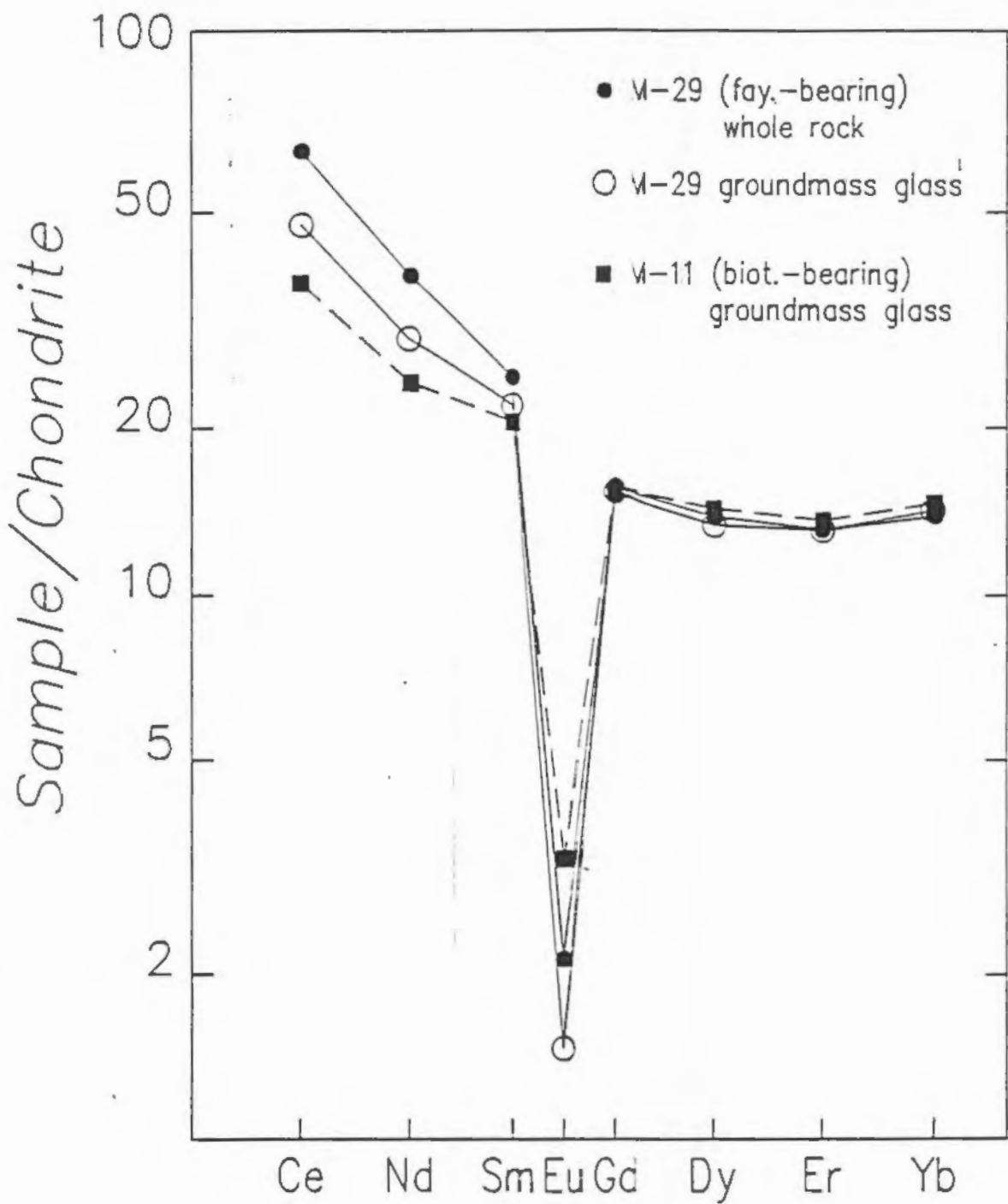


Figure 18:

REE whole rock/groundmass glass pair of a fayalite-bearing dome, and one groundmass glass analysis of the most differentiated biotite-bearing dome, M-11. The fayalite-bearing glass is strongly depleted in LREE relative to the whole rock, and both glasses are more depleted in LREE than any of the HSR lavas.

minated assemblage. The Rayleigh fractionation model, summarized in figure 19, requires reasonable published K' 's (table 6), and is in excellent agreement with the observed assemblage and proportions of phases. Zr was modeled by mass balance due to non-Henry's law behavior of Zr in zircon, and the mass fraction required was used in the Rayleigh calculations. Objections to the model might be the amount of allanite required (.08%) however, the orthopyroxene-bearing domes are the most allanite-rich, and crystals up to 1mm are observed. Rb, Nb, and Y are more enriched and Gd is depleted in the calculated daughter by as much as 7.5%. These differences however, are similar to or less than the range of concentrations for these elements in the fayalite and crystal poor lavas (table 3).

One sparsely porphyritic dome, M-16, also has a subtle but significantly different trace element signature than the other sparsely porphyritic facies lavas. In particular, Sr, Ba, and Rb are enriched and Ce, Nd, and Zr are depleted in this dome, relative to the other fayalite and crystal poor lavas, by as much as 30% (fig. 13a, b, table 3). M-16 also has more Mg-rich hornblendes than the fayalite-bearing lavas (fig. 5); thus, M-16 appears to be a separate magma batch.

Relationship Between the Inyo Domes and MC-MLL Rhyolites

The temporal and spatial relationship between the Mono Craters and Inyo Domes makes the hypothesis of a genetic tie between them very attractive. Moreover, the sense of change in the chemistry of the most evolved "fp" lava (Sampson and Cameron, in review) of the Inyo

chain and the fayalite and crystal poor HSRs is consistent with an allanite-bearing, rhyolitic assemblage. In detail, however, the chemical and petrologic data indicate that the Mono Craters and Inyo lavas are not linked to a single liquid line of descent from a compositionally zoned magma body.

The the crystal fractionation model, summarized in figures 20a and 20b, fails to satisfactorily reproduce the trace element concentrations of the observed MC HSRs. Specifically, Nb, Rb, and the LREE (especially Nd) are more depleted in the MC HSRs than can be explained by a reasonable model unless exorbitant proportions of trace phases and partition coefficients are invoked for these elements. For example, the weight fraction of trace phases used in the model (fig. 20a) is at least 5x that observed; the high K^d s required for Rb and Nb in sanidine and magnetite respectively, is equally unrealistic. The cross between Gd and Dy is also difficult to resolve using the observed phenocryst mineralogy in the proportions required to satisfy the major elements. For example, the model in fig. 20b has a bulk D Gd/Dy ratio of .96, opposite the approximately 1.1 required to match the HSR concentrations. Furthermore, the HREE and Y contents are constant to increasing in the MC HSRs, relative to the Inyo fp lavas, while the calculated HREE and Y concentrations are decreasing. The proportions of phenocryst phases controlling the concentrations of these elements (hornblende, zircon, apatite, and allanite), are restricted by major and other trace element requirements.

Rayleigh Fractionation Model: Inyo fp Rhyolite to MC HSR Fayalite
and Crystal Poor Lavas

assemblage (wt.%):

| plag | san | qtz | fay | hbld | magn | apat | zirc | alla |
|------|------|------|-----|------|------|------|------|------|
| 27.0 | 52.0 | 15.3 | 0.0 | 4.0 | 1.2 | 0.3 | 0.15 | 0.1 |

f = 0.600

conc.: Inyo-fp calc HSR-ol

| | | | |
|------|-------|-----|------|
| la = | 120 | 37 | |
| ce = | 138.0 | 51 | 51.0 |
| nd = | 46.9 | 29 | 22.0 |
| sm = | 6.70 | 4.8 | 4.7 |
| eu = | 0.39 | 0.1 | .15 |
| gd = | 4.69 | 4.5 | 3.95 |
| dy = | 4.38 | 4.2 | 4.45 |
| er = | 2.55 | 2.3 | 2.65 |
| yb = | 2.62 | 2.1 | 2.85 |
| ba = | 355 | 45 | 51 |
| sr = | 38 | 83 | 7 |
| rb = | 156 | 185 | 184 |
| zr = | 235 | 127 | 118 |
| nb = | 22 | 27 | 25 |
| y = | 28 | 30 | 37 |

partition coefficients used for the above model

| plag | san | qtz | fay | hbld | magn | apat | zirc | alla | |
|-------|------|-----|------|-------|------|------|-------|------|----|
| .200 | .10 | 0 | 1.08 | 1.5 | 11.0 | 52.5 | 7.2 | 2827 | la |
| .270 | .04 | 0 | .93 | 1.5 | 9.7 | 52.5 | 10.0 | 2494 | ce |
| .210 | .05 | 0 | .77 | 4.3 | 6.9 | 81.1 | 4.6 | 1340 | nd |
| .130 | .03 | 0 | .50 | 7.8 | 3.8 | 89.8 | 11.0 | 977 | sm |
| 2.850 | 3.00 | 0 | .09 | 5.1 | 0.9 | 50.2 | 20.0 | 100 | eu |
| .097 | .03 | 0 | .31 | 10.0 | 2.0 | 78.0 | 37.0 | 311 | gd |
| .064 | .05 | 0 | .90 | 13.0 | 2.0 | 69.2 | 108.0 | 150 | dy |
| .055 | .02 | 0 | .90 | 12.0 | 2.0 | 51.2 | 300.0 | 83 | er |
| .049 | .05 | 0 | 1.26 | 8.40 | 2.0 | 37.0 | 564.0 | 37 | yb |
| .610 | 9.35 | 0 | .01 | 0.044 | 0.01 | 0.01 | 0.01 | 0.01 | ba |
| 7.500 | 4.00 | 0 | .01 | 0.022 | 0.01 | 0.01 | 0.01 | 0.01 | sr |
| .041 | 1.25 | 0 | .01 | 0.014 | 0.01 | 0.01 | 0.01 | 0.01 | rb |
| .100 | .10 | 0 | .01 | 4.0 | 0.80 | 0.10 | 1300 | 1.00 | zr |
| .060 | .06 | 0 | .01 | 6.0 | 15.0 | 4.1 | 50.0 | 4.4 | nb |
| .100 | .10 | 0 | .01 | 6.0 | 2.00 | 30.0 | 270.0 | 37.0 | y |

NOTE: THESE K^d s ARE AT THE EXTREME END OF THE VALUES PRESENTLY AVAILABLE IN THE LITERATURE (see table 6 for references)

NOTE: K^d FOR RB IN SANIDINE IS >1; NASH AND CRECROFT (1985) REPORT VALUES IN THIS RANGE FOR THE TWIN PEAKS RHYOLITES HOWEVER, THIS IS THE ONLY PUBLISHED VALUE >1

NOTE: THERE ARE NO PUBLISHED VALUES FOR Nb FOR HIGHLY EVOLVED ROCKS, THUS THE PARTITION COEFF. FOR MAGNETITE AND ZIRCON ARE POORLY CONSTRAINED.

Figure 20a:

Petrogenetic model between the MC fayalite bearing HSR and the most evolved Inyo-fp series magma. The calculated daughter is a poor fit to the observed data requiring unrealistic proportions of accessory phases and maximized partition coefficients for most elements (e.g. Rb in sanidine and Nb in magnetite). See discussion.

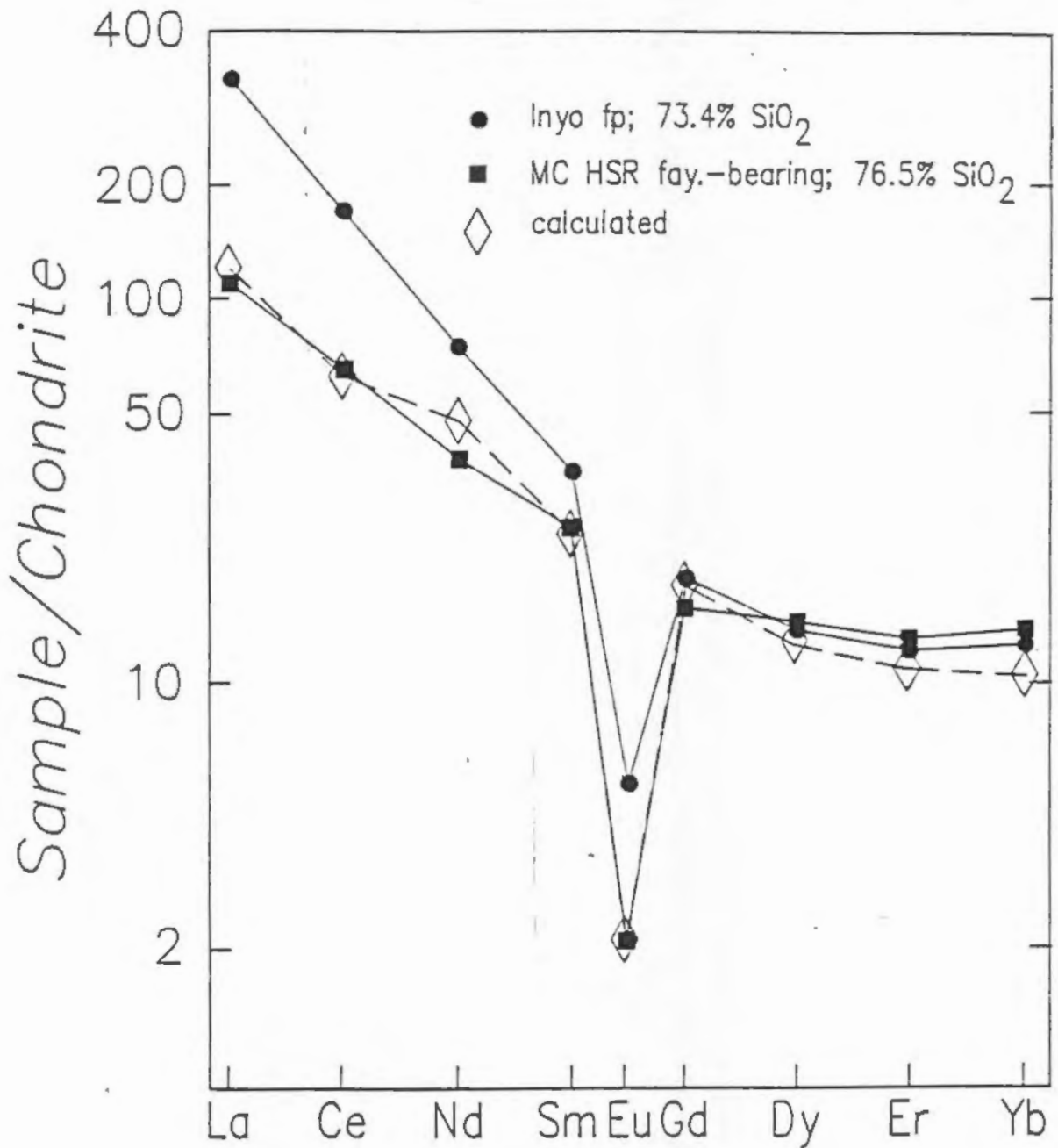


Figure 20b:

Summary of modeling between the most evolved Inyo "fp" rhyolite and the MC fayalite and crystal poor HSRs. See figure 20a for partition coefficients used. The Nd "spike" in the calculated pattern reflects the allanite partition coefficient pattern. Note that the HREEs of the modeled rhyolite (diamonds) are decreasing with fractionation, but the observed rhyolite (solid square) is constant to increasing, relative to the Inyo REE pattern.

The petrology of the two rhyolite suites is also different and difficult to conceptualize in a single, compositionally zoned magma. The Inyo fp lavas are two pyroxene- and biotite-bearing, and have approximately 3.5:1 plagioclase to sanidine ratios. In the fayalite-bearing MC lavas, hornblende is the primary ferromagnesian phase, biotite and pyroxene are absent, and plagioclase to sanidine ratios are approximately 1:1 to 1:2. Moreover, it is not readily apparent why a zoned magma chamber would erupt petrologically and chemically distinct magmas, at the same time, in geographically separate and restricted areas.

Assimilation of crustal material during residence time in a magma chamber, or ascent to the surface, is an improbable explanation to account for the chemical differences between the two lava suites. Likely assimilants, ie. Sierran granitics, have on average, 500 ppm Sr, while the majority of the MC HSR's average 6 ppm. The low Sr abundances of these lavas, therefore, precludes assimilation alone. Combined fractional crystallization and assimilation (AFC) is possible but requires extremely small values for r (mass rate of assimilation/mass rate of crystallization). There is also no physical evidence for mixing in the HSRs. Moreover, the fayalite and crystal poor lavas are chemically uniform which argues against random or selective contamination processes.

The Inyo fp series also appears chemically similar to the rhyolites of the Mono Lake Islands. However, these two lava suites cannot

be comagmatic for two main reasons. First, the FeO^*/MgO ratios are radically different (fig. 21); the Paohan rhyolites range from 9-14, while Inyo fp lavas are between 5-6. Secondly, relative to the Inyo fp series at the same SiO_2 content, the Paohan rhyolites are enriched in Ba and Zr and depleted in Ti, Mg, Y, and Nb concentrations and ratios of these elements (fig. 21). Thus, the chemical and isotopic similarity of the two suites of lavas probably reflects the common signature of the source region and not strictly a common parent.

Constraints on Source Regions

Most investigators agree that no single, homogeneous source region can explain the isotopic variations of the Sierra Nevada Province, and invoke some combination of mantle and crustal components (see for example: Leeman, 1982, Bacon and Metz, 1983, Bacon, et al., 1983, Domenick, et al., 1983, Menzies, et al., 1983). Studies of mantle and crustal xenoliths (Domenick, et al., 1983), alkalic to ultrapotassic basalts (Van Kooten, 1980, 1981), and the basalts of the Coso and MC-MLI volcanic complexes document gross mantle and crustal heterogeneities with time integrated LILE enrichments. Figure 22 is a Nd-Sr isotopic plot of the Sierra Nevada Province basaltic lavas, crustal and mantle nodules, and Mesozoic intrusives. Based on these data three distinct source regions are distinguished: 1) An isotopically enriched mantle source with high $^{87}\text{Sr}/^{86}\text{Sr}$ ($>.7053$) and lower ϵ_{Nd} (+1.5- -6.0), 2) a less enriched, more oceanic basalt-like mantle source, with $^{87}\text{Sr}/^{86}\text{Sr}$ of about .7045 and $\epsilon_{\text{Nd}} > +4$, and 3) an old

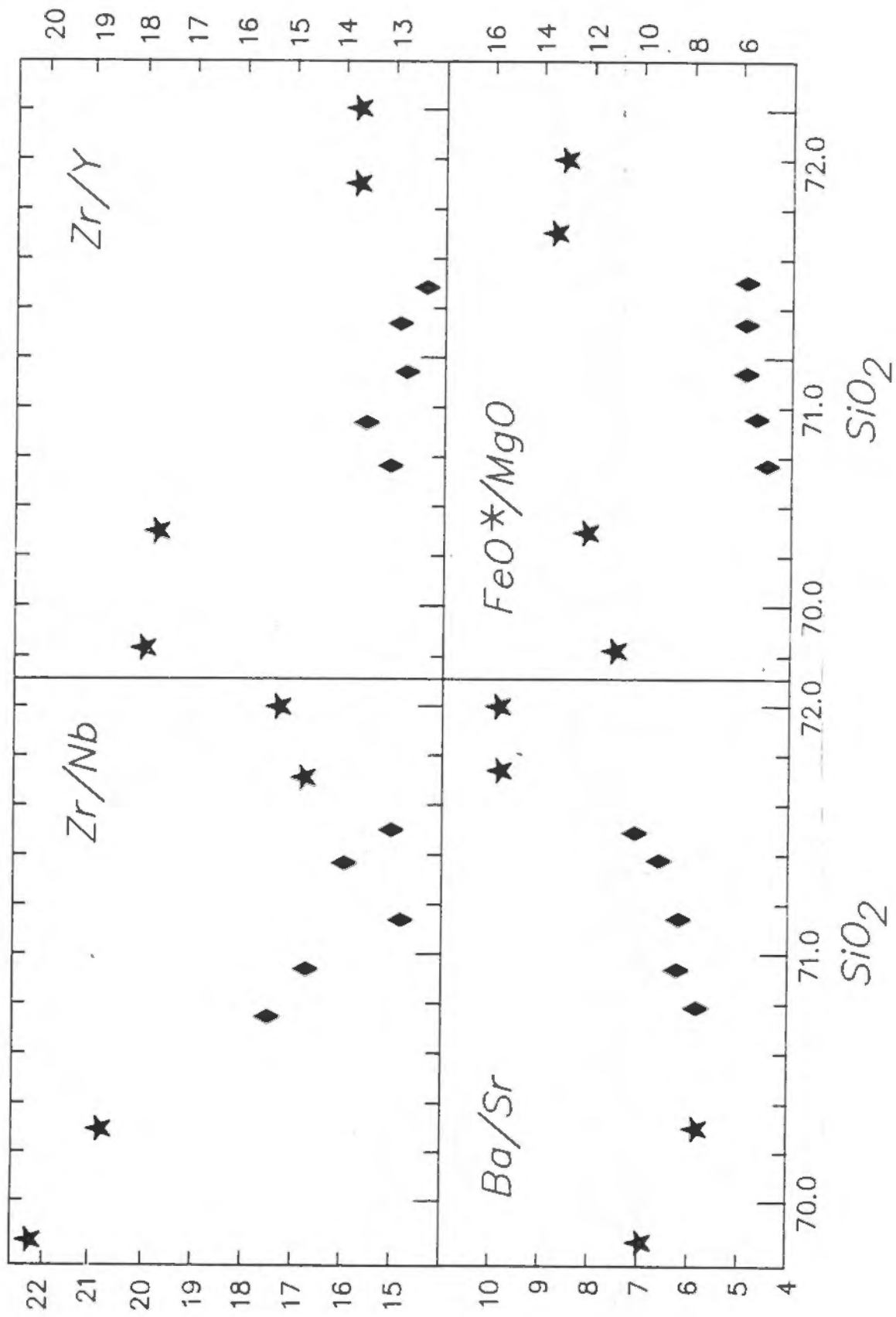


Figure 21:

Trace element and FeO^*/MgO ratios for the MLI rhyolites and the Inyo fp series lavas. Relative to the MLI rhyolites (stars), the Inyo lavas (diamonds) have, at similar SiO_2 contents, lower FeO^*/MgO , HFS element, and Ba/Sr ratios.

crustal source including pre-Cenozoic metasedimentary rocks and Mesozoic intrusives that have $^{87}\text{Sr}/^{86}\text{Sr}$ ratios $> .7090$, and low ϵ_{Nd} values (< -8.0). The latter source rocks act as reservoirs for assimilation/contamination, but not as source rocks for the generation of mafic magmas.

Two trace element signatures overprint the isotopically distinct source regions. One has a subduction related, arc-like, trace element pattern (fig. 12b) and is present in all of the Sierra Nevada Province volcanic rocks regardless of isotopic character. Furthermore, the arc-like component persists throughout the Devil's Garden Lava Field, except in the lowest-K ($< .15\% \text{K}_2\text{O}$) LAOT basalts (Bullen, in press), and throughout the basalt and associated andesites of the Lassen volcanic field (Bullen, pers. comm.).

The second component is characterized by a "within plate basalt" trace element signature typified by Nb, and Ta enrichments, lower Ba/Ta, Ba/Nb, and Ce/Yb ratios, and slightly higher Ti and Zr contents. The "within plate basalt" component is less prevalent, and, at least within the Sierra Nevada Province, is coupled with the less isotopically enriched mantle source. For example, the low-Ba basaltic and andesitic inclusions of the MC-MLI volcanic complex, the uncontaminated basalts of the Coso field, and one alkali olivine basalt of the Sierra Nevada ultrapotassic suite, all have a "within plate basalt" component, and have average $^{87}\text{Sr}/^{86}\text{Sr}$ ratios of $.7045$.

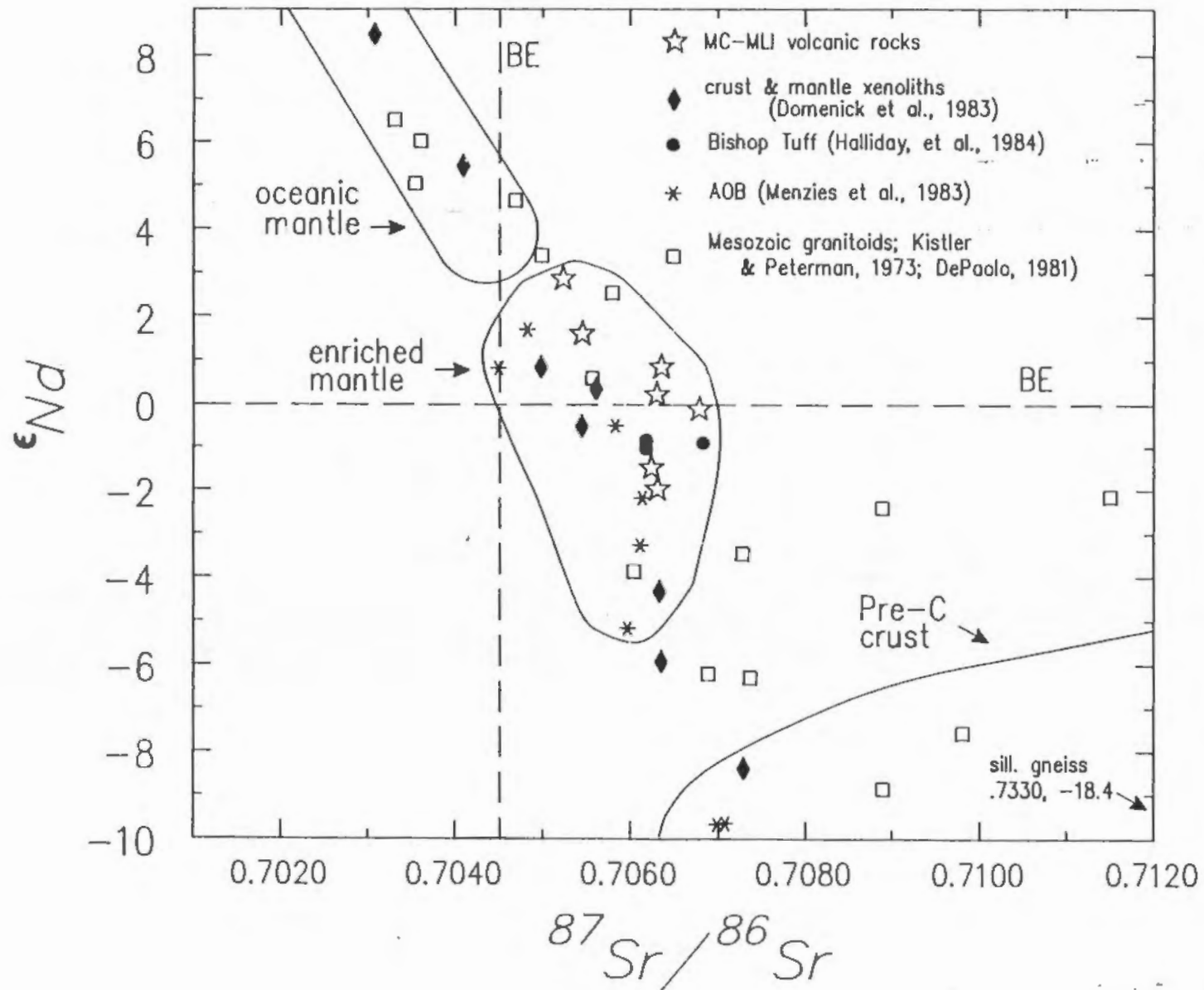


Figure 22:

Nd and Sr isotopic ratio diagram of: MC-MLI volcanic rocks, Inyo domes, Bishop Tuff, crustal and mantle nodules, Mesozoic intrusives and Late Cenozoic basalts of the Sierra Nevada Province (see text for sources). Bulk earth (BE) is drawn for reference. See figure for key to symbols. Not included on the diagram are uncontaminated basalt $87\text{Sr}/86\text{Sr}$ ratios from the Coso lava field; these lavas have ratios between .7037 and .7047. The three fields in the figure (labeled, with arrows) represent isotopically distinct source regions discussed in the text.

In addition, the isotopically enriched basalts of the Sierran Province that have a strong arc-like trace element signature, (i.e. high-Ba basalts of the MC-MLI, ultrapotassic and alkali olivine basalts, (Van Kooten, 1981), and the .08 M.Y. Long Valley basalt (Sampson, unpublished data), fig. 12b), have REE patterns that require residual hornblende or garnet. In contrast, the basalts that show evidence for a "within plate basalt" component have much flatter REE patterns that suggest a residual HREE phase is not present.

One scenario to explain the mantle source components is that melts are derived from two regions: 1) convecting, garnet-bearing asthenosphere and, 2) subcontinental lithosphere. Both source regions have been strongly affected by incompatible element rich fluids derived from the dehydrating, subducted crust, and inherit an arc-like trace element signature. The subcontinental lithospheric mantle is less affected, however, due its distance from the downgoing plate and non-convecting nature. This source, therefore, preserves some of its "within plate" component and more primitive isotopic mantle values. The above scenario implies, either relatively recent (? early Mesozoic) incompatible trace element enrichments in the subcontinental lithosphere and old (Pre-Cambrian?) enrichments in the asthenospheric mantle, or a young, enriched, subcontinental mantle "keel".

The potential source regions of the more evolved rocks of the MC-MLI complex are: 1) upper crustal, Mesozoic intrusive rocks of the Sierra Nevada Batholith (e.g. Doe and Delevaux, 1973, Kascor, MS

thesis, 1984), 2) enriched upper mantle, or 3) enriched lower crust (Halliday et al., 1983). The first possibility can be eliminated on the basis of Sr and limited Nd isotopic data. Intrusive rocks from the MC-MLI area generally have more present day radiogenic Sr and lower Nd values than the HSRs or MLI rhyolites (fig. 22, and Farmer, et al., 1985). Halliday et al. (1983) report average crustal $^{87}\text{Sr}/^{86}\text{Sr}$ values $>.708$ for the Long Valley area. This lead them, in part, to conclude a lower crust or enriched upper mantle source for the Bishop Tuff. The Bishop Tuff has Nd and Sr isotopic ratios similar to the rhyolites of the MC-MLI (fig. 15). Thus, the MLI rhyolites and MC HSRs were most likely derived from a similar enriched mantle or lower crustal source.

Summary

The volcanic rocks of the Mono Craters-Mono Lake Islands volcanic complex comprise several magma bodies that were not derived from a single liquid line of descent. The petrologic, chemical, and isotopic data indicates: 1) that the high- and low-Ba rocks cannot be related. 2) Within each group, none of the lavas can be directly linked by crystal liquid processes or by mixing of magmas represented by the exposed rock types, although fractional crystallization of a high-Ba basalt compositionally similar to Black Point to produce the MLI dacites is proposed. 3) Two component mixing between trace element enriched basalts and highly evolved materials is consistent with the petrologic and chemical data for the andesitic inclusions and MC dacite but is poorly constrained. 4) The MC HSRs are chemically

variable and fall into three distinct groups that correlate with petrologic subdivisions and eruption ages. The chemical data suggests that the fayalite and crystal poor lavas were derived from a magma with similar trace element contents as the orthopyroxene-bearing lavas. The biotite bearing domes comprise an older, chemically distinct magmatic event. 5) None of the MC-MLI lavas can be directly related to the Inyo rhyolites. It is therefore clear that the MC-MLI complex does not consist of a single evolving magma chamber/incipient caldera forming magmatic system (Bailey, et al., 1976, Kilborne, et al., 1980) rather, it comprises a plethora of magmas and magmatic processes that existed contemporaneously at several crustal levels.

The isotopic and trace element data of the MC-MLI complex documents sub-continental mantle heterogeneity and, combined with data from several Late Cenozoic volcanic centers throughout the Sierra Nevada Province, define two mantle components. The dominant component is characterized by an arc-like trace element signature. The second component is characterized by a within plate basalt enrichment in HFS elements which correlates with lower $^{87}\text{Sr}/^{86}\text{Sr}$ and Ce/Yb, and higher ϵ_{Nd} .

The MLI rhyolites and MC HSRs have similar isotopic ratios to the Inyo domes and the Bishop Tuff. These lavas are not directly comagmatic, and therefore, reflect a similar lower crust or enriched upper mantle source region, but not a common parent.

References

- Arth, J. G., Behavior of Trace Elements During Magmatic Processes--A Summary of Theoretical Models and their Applications, J. RES. U.S.G.S. 4 No. 1, p. 41 - 47, 1976
- Bacon, C. R., Magmatic Inclusions in Silicic and Intermediate Volcanic Rocks, J. Geophys. Res., 91 No. B6, p. 6091 - 6112, 1986
- Bacon, C. R., W. A. Duffield, and K. Nakamura, Distribution of Quaternary Rhyolite Domes of the Coso Range, California: Implications for Extent of the Geothermal Anomaly, J. Geophys. Res., 85 No. B5, p. 2425 - 2433, 1980
- Bacon, C. R., H. Kurasawa, M. H. Delevaux, R. W. Kistler, and B. R. Doe, Lead and strontium isotopic evidence for crustal interaction and compositional zonation in the source regions of Pleistocene basaltic and rhyolitic magmas of the Coso volcanic field, California, Contrib. Mineral. Petrol., 85, p.366-375, 1984
- Bacon, C. R., R. Macdonald, R. L. Smith, and P. A. Baedecker, Pleistocene High-Silica Rhyolites of the Coso Volcanic Field, Inyo County, California, J. Geophys. Res., 86 No. B11, p. 10223 - 10241, 1981
- Bacon, C. R., and Metz, J., Magmatic Inclusions in Rhyolites, Contaminated Basalts, and Compositional Zonation beneath the Coso Volcanic Field, California, Contrib. Mineral. Petrol., 85, p. 346 - 365, 1984
- Bailey, R. A., Structural and Petrologic Evolution of the Long Valley, Mono Craters, and Mono Lake Volcanic Complexes, Eastern California, EOS Trans. AGU, 61 No. 46, p. 1149, 1980
- Bailey, R. A., Postcaldera Evolution of the Long Valley Magma Chamber, Eastern California, EOS Trans. AGU, 64 #45, p.889, 1983
- Bailey, R. A., Chemical Evolution and Current State of the Long Valley Magma Chamber, U.S.G.S. PROC. WKSHP. XIX, p.25- 40, 1984
- Bailey, R. A., G. B. Dalrymple, and M. A. Lanphere, Volcanism, Structure, and Geochronology of Long Valley Caldera, Mono County, California, J. Geophys. Res. v.81 No. 5, p.725 - 744, 1976

- Bailey, R. A., R. A. Macdonald, and J. E. Thomas, The Inyo-Mono Craters: Products of an Actively Differentiating Rhyolite Magma Chamber, Eastern California, Eos Trans. AGU, 64 No. 18, p. 336, 1983
- Bateman, P. C., and J. P. Eaton, Sierra Nevada Batholith, Science, 158 #3807, p. 1407 - 1417, 1967
- Cameron, K. L., P. C. Kelleher, D. E. Sampson, and Farmer, L., A Nd and Sr Isotopic Study of the Inyo Dome--Mono Crater Rhyolites, Eastern California, Geol. Soc. Am. Abs. with Prog., 17 No. 7, p. 538, 1985
- Carmichael, I.S.E., The Iron-Titanium Oxides of Salic Volcanic Rocks and their Associated Ferromagnesian Silicates, Contrib. Mineral. and Petrol., 14, p. 36-64, 1967
- Christensen, M. N., and C. M. Gilbert, Basaltic Cone Suggests Constructional Origin of Some Guyots, Science, 143, p. 240-242, 1964
- Dalrymple, G. B., Potassium-Argon Ages of Recent Rhyolites of the Mono and Inyo Craters, California, Earth Planet. Sci. Lett., 3, p. 289 - 298, 1967
- DePaolo, D. J., A Neodymium and Strontium Isotopic Study of the Mesozoic Calc-Alkaline Granitic Batholiths of the Sierra Nevada and Peninsular Ranges, California, J. Geophys. Res., 86 No. B11, p.10470-10488, 1981
- Doe, B. R., and M. H. Delevaux, Variations in Lead-Isotopic Compositions in Mesozoic Granitic Rocks of California: A Preliminary Investigation, Geol. Soc. Am. Bull., 84, p. 3513 - 3526, 1973
- Domenick, M. A., R. W. Kistler, F.C.W. Dodge, and M. Tatsumoto, Nd and Sr Isotopic Study of Crustal and Mantle Inclusions from the Sierra Nevada and Implications for Batholith Petrogenesis, Geol. Soc. Am. Bull., 94, p. 713 - 719, 1983
- Farmer, G. L., and D. J. DePaolo, Origin of Mesozoic and Tertiary Granite in the Western United States and Implications for Pre-Mesozoic Crustal Structure 1. Nd and Sr Isotopic Studies in the Geocline of the Northern Great Basin, J. Geophys. Res., v.88 #B4, p. 3379 - 3401, 1983

- Gilbert, C. M., M.N. Christensen, Yehya Al-Rawi, and K. R. Lajoie, Structural and Volcanic History of Mono Basin, California-Nevada, Geol. Soc. Am. Mem., v. 116, p. 275 - 326, 1968
- Gill, J.B., Orogenic Andesites and Plate Tectonics, Springer-Verlag, 390 pp., 1981
- Halliday, A. N., A. E. Fallick, J. Hutchinson, and W. Hildreth, A Nd, Sr and O Isotopic Investigation into the Causes of Chemical and Isotopic Zonation in the Bishop Tuff, California, Earth Planet. Sci. Lett., 68, p. 379 - 391, 1984
- Hanson, G. N., The Application of Trace Elements to the Petrogenesis of Igneous Rocks of Granitic Composition, Earth Planet. Sci. Lett., v.38, p. 26 - 43, 1978
- Hanson, G. N., Rare Earth Elements in Petrogenetic Studies of Igneous Systems, Annual Review Earth and Planetary Science Letters, v.8, p. 371-406, 1980
- Hart, W. K., Chemical and Isotopic Evidence for Mixing between Depleted and Enriched Mantle NW USA, Geochim. Cosmochim. Acta, v.49 #1, p. 131-150, 1984
- Hedge, C. E., and D. C. Noble, Upper Cenozoic Basalts with High Sr87/Sr86 and Sr/Rb Ratios, Southern Great Basin, Western United States, Geol. Soc. Am. Bull., v. 82, p.3503 - 3510, 1971
- Hermance, J. F., W. Slocum, and G. A. Neumann, The Long Valley/Mono Basin Volcanic Complex: Status of Present Magnetotelluric Investigations, Eos Trans. AGU, 64 No. 45, p.890, 1983
- Kaczor, S. M., A Petrographic and Chemical Study of the Natural Melting of the Rattlesnake Gulch Granite, California, MS thesis, 136 pp., SUNY Stony Brook, Stony Brook, NY, 1984
- Kelleher, P.C., and Cameron, K.L. Petrologic and Geochemical Evolution of the Rhyolites of the Mono Craters, Eastern California, Eos Trans. AGU, v.65 No. 45, p. 1128, 1984
- Kelleher, P. C., K. L. Cameron, and G. J. Nimz, Evidence for Several Magma Batches at Mono Craters(MC)-Mono Lake Islands (MLI), California, Eos Trans. AGU, v.66 No. 46, p. 1112, 1985

- Kilbourne, R. T., S. H. Wood, and C. W. Chesterman, Recent Volcanism in the Mono Basin-Long Valley Region of Mono County, California, CA. DIV. MIN. GEO S.R. 150, p. 7- 22, 1980
- Kistler, R. W., Structure and Metamorphism in the Mono Carters Quadrangle, Sierra Nevada, California, U.S.G.S. BULL. 1221-E, p. 53, 1966
- Kistler, R. W., and Z. E. Peterman, Variations in Sr, Rb, K, Na, and Initial Sr87/Sr86 in Mesozoic Granitic Rocks and Intruded Wall Rocks in Central California, Geol. Soc. Am. Bull., v. 84, 3489 - 3512, 1973
- Lajoie, K. R., Late Quaternary Stratigraphy and Geologic History of the Mono Basin, Eastern California, Ph. D. thesis, Univ. of Calif., Berkeley, 271p., 1968
- Leeman, W. P., Tectonic and Magmatic Significance of Strontium Isotopic Variations in Cenozoic Volcanic Rocks from the Western United States, Geol. Soc. Am. Bull., v.93, p. 487 - 503, 1982
- Leeman, W. P., and D. W. Phelps, Partitioning of Rare Earths and Other Trace Elements Between Sanidine and Coexisting Volcanic Glass, J. Geophys. Res., v.86 No. B11, p.10193 - 10199, 1981
- Leeman, W. P., and J.W. Rogers, Late Cenozoic Alkali-Olivine Basalts of the Basin-Range Province, USA, Contrib. Mineral. Petrol., v.25, 1 - 24, 1970
- Loney, R. A., Flow Structure and Composition of the Southern Coulee, Mono Craters, California--A Pumiceous Rhyolite Flow, GSA Memoirs, v.116, p.415 - 440, 1968
- Mahood, G., and W. Hildreth, Large Partition Coefficients for Trace Elements in High-Silica Rhyolites, Geochim. Cosmochim. Acta, v.47, p.11 - 30, 1983
- McKee, E. H., W. Duffield, and R. Stern, Early Pliocene- Late Miocene Basaltic Rocks and Their Implications for Crustal Structure, Northeastern California and Southcentral Oregon, Geol. Soc. of America Bull., v.94, 1983
- Menzies, M. A., W. P. Leeman, and C. J. Hawkesworth, Isotope Geochemistry of Cenozoic Volcanic Rocks Reveals Mantle Heterogeneity Below Western USA, Nature, v.303, 205 - 209, 1983

- Miller, C. D., Chronology of Holocene Eruptions at the Inyo Volcanic Chain, California, *Eos Trans. AGU*, v.64 #44, p. 198, 1983
- Moore, J. G., and F.C.W. Dodge, Late Cenozoic Volcanic Rocks of the Southern Sierra Nevada, California: I. Geology and Petrology: Summary, *Geol. Soc. Am. Bull.*, v.91 Part I, p. 515 - 518, 1980
- Nash, W. P., and H. R. Crecraft, Partition Coefficients for Trace Elements in Silicic Magmas, *Geochim. Cosmochim. Acta*, v.49, p. 2309 - 2322, 1985
- Oliver, H. W., Gravity and Magnetic Investigations of the Sierra Nevada Batholith, California, *Geol. Soc. Am. Bull.* v.88, p.445 - 461, 1977
- Pakiser, L. C., F. Press, and M. F. Kane, Geophysical Investigation of Mono Basin, California, *Geol. Soc. Am. Bull.*, v.71, p. 415 - 448, 1960
- Pearce, J. A., and M. J. Norry, Petrogenetic Implications of Ti, Zr, Y and Nb Variations in Volcanic Rocks, *Contrib. Mineral. Petrol.*, v.69, p. 33 - 47, 1979
- Pearce, J.A., in *Continental Basalts and Mantle Xenoliths*, eds. Hawkesworth, C.J. and Norry, M.J., Shiva, Orpington p.239-249, 1983
- Putnam, W. C., The Mono Craters, California, *GEOG. REV.*, p. 68 - 82, 1838
- Sampson, D. E., C. P. Ardito, P. C. Kelleher, K. L. Cameron, and T. D. Bullen, The Geochemistry of Quaternary Lavas from the Inyo-Mono Chain: Evidence for Several Magma Types, *Eos Trans. AGU*, v.64 No. 44, p. 889 -, 1983
- Sampson, D. E., and K. L. Cameron, Geochemistry of the Most Recent Eruptive Event in the Inyo Volcanic Chain, Eastern California: the Intersection of Two Magmatic Systems, *Geol. Soc. Am. Abs. with Pro.*, v.16 No. 6, 1984
- Sampson, D. E., and K. L. Cameron, The Geochemistry of the Inyo Volcanic Chain: Multiple Magma Systems in the Long Valley Region, Eastern California, In Review, p. 25, 1986

- Sieh, K., Most Recent Eruption of the Mono Craters, Eastern Central California, USGS Proc. Wkshp. XIX, I, p.96 - 129, 1984
- Sieh, K., and M. Bursik, Most Recent Eruption of the Mono Craters, Eastern Central California, In Review p.80,
- Sieh, K., S. H. Wood, and S. Stine, Most Recent Eruption of the Mono Craters, Eastern Central California, Eos Trans. AGU, v.64 No. 45, p. 889, 1983
- Stewart, J. H., Cenozoic Structure and Tectonics of the Northern Basin and Range Province, California, Nevada and Utah, GEOTH. RES. COUN. S.R. NO. 13, p. 25 - 39, 1983
- Stewart, J. H., G. W. Walker, and F. J. Kleinhampl, Oregon-Nevada Lineament, Geology., v.3, p. 265 - 268, 1975
- Stork, A., D.K. Smith, J.B. Gill, Automated XRF analyses of geochemical reference standards, submitted to Geostandards Newsletter, 1986
- Tanzer, M. O., and J. D. Maccougall, ²³⁰Th-²³⁸U Disequilibrium Systematics from Long Valley and Mono Domes, California: Evidence for Magma Replenishment Since 0.1 m.v. Ago, Eos Trans. AGU, 65 No. 45, p. 1128, 1984
- Van Kooten, G. K., Mineralogy, Petrology, and Geochemistry of an Ultrapotassic Basaltic Suite, Central Sierra Nevada, California, U.S.A., J. Petrol., v.21 Part 4, p. 651 - 684, 1980
- Van Kooten, G. K., Pb and Sr Systematics of Ultrapotassic and Basaltic Rocks from the Central Sierra Nevada, California, Contrib. Mineral. Petrol., v.76, p. 378 - 385, 1981
- Whitcomb, J. H., and J. Rundle, Gravity Variation in the Mammoth Lakes, Mono Lake and Owens Valley, California Regions, Eos Trans. AGU, v.65 No. 45, p. 890, 1983
- Wood, S. H., Chronology of Late Pleistocene and Holocene Volcanics, Long Valley and Mono Basin Geothermal Areas, Eastern California, U.S. Geol. Surv. Open File Rep., p. 1 - 55, 1977

Wood, S. H., Distribution, correlation, and radiocarbon dating of late Holocene tephra, Mono and Inyo craters, eastern California, Geol. Soc. Am. Bull., v.88, p.89 - 95, 1977

Wright, L., Late Cenozoic Fault Patterns and Stress Fields in the Great Basin and Westward Displacement of the Sierra Nevada Block, Geology, v. 4, p.489 - 494, 1976

Explanation

Map units for lavas



talus



low density, homogeneous, gray to black pumice



intermediate density, brn.-black color, irregular, flowbanded obsidian and lens shaped, coarsely vesicular pockets



highest density, slate gray color, finely vesicular, planar flowbands slaty cleavage



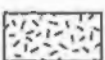
highest density, pale red color, micro-vesicular, irregular vesicle pockets planar flowbands, blocky fracture



unconsolidated tephra, predom. gray color little juvenile material



predom. marginal facies, chaotic blocks of breccia and obsidian; obsid. rich at flow margins, locally breccia rich



porphyritic, perlitic, dacite with plagioclase, megacrysts and basaltic inclusions

Map units for tephras



predom. airfall, local surge and pyroclastic flows



pyroclastic flows and block avalanche deposits of North Coulee, Panum, and Crater, and Pumice Pit dome



pyroclastic flows of Northwest and South Coulees



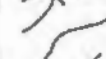
unconsolidated, explosion breccia of dome M-18



scarp/crater rim, hachures on downthrown/lee side



lava flow lineations, single barb; ridge double barb; depression



lithologic contact



strike and dip of flow foliation



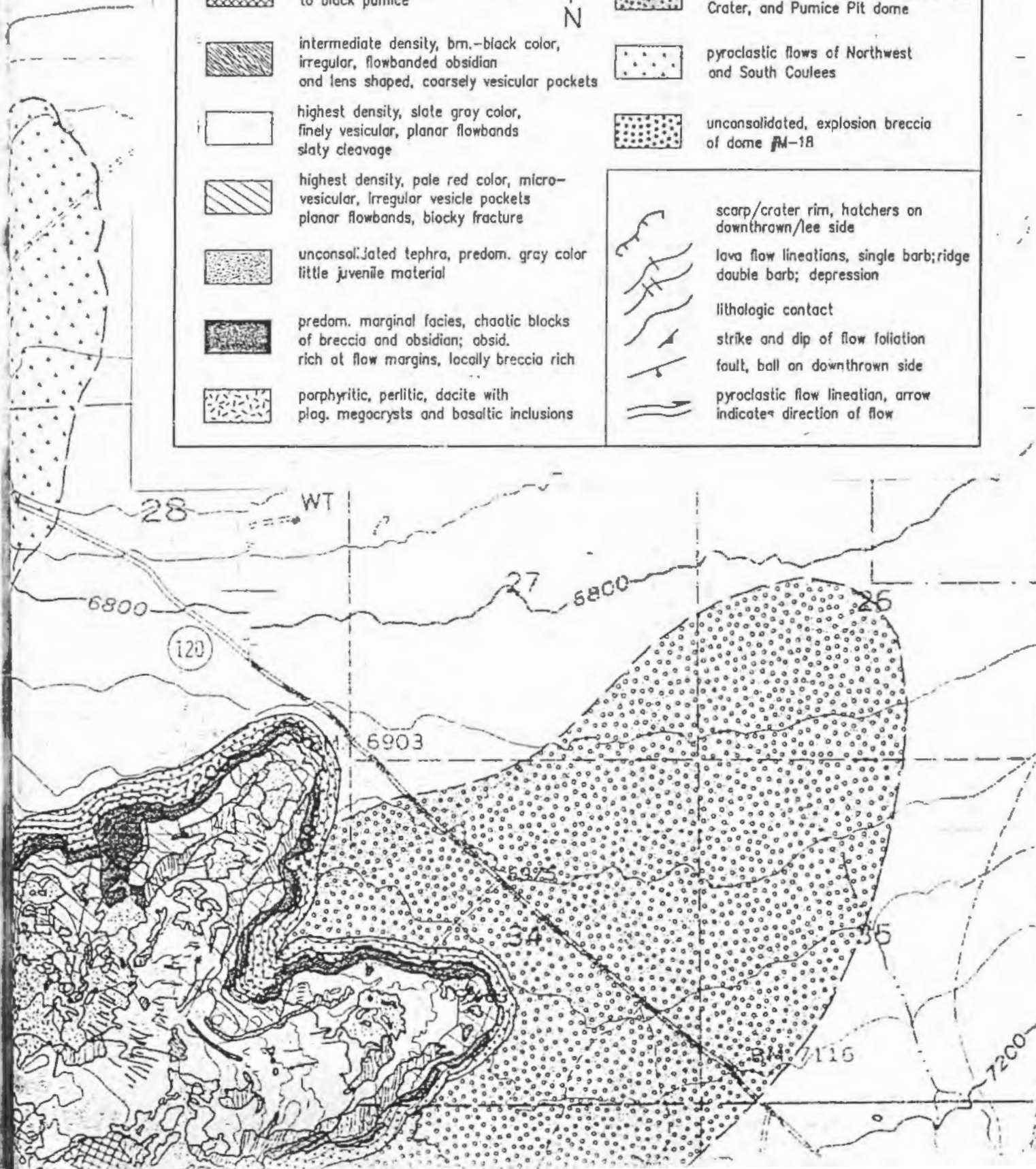
fault, ball on downthrown side

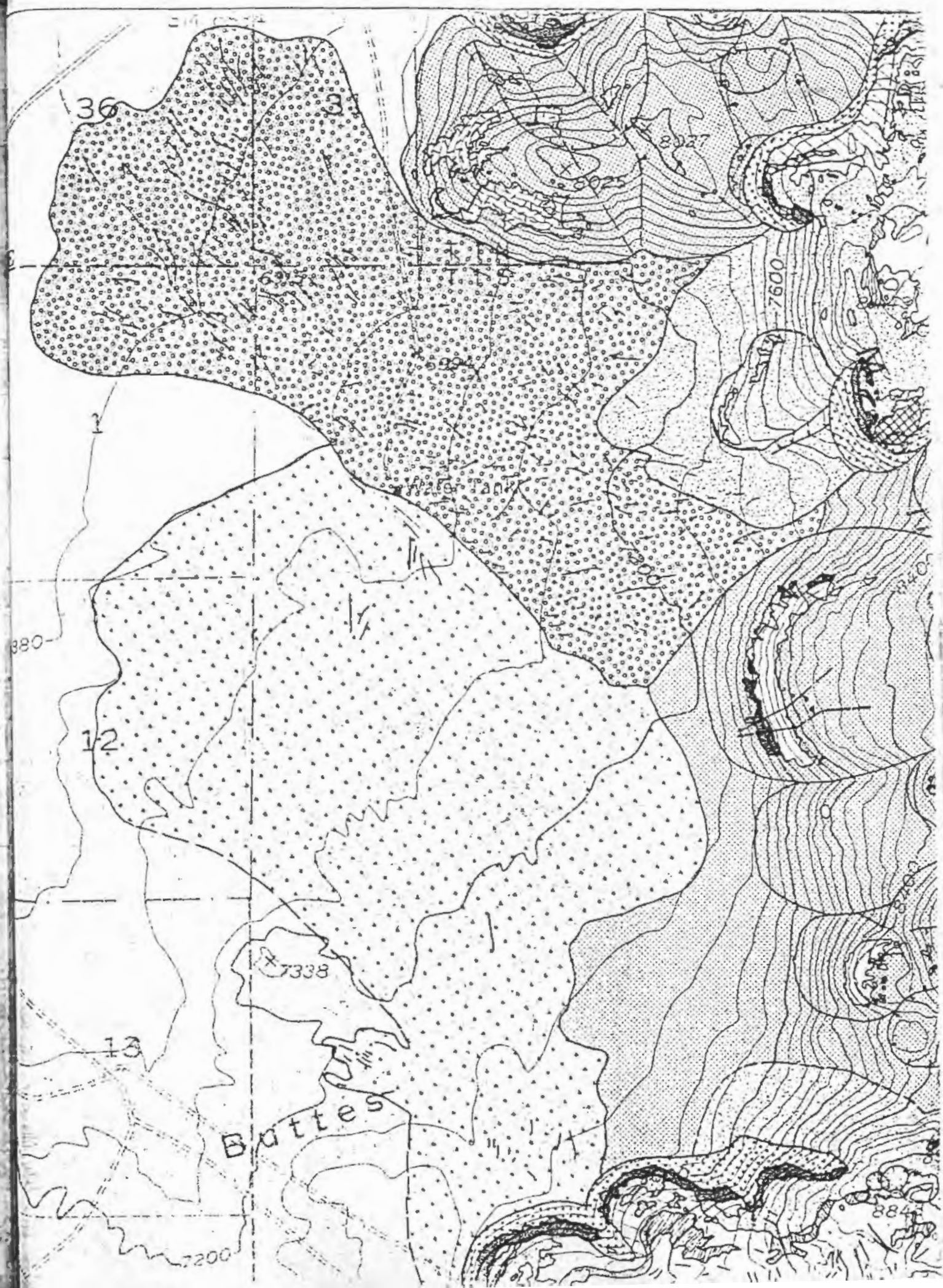


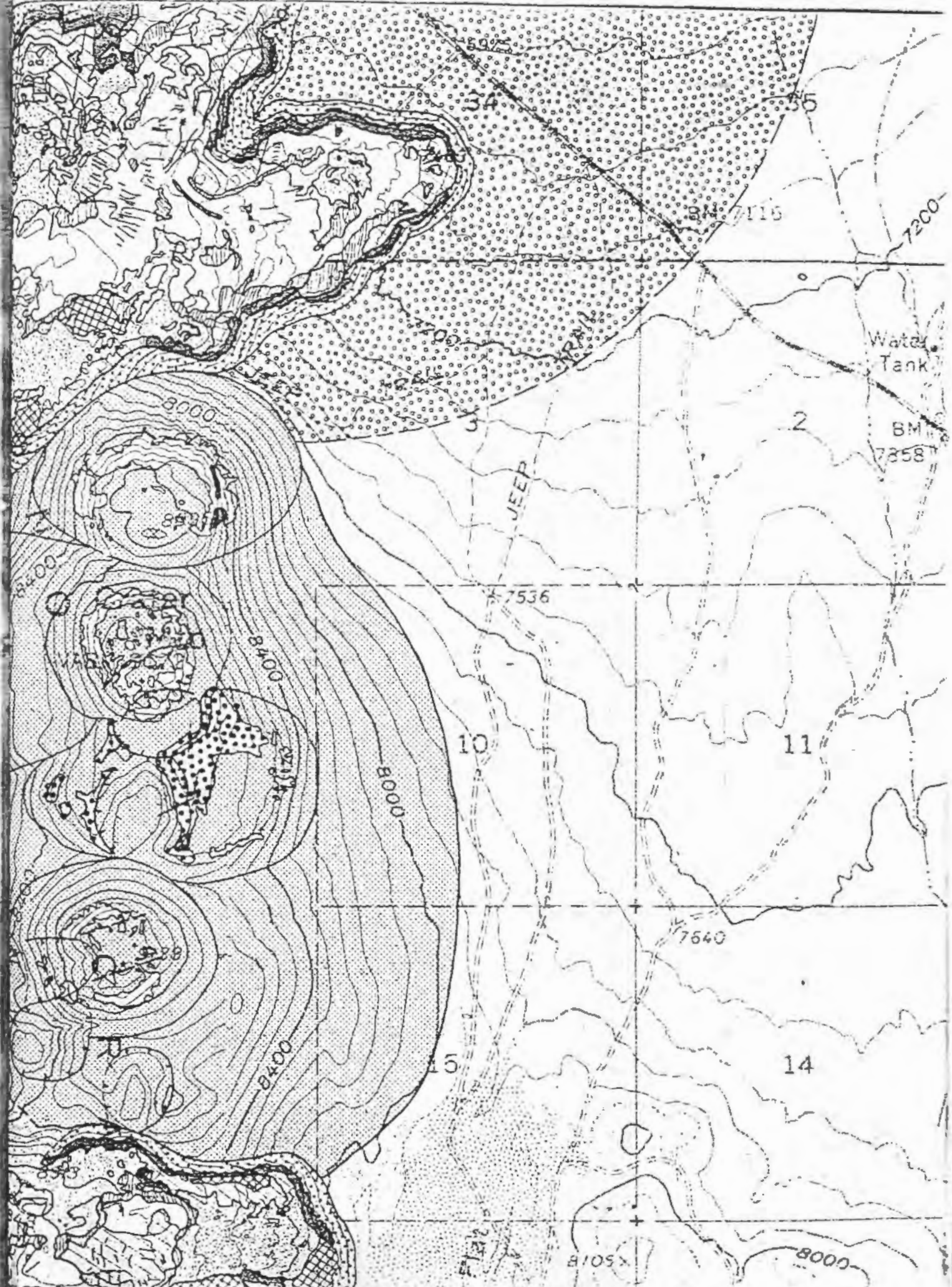
pyroclastic flow lineation, arrow indicates direction of flow

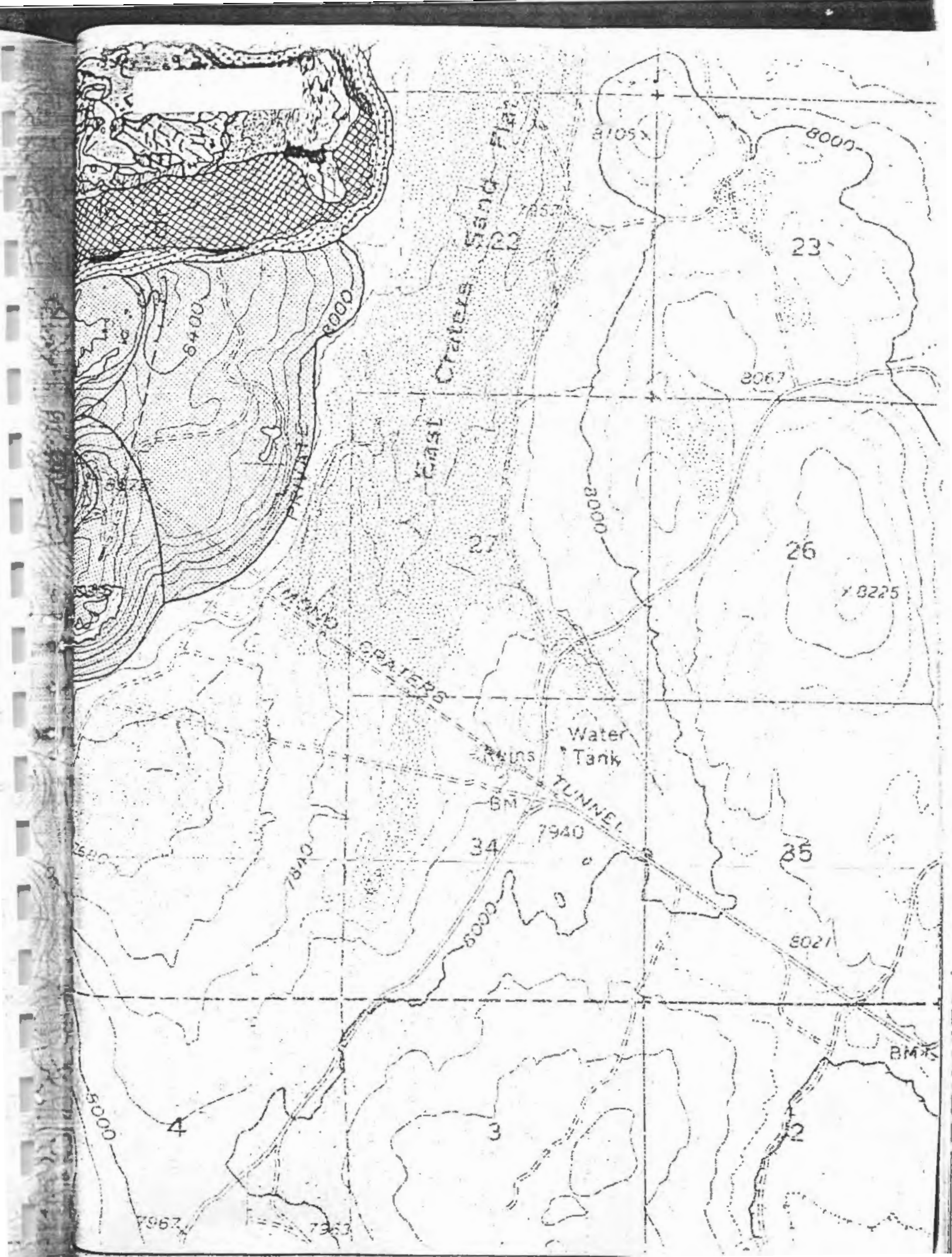


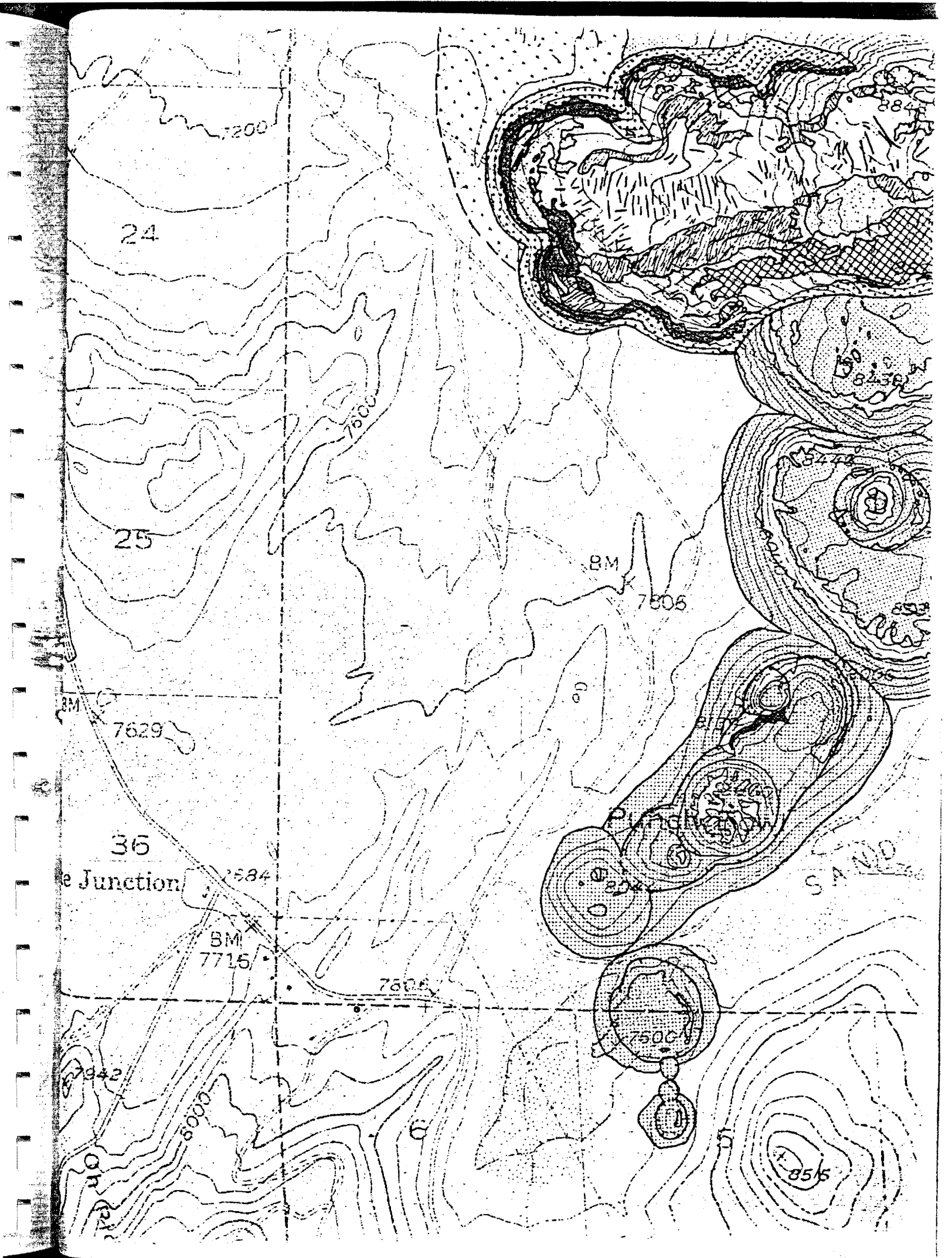
N

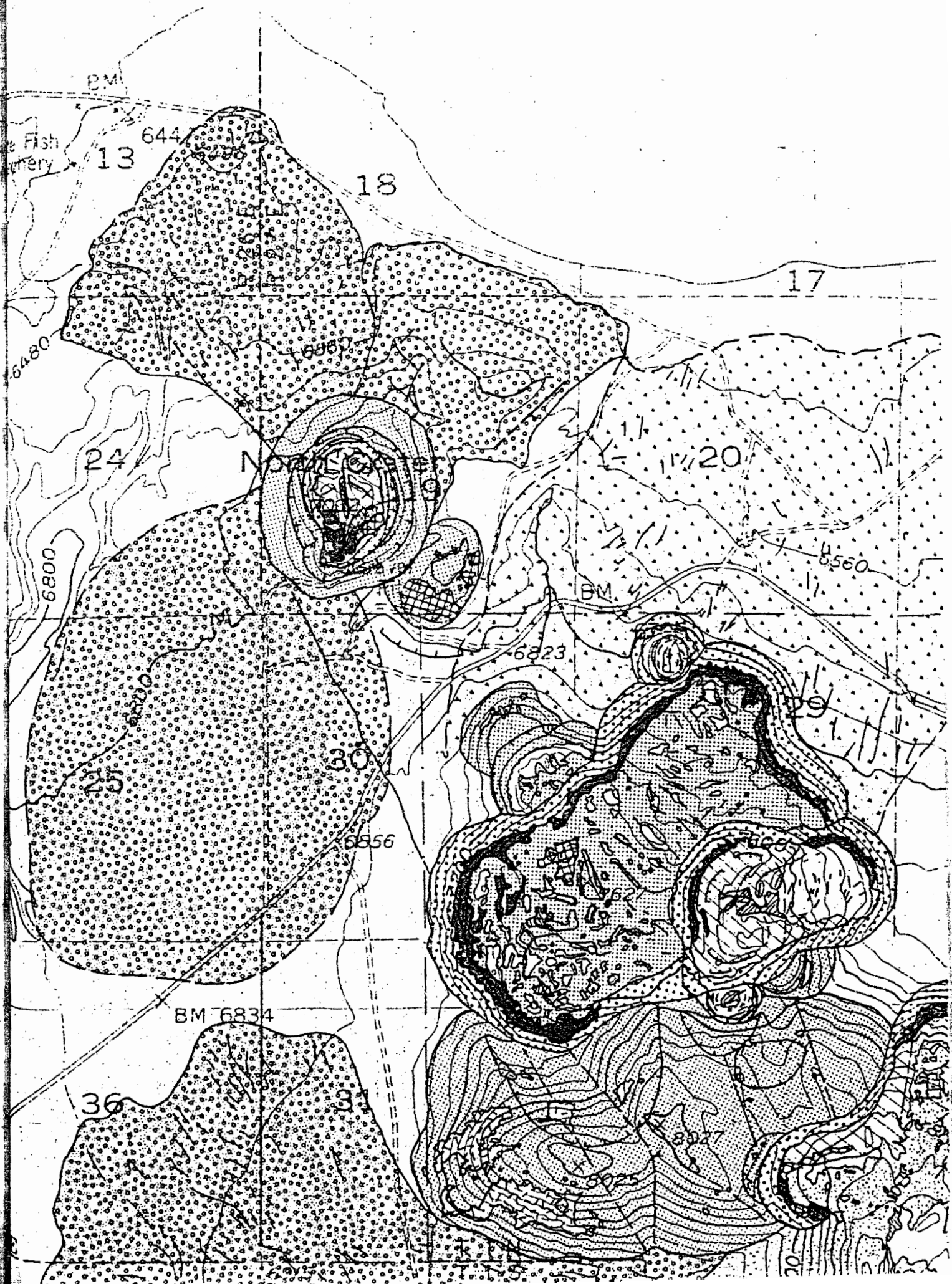












BM

Fishery

13

6440

18

17

6480

6800

24

M

1/2

1/2

20

6560

6800

BM

6823

25

30

19

6856

BM 6834

36

34

30

20